The Dissertation Committee for Md Sarwar Siddiqui Certifies that this is the approved version of the following dissertation:

Effect of Portland Cement Concrete Characteristics and Constituents on Thermal Expansion

Committee:

David W. Fowler, Supervisor

Maria Juenger

Amit Bhasin

Moon Won

Harovel G. Wheat

Effect of Portland Cement Concrete Characteristics and Constituents on Thermal Expansion

by

Md Sarwar Siddiqui, B.E.; M.S.

Dissertation

Presented to the Faculty of the Graduate School of

The University of Texas at Austin

in Partial Fulfillment

of the Requirements

for the Degree of

Doctor of Philosophy

The University of Texas at Austin

August 2014

Dedication

To my late father, Mr. Md Nurul Karim who was not able to see me reaching to the highest level.

Acknowledgements

First, I would like to express my profound gratitude to my advisor, Dr. David Fowler, for providing me invaluable support, guidance, and encouragement throughout this study. I am truly grateful for his role in my personal and professional development.

I am grateful to the committee members—Dr. Maria Juenger, Dr. Amit Bhasin, Dr. Moon Won, and Dr. Harovel Wheat—for providing helpful comments and suggestions on my Ph.D. research work. Also, I would like to acknowledge Dr. Zachary Grasley for his help and guidance in developing the analytical model.

I acknowledge the financial support of the Texas Department of Transportation (TxDOT). A number of TxDOT personnel helped me in many ways, including Elizabeth Lukefahr, Ryan Barborak, Hua Chen, and Andy Naranjo. Without their help, this study would not be possible.

Thanks to my colleagues in my research group for their strong support in the lab and academic conversations, particularly David Whitney, Michael Rung, Dr. Mark Rached, and Ali Al-Qarni. I would also like to thank the departmental staff for their kind assistance with several issues. I want to acknowledge my friends, who have always encouraged me.

I cannot adequately express my gratitude to my parents, Mr. Md Nurul Karim and Mrs. Door Afsan Khanam, and my siblings for their love, encouragement, and support. Finally, I wish to thank my wife Sharmin for her patience and kindness. Words cannot describe her inspiration during this long process.

Effect of Portland Cement Concrete Characteristics and Constituents on Thermal Expansion

Md Sarwar Siddiqui, Ph.D.

The University of Texas at Austin, 2014

Supervisor: David W. Fowler

The coefficient of thermal expansion (CTE) is one of the major factors responsible for distresses in concrete pavements and structures. Continuously reinforced concrete pavements (CRCPs) in particular are highly susceptible to distresses caused by high CTE in concrete. CRCP is a popular choice across the U.S. and around the world for its long service life and minimal maintenance requirements. CRCP has been built in more than 35 states in the U.S., including Texas. In order to prevent CRCP distresses, the Texas Department of Transportation (TxDOT) has limited the CTE of CRCP concrete to a maximum of 5.5 x10^{-6} strain/^{o}F (9.9 x10^{-6} strain/^{o}C). Coarse aggregate sources that produce concrete with CTE higher than the allowable limit are no longer accepted in the TxDOT CRCP projects. Moreover, CTE is an important input in the *Mechanistic-Empirical Pavement Design Guide* (MEPDG). Small deviations in input CTE can affect the pavement thickness significantly in MEPDG designs. Therefore, accurate determination of concrete CTE is important, as it allows for enhanced concrete structure and pavement design as well as accurate screening of CRCP coarse aggregates. Moreover, optimizing the CTE of concrete according to a structure's needs can reduce that structure's cracking potential.

This will result in significant savings in repair and rehabilitation costs and will improve the durability and longevity of concrete structures.

This study found that the CTEs determined from saturated concrete samples were affected by the internal water pressure. As a result, the TxDOT method yielded higher values than did the American Association of State Highway and Transportation Officials (AASHTO) method. To further investigate the effect of internal water pressure, an analytical model was developed based on the poroelastic phenomenon of concrete. According to the model, porosity, permeability, and the rate of temperature change are the major factors that influence the internal water pressure development. Increasing the permeability of concrete can reduce the internal water pressure development and can thus improve the consistency of measured CTE values. Preconditioning concrete samples by subjecting them to several heating and cooling cycles prior to CTE testing and reducing the rate of temperature change improved the consistency of the CTE test results.

Concrete CTE can be reduced by blending low-CTE aggregates with high-CTE aggregates and reducing the cement paste volume. Based on these findings, a concrete CTE optimization technique was developed that provides guidelines for the selection of concrete constituents to achieve target concrete CTE. A concrete proportioning technique was also developed to meet the need for CTE optimization. This concrete proportioning technique can use aggregate from any sources, irrespective of gradation, shape, and texture. The proposed technique has the potential to reduce the cement requirement without sacrificing performance and provides guidelines for multiple coarse and fine aggregate blends.

Table of Contents

List of Tables

List of Figures

Chapter 1: Introduction

1.1 INTRODUCTION

Materials, when subjected to temperature change, typically change dimensions (length, area, and volume). Generally, materials expand when temperature increases and contract when temperature decreases. This fundamental property of materials is termed the coefficient of thermal expansion (CTE). The CTE is an important concrete property, as it is one of the properties responsible for distresses in concrete structures. The CTE of concrete is generally measured as the linear CTE and can be defined as the strain that develops in response to unit changes in temperature. When concrete members are subjected to temperature change, they deform, creating tensile and compressive stresses if the members are restrained. Concrete is stronger in compression; thus, any compressive stress created by temperature change is less likely to cause cracking. In contrast, concrete is weaker in tension, so any tensile stress created by temperature change could potentially exceed concrete's tensile strength and causes cracking. Early-age concrete has lower strength and higher CTE than does hardened concrete (Kada et al. 2002). Therefore, early-age concrete is more prone to cracking due to temperature changes.

1.2 MOTIVATION

The CTE of concrete is an important design parameter in the concrete pavement designs provided by the *Mechanistic-Empirical Pavement Design Guide* (MEPDG) (NCHRP and ARA 2004). A number of studies have shown that small deviations of input

concrete CTE from the MEPDG-prescribed value significantly affected the concrete pavement thickness (Kannekanti and Harvey 2006; Chung and Shin 2011; Kim and Won 2004; Choi et al. 2011; Jahangirnejad et al. 2009; Mallela et al. 2005; Tanesi et al. 2006, 2007). Moreover, continuously reinforced concrete pavements (CRCPs) showed higher distresses when high-CTE concrete was used (Choi et al. 2011; Kim and Won 2004). CRCP is a popular pavement choice across the U.S. and around the world for its minimal maintenance requirements and longer service life. Thirty-five states, including Texas, have CRCP pavements. To prevent CRCP distresses, the Texas Department of Transportation (TxDOT) imposed a statewide limit on the CTE of CRCP concrete: a maximum of 5.5 $x10^{-6}$ strain/^{o}F (9.9 $x10^{-6}$ strain/^{o}C). Furthermore, TxDOT's Houston District has a lower CTE limit for CRCP concrete of 5.0 $x10^{-6}$ strain/^{o}F (9.0 $x10^{-6}$ strain/^{o}C). As a result, coarse aggregate sources, which produce concrete with CTE values higher than the allowable limit, are no longer accepted in TxDOT CRCP projects. Therefore, it is important to precisely measure the CTE of concrete to achieve accurate design thickness of concrete pavements based on the MEPDG and to better screen the unacceptable high-CTE coarse aggregates for TxDOT CRCP projects.

The CTE of concrete is affected by the moisture content. Therefore, concrete CTE is determined using saturated concrete samples in an attempt to minimize the effect of variable moisture content on the measured CTE. The two most popular CTE testing procedures in the U.S. are proposed by the American Association of State Highway and Transportation Officials (AASHTO) (AASHTO T 336-11 2011) and TxDOT (Tex-428-A 2011). Other countries around the world have either adopted one of these methods or use a method that is very similar to one of these methods. In the U.S., all the state agencies

except TxDOT use the AASHTO T 336 method; only TxDOT uses Tex-428-A to determine the concrete CTE. Both of these methods are modified versions of the provisional CTE test procedure, AASHTO TP 60 (2000), which is often criticized for poor accuracy and repeatability. To improve the accuracy, Won (2005) proposed the Tex-428-A method in 2005 and AASHTO proposed AASHTO T 336 in 2011. However, both these methods still need improved consistency and repeatability. The reasons for the inconsistency in measured CTE can likely be explained by the porous structure of concrete. The focus of this research project is not to criticize the test methods, but to reveal the reasons for the inconsistency of the CTE measured in saturated concrete samples, as that inconsistency may be associated with the properties of the concrete. Inconsistencies of the CTE results are typically determined by the differences in the CTE of replicate concrete cylinders and the variation between the apparent CTE calculated from the displacement readings during heating and cooling for the same sample. Therefore, to improve the consistency of the CTE test methods, it is important to identify the reasons for inconsistency of the measured CTE.

High-CTE concrete is more likely to produce higher stress for a given temperature change than is a relatively lower CTE concrete. As described previously, stress development due to temperature change is responsible for distresses in concrete structures. Thermal stresses can be reduced by reducing the CTE of concrete, thus reducing the cracking potential of concrete due to temperature change. The CTE of concrete depends on the CTE of the concrete's constituents. Concrete CTE can be reduced by using low-CTE aggregates and/or reducing the volume of cement paste, which is considered to be uneconomical (Mallela et al. 2005). However, significant savings can be achieved in terms

of reduced repair and rehabilitation cost by optimizing the CTE of concrete according to the need of the structural application. Moreover, concrete CTE reduction will improve the durability and longevity of concrete structures.

1.3 RESEARCH OBJECTIVES

The goals of this research project were to improve the consistency of the CTE testing procedures and to develop a concrete CTE optimization technique that has the potential to reduce the cracking of concrete structures. The primary objectives of this research project were the following:

- Compare the effects of length-change measuring devices and the calculation techniques on the measured CTE.
- Develop an analytical model to better understand the effect of calculation techniques and determine the factors that are responsible for inconsistent CTE results.
- Evaluate techniques to improve the consistency of the CTE test methods.
- Develop a rational, sustainable concrete mixture design that allows multiple aggregate blends and rationally reduces cement paste volume, and that has the potential to optimize the CTE of concrete.
- Develop a model based on the rule of mixture to optimize the CTE of concrete.

1.4 CONTENT

This dissertation is divided into nine chapters. Chapter 2 summarizes the literature search, which includes a brief description of the importance of concrete CTE in the

durability and longevity of concrete pavements and structures, the factors that affect concrete CTE, and the CTE testing procedures.

Chapter 3 includes the measured physical properties of the coarse aggregates that were used throughout the research project.

Chapter 4 summarizes the effect of length-change measuring devices and the calculation techniques (TxDOT and AASHTO) on the measured CTE. The effect of calculation techniques is also explained using the internal water pressure development in saturated concrete subjected temperature change.

Chapter 5 presents an analytical model to explain the effect of internal water pressure on the CTE of concrete. A sensitivity analysis was also performed to determine the effects of various factors—such as porosity, permeability, rate of temperature change, and specimen dimension—on the axial strain and internal water pressure development in concrete cylinders subjected to temperature change.

Chapter 6 discusses the various techniques that might be helpful to improve the consistency of the CTE test procedures.

Chapter 7 proposes a rational concrete mixture design technique, one that can produce more economical and sustainable concrete and can use aggregates from any source, irrespective of gradation, shape and texture. It also provides rational guidelines for cement paste reduction and allows multiple aggregate blending. Cement paste volume reduction and aggregate blending are important in developing a CTE optimization technique.

Chapter 8 proposes a concrete CTE optimization model based on the rule of mixture.

Chapter 9 summarizes key findings and conclusions from the dissertation and provides a list of recommendation for future research.

Chapter 2: Literature Review

2.1 INTRODUCTION

The coefficient of thermal expansion (CTE) is a material characteristic that represents the change in strain due to unit temperature change. It is an important fundamental property of concrete and a key design parameter for concrete pavements and structures. The CTE of concrete is one of the important factors responsible for distresses in concrete infrastructures (Darwin et al. 2010; Huang 2003; Kim and Won 2004; Mallela et al. 2005). This chapter will review literature that pertains to the importance of CTE in terms of the durability of concrete pavement and structures, various factors that affect concrete CTE, and different concrete CTE measuring methods.

2.2 IMPORTANCE OF THE COEFFICIENT OF THERMAL EXPANSION ON THE DURABILITY OF CONCRETE PAVEMENTS AND STRUCTURES

Concrete pavements and structures experience thermal movements (expansion and contraction) when subjected to temperature change. These thermal movements can result in stresses in restrained concrete. The magnitude of the thermal stresses depends on the amount of temperature change, material properties, and degree of restraint. If the developed stresses are higher than the tensile strength of the concrete, cracks occur. Typically, these thermal cracks occur at an early age, when the concrete strength is low, but can occur at a later age if greater temperature changes occur. Early-age cracking can have significant detrimental effects on the service life of concrete structures (Schindler and McCullough 2002). A number of studies presented the effect of temperature on the deterioration of

concrete pavements and structures (Bentz et al. 2011; Branco and Mendes 1993; Ceylan et al. 2008; Choi et al. 2011; Chung and Shin 2011; Garboczi 1997; Hale et al. 2012; Iskander et al. 2012; Jahangirnejad et al. 2009; Kim and Won 2004; Krauss and Rogalla 1996; Mallela et al. 2005; Moorty 1990; Ndon and Bergeson 1995; Sandepudi 1991; Schindler and McCullough 2002; Tanesi et al. 2012; Tindal and Yoo 2003). Krauss and Rogalla (1996) studied the early-age cracking of bridge decks in the U.S. and observed that over 10,000 bridge decks exhibited early-age cracking. One of the major causes of this early-age cracking was thermal stress (Sakyi-Bekoe 2008). Thermal stresses are also major causes of concrete pavement distresses (Mallela et al. 2005).

Figure 2.1 shows a graphical representation of early-age thermal stress development in concrete for a typical summer placement. Concrete temperature increases with time, due to the heat of hydration, and continue to increase beyond the final setting, as shown by line A. Concrete expands as the temperature of the concrete increases and reaches peak temperature, as shown by line B. As concrete expansion is typically restrained, concrete will be in compression at peak temperature. At this early age, permanent relaxation can occur due to the presence of compressive stresses during the low strength phase. After peaking, the temperature starts to decrease and concrete begins to contract and reach a zero stress state, as shown by line C. If the temperature further decreases, the concrete continues to contract and experiences tensile stress. When this tensile stress is equal to the tensile strength, cracking occurs, as shown by line D. These early-age cracks are a significant cause of premature deterioration in concrete pavements and structures.

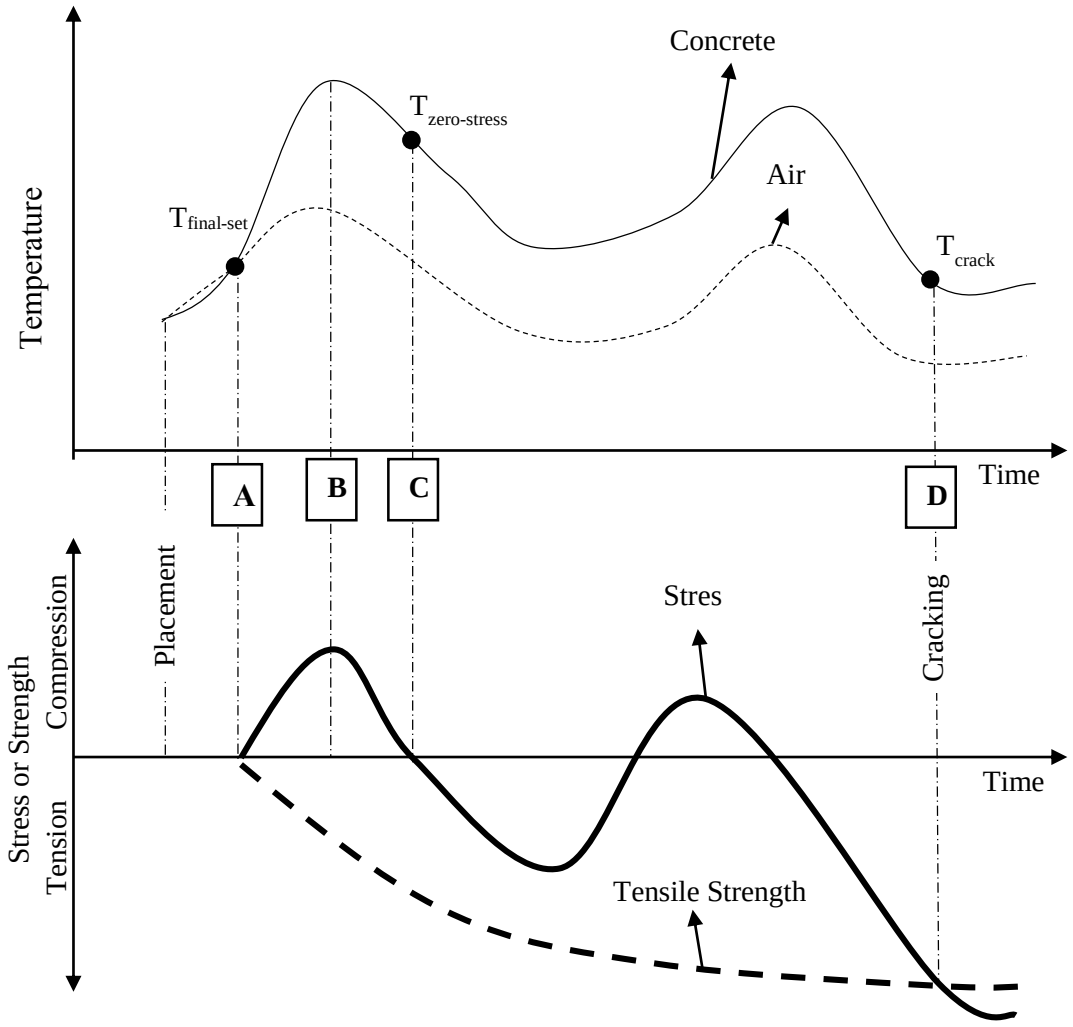

Figure 2.1 A graphical representation of thermal stress development in fresh concrete (reproduced from Schindler and McCullough 2002)

2.2.1 Concrete pavements

Concrete's CTE is a significant factor in concrete pavement performance. CTE is considered to be a major cause of pavement distresses, including cracking, faulting, punchouts, and delamination (Choi et al. 2011; Kim and Won 2004). State agencies, such as the Texas Department of Transportation (TxDOT), recognize the thermal

incompatibility between mortar and aggregates as one of the major causes of distresses in continuously reinforced concrete pavement (CRCP). Some TxDOT districts have limited the CTE of CRCP concrete for years to minimize pavement distresses. Spalling has significantly diminished after limiting the CTE of CRCP concrete in the Houston district (Naranjo 2013). Very recently, TxDOT imposed a statewide maximum qualifying limit on the CTE of CRCP concrete of 5.5 $x10^{-6}$ strain/^{o}F (9.9 $x10^{-6}$ strain/^{o}C). Moreover, some districts, such as Houston, enforce an even lower CTE maximum value of 5.0 $x10^{-6}$ strain/^{o}F (9.0 $x10^{-6}$ strain/^{o}C) for concrete used in CRCP.

Won and his colleagues (Choi et al. 2011; Kim and Won 2004) investigated the horizontal cracking of CRCP pavements. They identified CTE as one of the major factors that is responsible for this distress. Kim and Won (2004) performed numerical analyses to determine the effect of concrete CTE on the shear and normal stress development in CRCP. Two CTEs for concrete were considered: 4.0 and 8.0 $x10^{-6}$ strain/^{o}F (7.2 and 14.4 $x10^{-6}$ strain/^{o}C). They observed that for both one-mat and two-mat steel, higher CTE generates higher stresses at the reinforcement level, which contributes to horizontal cracking in CRCP pavements.

Choi et al. (2011) conducted laboratory and field investigations to identify the cause of horizontal cracking. As a part of the laboratory investigation, a horizontal concrete cracking frame was used to determine the effect of thermal loading on cracking in CRCP. After the concrete was placed, the temperature was maintained at 39^{o}C (102.2^{o}F) for 74 hours from mixing to give the concrete sufficient time to gain strength. Then the temperature was gradually reduced to 21.1^{o}C (70^{o}F). As the temperature decreased, the concrete contracted and developed tensile stress. The temperature-induced tensile stress at

the age of about 82 hours and about 27°C (80°F) was greater than the concrete tensile strength, so the concrete cracked. It can be concluded from their study that higher CTE generates higher vertical stresses and has the potential to cause horizontal cracking.

It is evident from the prior discussion that CTE plays a major role in the deterioration of concrete pavements. Although CTE was used in the American Association of State Highway and Transportation Officials (AASHTO) design guide to calculate the transverse joint width and sealant reservoir dimension, it has only recently been used as a parameter to design pavement thickness. In 2004, the *Mechanistic-Empirical Pavement Design Guide* (MEPDG) designated CTE as an important design parameter for concrete pavements. Some studies showed that a small deviation from the prescribed CTE can cause a significant change in the required pavement thickness (Kannekanti and Harvey 2006; Chung and Shin 2011; Kim and Won 2004; Choi et al. 2011; Jahangirnejad et al. 2009; Mallela et al. 2005; Tanesi et al. 2006, 2007). The MEPDG has three levels of CTE input: (1) level one input obtains the CTE from the actual test results, which is the most desirable as it imparts higher accuracy, (2) level two input uses the CTE calculated from individual concrete components, using an empirical formula, and (3) level three input recommends a design CTE from the agency database, user-selected values, typical average CTE for the design area, or default values based on the types of coarse aggregates used (Hossain et al. 2006).

Mallela et al. (2005) and Tanesi at al. (2007) extensively investigated the effect of CTE on concrete pavements designed by the MEPDG. Their research focused on three key distresses commonly found in jointed plain concrete pavements (JPCP): slab cracking, joint faulting, and ride quality, as measured by the International Roughness Index (IRI). Chert

had the highest cracking potential, followed by sandstone, quartz, dolomite, and granite (Mallela et al. 2005). Tanesi at al. (2007) observed that CTE has an exponential relationship with the percentage of JPCP slabs that cracked. At a CTE of 4.5 $x10^{-6}$ strain/^{o}F (8.1 $x10^{-6}$ strain/^{o}C), the percentage of slab cracked was negligible, but cracked slabs increased to about 50% at a CTE of 7.5 $x10^{-6}$ strain/^{o}F (13.5 $x10^{-6}$ strain/^{o}C). It is also observed that an increase in CTE beyond 6.0 $x10^{-6}$ strain/^{o}F (10.8 $x10^{-6}$ strain/^{o}C) significantly increased the percentage of cracked slabs. Pavement faulting is defined as the difference in elevation across a joint or a crack. Faulting in joints is one of the major types of concrete pavement distress. Change in faulting over time is an indication of JPCP pavement performance. According to Mallela et al. (2005) and Tanesi at al. (2007), an increase in CTE significantly increases the joint faulting potential.

Smoothness of ride is another important parameter used to rate pavements. Ride comfort is dependent on the pavement smoothness, which is a function of road roughness, the vehicle's response to the road, and human response to the resulting vibration (bumpiness). The IRI value indicates the pavement smoothness on a scale, based on the simulated response of a motor vehicle to the roughness experienced during a single wheel pass of the road surface. The MEPDG considers the effect of transverse cracking, transverse joint spalling, patching, and corner breaks to predict the IRI of JPCP (Tanesi et al. 2007). There is no direct effect of CTE on IRI. However, cracking and faulting resulting from thermal loading affect IRI. Therefore, high-CTE aggregates relate to poor IRI (Mallela et al. 2005) and small increases in CTE beyond 5.5 $x10^{-6}$ strain/^{o}F (9.9 $x10^{-6}$ strain/^{o}C) significantly exacerbate pavement roughness (Tanesi et al. 2007).

It is evident from the previous discussions that CTE is an important concrete property in concrete pavement design and one of the important parameters responsible for concrete pavement deterioration.

2.2.2 Bridge decks

Bridges are the most expensive component of the transportation infrastructure. Concrete bridges experience thermal loading from daily temperature cycles, heat of hydration during construction, and placement of asphalt concrete on the deck. Temperature change influences the girder axial force, girder moment, pile lateral force, pile moment, and pile head/abutment displacement (Kim and Laman 2010). Thermal stresses are also responsible for joint and bearing distress (Moorty and Roeder 1990). During the construction period, thermal movement occurs due to the daily temperature change. These displacements should be analyzed by the contractor, since they are important for the design of the falsework, control of the structural behavior, and the bridge survey (Branco and Mendes 1993). Due to thermal movement of the bridge deck and the associated redistribution of reaction, the falsework of a viaduct in New Zealand collapsed (Imbsen et al. 1985). The Elbow River bridge in Canada collapsed due to poor design of the supports and excessive thermal displacements of the bridge deck (Paul 1981). Therefore, thermal expansion is shown to play a major role in the durability and safety of concrete bridge construction and operation. This is particularly true in modern long-span prestressed concrete bridges with limited numbers of expansion joints and bearings (Pritchard 2003).

In a typical bridge deck, approximately the top half of the deck is influenced primarily by solar radiation; the temperature of the bottom one-third of the deck depends

on the immediate shade temperature and the amount of heat reflected or re-radiated from the ground beneath the bridge; and the temperature of the rest of the deck is the result of radiation and shade temperature levels of the previous two days (Emerson 1981).

Im and Chang (2000) conducted a comprehensive study of temperature effect on the composite box girder bridge. Daily temperature change creates significant stresses in the composite box girder. According to their study, daily temperature change can generate significant stress in box girders. Maximum compressive and tensile stresses of about 6527 psi (45 MPa) and 1450 psi (10 MPa), respectively, were observed in the studied box girder due to daily temperature change.

The durability and safe operation of the bridge depends to a great extent on the thermal stress and movement developed in the bridge deck. The CTE of concrete is an important parameter for bridge design and construction as well as a major factor influencing thermal stresses and movements.

2.2.3 Mass concrete

According to the American Concrete Institute's (ACI) *Manual of Concrete Practice* (ACI 2013), mass concrete is defined as "any volume of concrete with dimensions large enough to require that measures be taken to cope with the generation of heat from hydration of the cement and attendant volume change to minimize cracking." It is evident from the ACI definition of mass concrete that thermal distress is an important factor to be considered when designing for mass concrete. Typically, a great deal of heat is generated at the core of the mass concrete due the heat of hydration of cementitious materials. Several factors affect heat generation, including the thermal conductivity of concrete, the heat of hydration

of cementitious materials, the specific heat of concrete components, and ambient temperature. Concrete is not a good conductor of heat. Therefore, heat generated from the hydration reaction cannot dissipate quickly, resulting in a high temperature at the core of the concrete mass. This high temperature causes the expansion of volume of the concrete core, which can cause undesirable distresses. Higher concrete CTE leads to a higher volume change and results in higher cracking potential.

Bentz et al. (2011) identified CTE as one of the important design parameters to alleviate thermal distresses. Their study (Bentz et al. 2011) presented a real-world mass concrete thermal distress problem. In fall 2006, the foundation of Tower One at the World Trade Center in New York City was under construction. Two different concrete proportioning mixtures were used. The cementitious material (i.e., cement + supplementary cementitious materials) contents of the two concrete mixtures were 1250 and 1040 lb/yd^3 (742 and 617 kg/m^3), and the portland cement contents were 700 and 520 lb/yd^3 (415 and 309 kg/m^3). This resulted in concrete with compressive strengths of 12000 and 8500 psi (83 and 59 MPa), respectively. Both concrete foundations showed severe cracking within the first 48 hours. Internal temperature for the 8500-psi (59 MPa) concrete was monitored and found to have reached about 170^{o}F (77^{o}C) at 24 hours and remained above 160^{o}F (71^{o}C) for more than a week. Later concrete cores were taken and tested for compressive strength. The measured strength was satisfactory. Thermal expansion seems to be the cause of the cracking.

Recent efforts to mitigate the thermal cracking in mass concrete have focused on reducing the heat of hydration of cementitious materials. Thermal stress in mass concrete

can be significantly reduced using concrete with a lower CTE. However, optimizing CTE for mass concrete is often neglected for economic reasons.

2.3 FACTORS AFFECTING THE COEFFICIENT OF THERMAL EXPANSION OF CONCRETE

Concrete CTE is affected by several factors. Aggregates typically occupy about 70 to 80% of concrete's volume. Therefore, the mineralogy and volume fraction of aggregates greatly influence the CTE of concrete (Emanuel and Hulsey 1977; Mallela et al. 2005; Sakyi-Bekoe 2008; Siddiqui and Fowler 2013b, 2014; Won 2005). Moisture content as well as types and amount of cement also have significant effect on the CTE of concrete (Bjøntegaard and Sellevold 2001; Emanuel and Hulsey 1977; Sakyi-Bekoe 2008; Scherer 2000a; b; Sellevold and Bjøntegaard 2006). Concrete age, water-to-cement ratio (w/c), and cylinder size also minimally affect the concrete CTE (Alungbe et al. 1992; Kohler et al. 2007). Various effects on the CTE of concrete are discussed in the following sections.

2.3.1 Effect of aggregates

Aggregate plays an important role in the CTE of concrete. Two aggregate factors in particular—mineralogy and used volume fraction—affect concrete CTE. Dettling (1964) studied the CTE of different types of aggregate, as shown in Table 2.1. Quartzite has the highest CTE and limestone has the lowest. Concrete CTE is directly related to the CTE of the aggregate used (Mehta and Monteiro 2006). From the findings of Mehta and Monteiro (2006), it can be observed that concrete made with limestone has the lowest CTE and concrete made with quartzite has the highest. Therefore, high-CTE aggregates produce high-CTE concrete.

Table 2.1 Average coefficient of thermal expansion of different types of aggregate (reproduced from Dettling 1964)

Aggregate mineralogy	CTE in $x10^{-6}$ strain/^{o}F ($x10^{-6}$ strain/^{o}C)
Quartzite, silica shale, chert	6.1–6.9 (11.0–12.4)
Sandstone	5.8–6.7 (10.4–12.1)
Quartz, sands, pebbles	5.6–6.9 (10.1–12.4)
Clay, mica shales	5.3–6.1 (9.5–11.0)
Granites, gneisses	3.6–4.7 (6.5–8.5)
Syenites, feldspathic porphyry diorites, andesite, phonolite gabbros, diabase, basalt	3.1–4.4 (5.6–7.9)
Dense, crystalline, porous limestone	1.9–3.3 (3.4–5.9)
Pure calcite	2.2–3.6 (4.0–6.5)
Marbles	2.2–3.9 (4.0–7.0)
Dolomites, magnesites	3.9–5.6 (7.0–10.1)

Won (2005) studied the CTE from 32 aggregate sources in Texas. Among the 32 sources, 21 were gravel and 11 were limestone aggregates. The variation of CTE among limestone concrete was about 0.72 $x10^{-6}$ strain/^{o}C (1.3 $x10^{-6}$ strain/^{o}F) and among gravel concrete was about 4.86 $x10^{-6}$ strain/^{o}C (8.7 $x10^{-6}$ strain/^{o}F). Concrete with the same type of aggregate sources showed different CTEs, which indicates the impact of an aggregate's mineralogical composition on concrete's CTE.

Won (2005) also studied the effect of aggregate volume on the CTE of concrete. According to his findings, concrete CTE decreases with the increased volume of coarse aggregate. An increase in aggregate volume reduces the volume of the cement paste. Since the CTE of cement paste is typically the highest among the concrete constituents (the CTE of some river gravel can be higher than that of cement paste), reducing the volume of cement also reduces the CTE. Further discussion of the effect of mineralogical composition and aggregate volume on the CTE of concrete is presented in the next two sections.

2.3.1.1 Aggregate mineralogical composition

The CTE of siliceous aggregates is higher than that of carbonate aggregates (Alungbe et al. 1992; Ziegeldorf et al. 1978). Mindess et al. (2002) observed that the CTE of an aggregate depends on its silica content. Aggregates with higher silica content, such as river gravel or quartz, have higher CTEs; lower silica content aggregates, such as limestone, have lower CTEs. McCullough et al. (2000) studied the effect of mineralogical composition on the CTE of aggregate. Figure 2.2 and Figure 2.3 show the effect of silicon dioxide and calcium oxide on the CTE of aggregates, respectively. The CTE increases significantly with the increase of silicon dioxide content. On the other hand, CTE decreases significantly with the increase of calcium oxide content up to 20%, followed by a moderate decrease up to 60%; above 60%, calcium oxide content has little impact on the CTE.

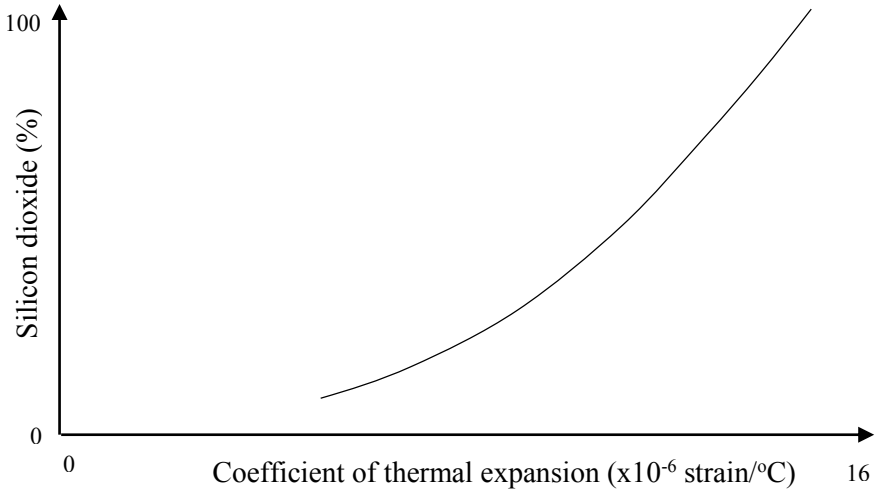

Figure 2.2 Effect of silicon dioxide content on the CTE of aggregate (reproduced from McCullough et al. 2000)

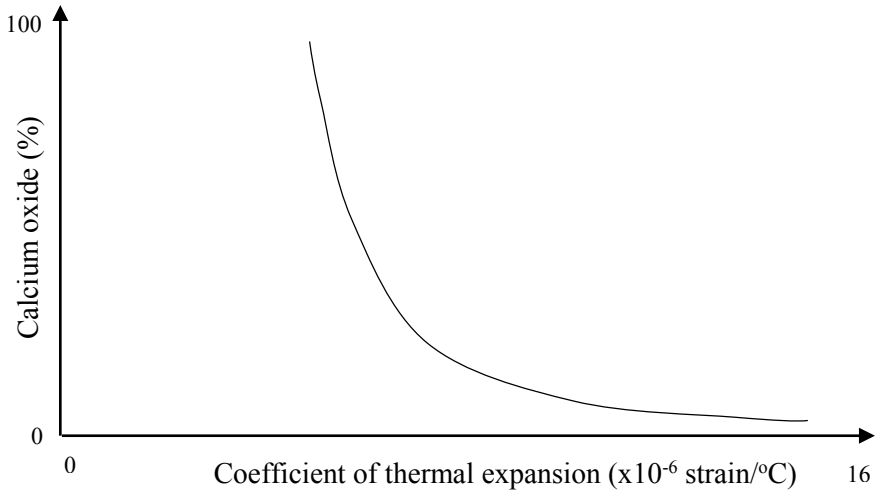

Figure 2.3 Effect of calcium oxide content on the CTE of aggregate (reproduced from McCullough et al. 2000)

2.3.1.2 Aggregate volume

Aggregate occupies the largest volume in concrete. An increase in the aggregate volume can increase or decrease the CTE of concrete, depending on the mineralogy of the aggregates.

Figure 2.4 shows the effect of aggregate volume and mineralogy on the CTE of mortar and concrete. From Figure 2.4 (a) it can be seen that an increase of siliceous sand volume increases the CTE of mortar. Conversely, an increase of limestone sand volume decreases the CTE of mortar. Similarly, it is observed from Figure 2.4 (b) that the CTE of concrete decreases with the increase of both siliceous sand/crushed limestone and limestone sand/crushed limestone. The rate of decrease in CTE for concrete with siliceous sand/crushed limestone is much higher than for the limestone sand/crushed limestone aggregate combination concrete. On the other hand, the limestone sand/ quartz gravel aggregate combination CTE increases with an increase in the volume of aggregate. For

siliceous sand/quartz gravel aggregate, the CTE remains almost unchanged with any increase in aggregate volume.

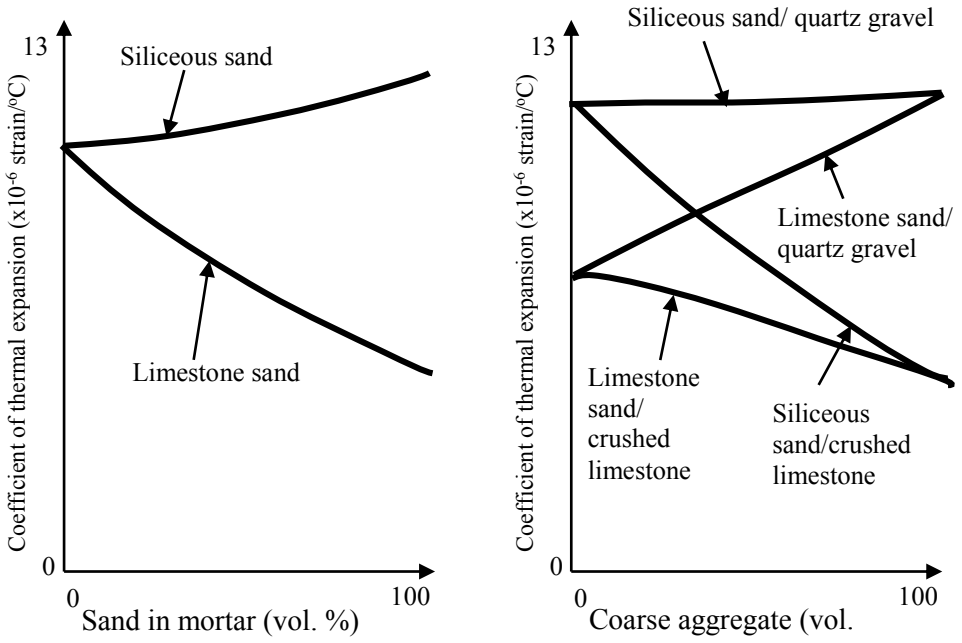

(a) Mortar (b) Concrete

Figure 2.4 Effect of aggregate volume and mineralogy on the CTE of concrete (reproduced from Mindess et al. 2002)

Neville and Brooks (1987) represented the effects of volume of aggregate and aggregate CTE on the CTE of concrete using the mathematical model developed by Hobbs (1971). According to their findings, concrete CTE decreases with increased aggregate volume, except for quartz coarse aggregate. CTE also decreased with the decrease of aggregate CTE for a given aggregate volume.

2.3.2 Effect of moisture content and relative humidity

Moisture content and relative humidity too play an important role in the CTE of cement paste and concrete (Chung and Shin 2011; Emanuel and Hulsey 1977; Mindess et al. 2002; Neville and Brooks 1987; Yeon et al. 2009). Emanuel and Hulsey (1977) documented the effect of moisture content on the CTE of cement paste. According to them, the CTE of dry cement paste is higher than that of saturated cement paste. Peak CTE occurs at about 60 to 70% moisture content, which is about twice that of the CTE for fully saturated paste and 60% higher than for completely dry paste. Chung and Shin (2011) studied the expansion and contraction of concrete due to the CTE and the related response to relative humidity change. Their findings showed that the peak CTEs for expansion and contraction were obtained at about 65 and 85% relative humidity, respectively. The expansion CTE for a concrete specimen at 100% relative humidity is about 7% lower than the peak expansion CTE, but the variation of the peak contraction CTE with respect to relative humidity is almost negligible.

Yeon et al. (2009) investigated the effect of relative humidity on the CTE of siliceous river gravel concrete and plain cement paste. Yeon et al. observed that the maximum CTE for concrete was obtained at 80% relative humidity. The CTE of 100% relative humidity concrete is slightly lower than the peak CTE but higher than CTE at relative humidity below 60%. A study was conducted on cement paste from 75 to 100% relative humidity and a similar effect was observed. However, these findings contradict the findings of Neville and Brooks (1987) and Mindess et al. (2002).

It is evident from the previous discussion that moisture content and relative humidity significantly affect the measured CTE of concrete. Therefore, while measuring

concrete CTE, comparable moisture content and relative humidity should be maintained for all samples.

2.3.3 Effect of age

There are contradictory findings observed in the literature regarding the dependency of CTE on the age of concrete age. Emanuel and Hulsey (1977) observed the influence of cement paste age on the measured CTE. The CTE of cement paste decreased with age. The effect of moisture content was also influenced by the paste age. For an age of 0 to 18 months, the peak CTE was observed at about 70% moisture content, which changes to 50% moisture content for 16-year old paste. Kada et al. (2002) studied the CTE of concrete during early hydration. At the initial state of hydration (before final setting), the CTE of concrete is much higher. The CTE reduced rapidly and then remained constant after the final setting time. Won (2005) studied the changes in concrete CTE for up to three weeks after mixing. It did not change significantly during the first three weeks. This supports the findings of Kada et al. (2002) but contradicts the findings of Emanuel and Hulsey (1977).

2.3.4 Effect of temperature

Wittmann and Lukas (1974) studied the CTE of concrete at different temperatures. They studied concrete sample at two relative humidities, 100% and 90%, and within the temperature range of 20 to -30^{o}C (68 to -22^{o}F). Concrete specimens at different ages from 5 to 55 days were tested. For samples with 100% relative humidity, the CTE remained the same from 20 to 10^{o}C (68 to 50^{o}F), followed by a sharp drop with a decrease in temperature

down to 0°C (32°F), and then a sharp rise with a temperature drop to -10°C (14°F). Below -10°C (14°F) the CTE remained unchanged. Steady state CTE after freezing was much higher than the steady state CTE before freezing. For samples at 90% relative humidity, the CTE remained steady from 20 to 10°C (68 to 50°F) and then gradually decreased with decreasing temperature.

2.3.5 Effect of water-to-cement ratio

Contradictory findings were observed regarding the effect of w/c ratio on the CTE of concrete. Berwanger and Sarkar (1976) studied reinforced concrete slab expansion and contraction for concrete with a w/c of 0.672 to 0.445. He concluded that CTE decreases with increased w/c. However, Alungbe et al. (1992) studied the CTE of concrete with a w/c of 0.53, 0.45, and 0.33. He did not observe any effect of w/c on the CTE of concrete, and thus is supported by the findings of Mindess et al. (2002).

2.3.6 Effect of concrete paste content and composition

The CTE of cement paste is higher than that of most aggregates. Therefore, concrete CTE increases with the increasing cement content (Bonnell and Harper 1950). A similar observation was made recently by Hossain at al. (2006). Bonnell and Harper (1950) also studied the effect of cement type on the CTE. The concrete was made with river gravel and river sand using identical proportions with different types of cement. The concrete samples were cured in air and water. The results are presented in Table 2.2. Air-cured concrete showed higher CTE than did wet-cured concrete. Portland blast-furnace cement had the highest CTE, followed by portland and high-alumina cement. Emanuel and Hulsey (1977)

also observed that the CTE increases with the increase of the fineness of cement. A summary of the factors affecting the concrete CTE based on the literature reviewed is presented in Table 2.3.

Table 2.2 Effect of cement type on the CTE of concrete (reproduced from Bonnell and Harper 1950)

Cement	CTE in $x10^{-6}$ strain/°F ($x10^{-6}$ strain/°C)	
	Air cured	Wet cured
Portland	7.3 (13.1)	6.8 (12.2)
High-alumina	7.5 (13.5)	5.9 (10.6)
Portland blast-furnace	7.9 (14.2)	6.9 (12.4)

Table 2.3 Summary of the effect of variables on the CTE of concrete (reproduced from Sakyi-Bekoe 2008)

Variables	Change	Effect on concrete CTE	Correlation
Coarse aggregate volume	Increase	Increase or decrease	Strong
Coarse aggregate type	Quartz: Increase	Increase	Strong
	CaO: Increase	Increase	Strong
Fine aggregate volume	Increase	Increase or decrease	Strong
Fine aggregate type	Siliceous: Increase	Increase	Strong
	CaO: Increase	Increase	Strong
Moisture content	Varies	Varies	Strong
Paste content	Increase	Increase	Strong
Water-to-cement ratio	Increase	Decrease	Moderate
Cement fineness	Increase	Increase	Moderate
Temperature	Varies		
Age	Increase	Varies	Inconclusive

2.4 COEFFICIENT OF THERMAL EXPANSION TESTING PROCEDURE

Various CTE test procedures are available. All U.S. state agencies (other than TxDOT) use AASHTO T 336 (2011) for CTE determination. TxDOT has their own CTE test method, Tex-428-A (2011). These two methods, the most popular in the U.S., are studied in this research program. This section will explain the AASHTO and TxDOT CTE methods and only briefly discuss other proposed CTE test methods.

2.4.1 Coefficient of Thermal Expansion of Hydraulic Cement Concrete: AASHTO T 336

The AASHTO T 336 is proposed and recommended by AASHTO for determining the CTE of hydraulic cement concrete cylinders. This method is a modified version of the previous AASHTO TP 60 (2000) method. AASHTO T 336 specifies that concrete specimens are to be tested in a saturated condition to prevent any influence of moisture content on the measured CTE. The concrete cylinders are submerged under limewater at 23 ± 2°C (73 ± 4°F) for at least 48 hours and until the weights in two successive measurements of the saturated surface-dry sample at a 24-hour interval show an increase of less than 0.5%. For CTE testing, 4-in. x 8-in. (100-mm x 200-mm) concrete cylinders are trimmed to 4-in. x 7-in. (100-mm x 175-mm) cylinders. This method specifies measurement for length change in a 4-in. x 7-in. (100-mm x 175-mm) concrete cylinder at two prescribed temperatures of 10 and 50°C (50 to 122°F) and calculates the CTE by dividing the total length change by the length of the sample and the temperature difference.

AASHTO T 336 also specifies that a rigid supporting frame should be used while measuring the length change of the concrete cylinders. The frame material should be non-

corroding and have a minimal CTE to minimize any effect on the measured length change of the concrete cylinder. The support for the test cylinder (where the cylinder rests) should be designed to facilitate the movement of the cylinders due to temperature change. The frame should be designed to be adjustable to accommodate different lengths of specimens. However, the frame must be calibrated every time after adjusting the length.

A correction factor must be determined to account for the length change of the frame. This correction factor is measured by measuring the CTE of a known sample. This procedure will be discussed in the next section. If the CTE of the calibration sample is CTE_c and the measured CTE is CTE_m, the correction factor, C_f, can be expressed as

$$C_f = CTE_c - CTE_m \quad (2.1)$$

2.4.1.1 Test procedure

The testing frame with the length-change measuring device is placed in the water bath. The water bath is then filled until the frame and the sample are completely submerged. The water bath should be sealed properly to prevent water loss and to maintain the same water level during calibration and CTE testing. The steps of the test process are as follows:

- Remove the concrete cylinder from the water and measure the length at room temperature to the nearest 0.004 in. (0.1 mm). Place the sample in the CTE frame so that the sample is sitting on the frame firmly and so that the tip of the length-change measuring device touches the mid-point of the top surface of the cylinder. Then the length-change measuring device is physically nulled at room temperature. AASHTO T 366 suggests using a linear variable differential transducer (LVDT) as the length-change measuring device. However, any length-change measuring

device with a resolution of 0.00001 in. (0.00025 mm) or better and a calibrated range suitable for the test is acceptable.

- Place the concrete sample and the cylinder in the water bath and set the temperature of the water bath to 10 ± 1°C (50 ± 2°F). After the water temperature reaches that target temperature, allow sufficient additional time for the sample to reach thermal equilibrium, which is indicated by consistent deformation readings taken every 10 minutes over a 30-minute period. The allowable difference between the three readings is 0.00001 in. (0.00025 mm) or less. If the obtained readings do not meet the requirement, continued readings should be obtained until four consecutive 10-minute interval readings are within the limit. Record the temperature to the nearest 0.1°C (0.2°F) and the length-change readings to the nearest 0.00001 in. (0.00025 mm).
- Change the temperature to 50 ± 1°C (122 ± 2°F), followed by another change to 10 ± 1°C (50 ± 2°F), and at each temperature follow the previous steps to obtain precise temperature and displacement readings.
- The CTE is calculated for both the heating and the cooling cycles, and the difference between the two CTE determinations should not be more than 0.3 $x10^{-6}$ strain/°C (0.2 $x10^{-6}$ strain/°F). If the criterion is not met, additional cycles of heating and cooling must be run until two successive test segments yield CTE values within 0.3 $x10^{-6}$ strain/°C (0.2 $x10^{-6}$ strain/°F) of each other. The average of the CTEs of heating and cooling cycles is the CTE of the sample.

- Two samples must be tested for CTE and the average of the two samples is the CTE of the concrete. The difference between the two values must be less than or equal to 0.5 x10^{-6} /^{o}F (0.3 x10^{-6} /^{o}C).

2.4.1.2 Calculation

Calculate the CTE of one expansion or contraction test segment of a concrete specimen as follows (reported in micro strains/°C):

$$CTE = \frac{\Delta L_a}{L_o * \Delta T}, \quad (2.2)$$

$$\Delta L_a = \Delta L_m + \Delta L_f. \quad (2.3)$$

Since the frame expands while the concrete specimen is expanding length change of the measuring apparatus during temperature change, ΔL_f becomes

$$\Delta L_f = C_f \text{ x } L_o \text{ x } \Delta T \quad (2.4)$$

where ΔL_a is the actual length change of the specimen during temperature change; L_o is measured length of the specimen at room temperature; ΔT is measured temperature change °C; ΔL_m is measured length change of the specimen during temperature change; C_f is correction factor accounting for the change in the length of the measurement apparatus.

2.4.2 Determining the Coefficient of Thermal Expansion of Concrete: Tex-428-A

Tex-428-A is a modified version of the provisional AASHTO TP 60 CTE test method. This method was proposed by Won (2005). Tex-428-A is very similar to AASHTO T 336, but there are some differences. This method uses heating and cooling cycles from 10 to 50^{o}C (50 to 122^{o}F) for CTE measurement. This method specifies that the heating and cooling rate should be adjusted in such a way that it takes at least 2 hours to

heat from 10 to 50ºC (50 to 122ºF), and similarly, at least 2 hours to cool from 50 to 10ºC (122 to 50ºF). The test setup, including the testing frame, water bath, length-change measuring devices, temperature measuring devices, and specimen dimensions, is the same as in the AASHTO T 336 method. The biggest difference in this method compared to the AASHTO method is the calculation technique.

Tex-428-A uses length-change readings from 15 to 45ºC (59 to 113ºF) for CTE determination. Length-change readings are taken as a function of temperature change. From the displacement vs. temperature plot, the slope of the best-fit straight line is determined. The CTE is calculated by dividing the obtained slope by the total length of the concrete specimen measured at room temperature. The correction factor is determined from a sample with a known CTE, using Eq. (2.1). A corrected CTE can be calculated from the following equation:

$$CTE = \frac{M}{L} + C_f \tag{2.5}$$

where M is the slope of the best-fit straight line; L is the measured length of the sample at room temperature.

The average CTE of the sample during heating and cooling is the CTE of the sample. The average CTE of two concrete cylinders is the CTE of the concrete. The maximum allowable difference between the CTE for heating and for cooling as well as two samples is 0.5 x10^{-6} strain/°C (0.3 x10^{-6} strain/°F).

This method also provides a specific proportioning for concrete, which consists of 23.45 lb. of cement, 11.49 lb. of water, 51.44 lb. of fine aggregate, and 85.2 lb. of coarse aggregate to batch 0.75 yd^3 of concrete. The TxDOT method also provides a specific

grading criterion for coarse aggregate, which is shown in Table 2.4. TxDOT is in the process of releasing a newer version of the CTE test method.

Table 2.4 Proposed gradation for coarse aggregate (reproduced from Tex-428-A 2011)

Sieve Size		Mass in pounds (kg)
Passing	**Retained**	
1”	3/4”	18.7 (8.48)
3/4”	1/2”	39.2 (17.78)
1/2”	#4	27.3 (12.38)

2.4.3 Vibrating wire extensometer method

This process was proposed by Kada et al. (2002) as suitable to monitor the CTE of concrete from its initial setting time. Concrete samples are cast in a PVC mold of 4 x 4 x 16-in. (100 x 100 x 400-mm), and a vibrating wire extensometer is installed at the center of the sample along the longitudinal axis. The vibrating wire extensometer is connected to a data acquisition system to monitor strain and temperature variation. The samples are demolded from the PVC mold at the onset of final setting. Two specimens are made from each concrete sample. After demolding, samples are wrapped in plastic bags to prevent moisture loss. Next, each sample is placed in a heat-controlled water bath at 50^{o}C (122^{o}F) and 10^{o}C (50^{o}F), respectively. When the samples reach temperature equilibrium, each sample is subjected to a temperature shock on the order of 40^{o}C (72^{o}F) and the strain developed in the concrete sample is measured by vibrating wire extensometer.

The material of the vibrating wire extensometer has a different CTE from the concrete. This contributes to an error in the measured strain and corrections must be made to the gross strain values to eliminate the strain caused by the differences in the thermal

expansion coefficients. The total deformation recorded can be expressed by the following equation:

$$\varepsilon_{total} = \varepsilon_{plastic} + \varepsilon_{drying} + \varepsilon_{carbonation} + \varepsilon_{thermal} + \varepsilon_{autogeneous} \quad (2.6)$$

where $\varepsilon_{plastic}$ is the shrinkage due to the evaporation of water from the fresh concrete when it is still at the plastic state; ε_{drying} is the shrinkage caused by the evaporation of water from capillary pores in the hardened concrete; $\varepsilon_{carbonation}$ is the shrinkage caused by the reaction of the hydrated cement paste with the carbon dioxide in the air when humidity is present; $\varepsilon_{thermal}$ is the thermal deformation linked to the expansion and contraction of the mass accompanying cement hydration (this deformation accounts for both the concrete and the vibrating wire sensor); $\varepsilon_{autogeneous}$ is the deformation caused by the reduction of available water for hydration because of the hydration process itself. If the duration of the thermal expansion coefficient measurement is less than one hour, the total deformation due to thermal shock can be represented as

$$\varepsilon_{total} = \varepsilon_{thermal} = \alpha_c \Delta T + \alpha_e \Delta T \quad (2.7)$$

where α_c and α_e are the CTE of the concrete and the vibrating wire extensometer respectively. Thus, the concrete CTE can be expressed as

$$\alpha_c = \frac{\varepsilon_{total} - \alpha_e \Delta T}{\Delta T} \quad (2.8)$$

2.4.4 Environmental extensometer method

This method was developed by Ndon and Bergeson (1995) to determine the CTE of concrete cores. An environmental chamber is used to heat and cool the concrete samples. The concrete is heated to 60^{o}C (140^{o}F) and cooled to -14^{o}C (7^{o}F) for CTE measurement.

Temperature and length change are measured at 10-minutes intervals. The CTE of the concrete can be determined from the following equation:

$$\alpha_c = \frac{\Delta L}{\Delta T \times L_i} \tag{2.9}$$

where ΔL is the change in length of the concrete specimen; L_i is the initial length of the concrete specimen.

The U.S. Army Corp of Engineers and the Bureau of Reclamation have their own CTE methods: CRD-C 39-81 and USBR 4910-92, respectively. Researchers have proposed other CTE test methods as well (Burnham and Koubaa 2001; Mukhopadhyay et al. 2007), including a test to measure the CTE of the aggregate alone to determine concrete CTE (Mukhopadhyay et al. 2003). However, none of these methods is widely used.

Chapter 3: Properties of Coarse Aggregates

3.1 INTRODUCTION

Coarse aggregate occupies typically about 40 to 50% of the volume of concrete. Consequently, the physical properties of concrete are significantly affected by the properties of coarse aggregates. As mentioned earlier, continuously reinforced concrete pavement (CRCP) is gaining worldwide popularity due to its low maintenance and longer service life. The Texas Department of Transportation (TxDOT) has about 16,400 lane miles of portland cement concrete pavement (PCCP). Approximately 75% of the concrete pavement in Texas is CRCP. As discussed in Chapter 2, significant distresses have been observed in CRCP when high-CTE coarse aggregates are used. Some TxDOT districts, such as Houston and Beaumont, do not have local, acceptable coarse aggregate sources that meet the CTE limit for CRCP aggregates. As a result, those districts have to haul aggregates over greater distances for CRCP construction projects. This increases both materials and overall project cost, and contributes to global CO_2 emission due to the associated fuel consumption. In addition to the CTE criterion, coarse aggregates considered for use in PCCP have to meet other physical and durability requirements. Therefore, it is important to determine all critical durability and physical properties of coarse aggregates for PCCP to evaluate the adequacy of specific aggregate sources for pavement use.

High-CTE coarse aggregates were selected from five TxDOT districts (Atlanta, Houston, Amarillo, Paris, and Wichita Falls), based on the volume of concrete pavement in each district and the scarcity of good quality local aggregate sources. This chapter

documents performance-critical physical properties of the selected coarse aggregates from each of the five districts.

3.2 OBJECTIVES

Good quality aggregates are rapidly depleting, because of the high volume of concrete use. In concrete structures, the use of incompatible aggregate usually causes premature deterioration. The objective of this chapter is to present the material selection process along with the measured durability and physical properties from laboratory testing for the selected aggregates.

3.3 MATERIALS

The district offices of Atlanta, Houston, Amarillo, Paris, and Wichita Falls were contacted and queried for aggregate source selections. Two sources of aggregates from each district were selected. Four sources were from Texas, four from Oklahoma, and the other two sources were from Arkansas. Four of the coarse aggregates were siliceous river gravel (RG), two were natural blends of siliceous and limestone gravel (RGLS), and one source consisted of granite (GR), rhyolite (RH), sand stone (SS), and slate (SL). Table 3.1 shows the aggregate sources suggested by the district personnel. The mineralogies of the aggregates were obtained from the TxDOT Concrete Rated Source Quality Catalog (CRSQC) data sheet. The RH, SS, and SL were not on the list and were identified by petrographic analysis performed by a TxDOT staff member. Particle size distribution of the coarse aggregates is presented in Figure 3.1. Existing gradation of coarse aggregate is not important for concrete mixture proportioning, because the concrete mixtures were

proportioned and the coarse aggregates were regraded according to Tex-428-A (2011) to produce comparable concrete mixtures for aggregates from different sources. However, the particle size distribution shown in Figure 3.1 helped to identify the missing aggregate sizes that are required for the Aggregate Image Measurement System (AIMS) to determine the angularity, shape, and texture of the aggregates. Further discussion on concrete mixture proportioning and AIMS will be found in the next section. An ASTM C150 (2012) Type I/II cement and a TxDOT-specified ASTM C33 (2013) river sand were also used for all laboratory concrete mixtures. Fineness modulus, specific gravity (SG), and absorption of fine aggregate were 2.73, 2.6, and 0.6%, respectively.

Table 3.1 List of coarse aggregates

Aggregate ID	TxDOT District
RG1	Houston
RG2	Houston
RG3	Atlanta
RG4	Atlanta
RGLS1	Amarillo
RGLS2	Amarillo
GR	Wichita Falls
RH	Wichita Falls
SS	Paris
SL	Paris

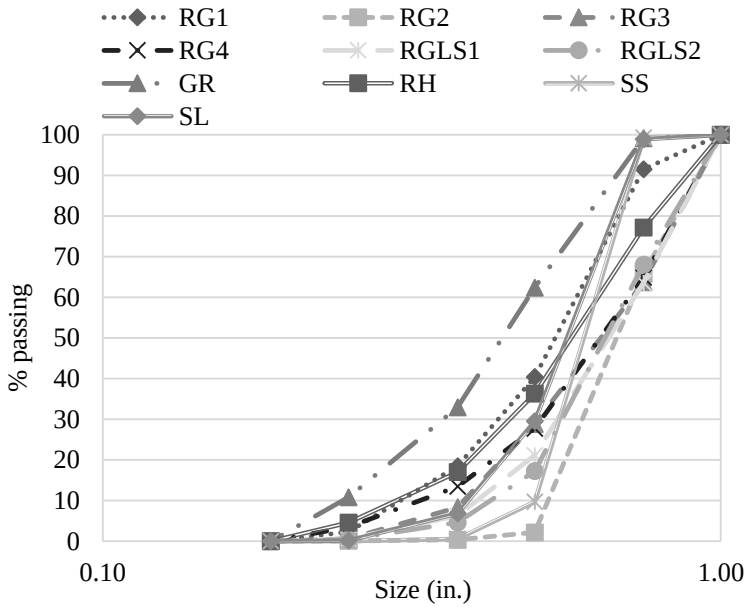

Figure 3.1 Particle size distribution of coarse aggregates

3.4 TEST PROCEDURES

Various laboratory tests were performed to determine the durability and physical properties of the specified coarse aggregates. The tests performed, along with the standards used (in parentheses), are shown below:

- SG and absorption (Tex-403-A (1999))
- Los Angeles (L.A.) abrasion (Tex-410-A (1999))
- Micro-Deval (Tex-461-A (2005))
- Sulfate soundness (Tex-411-A (2004))
- Aggregate angularity, texture, and shape as determined by AIMS
- Unconfined freeze-thaw (CSA A23.2-24A. (2004))
- Aggregate crushing value (ACV) (TxDOT provisional method Tex-1xx-E (Unpublished))

- Concrete compressive strength (Tex-418-A (2008))
- Concrete modulus of elasticity (ASTM C469 (2010))

Angularity, texture, and shape of aggregate were measured both before Micro-Deval (BMD) and after Micro-Deval (AMD) by AIMS. Aggregates retained on the 1/2-in., 3/8-in., 1/4–in., and #4 sieves were used in AIMS. The average angularity and texture values presented in this chapter are the average values for different particle sizes. Note that RG2 and SS did not have all the needed aggregate sizes and were crushed with a small laboratory crusher to get the missing particle sizes. It should be noted that the crushing process for both these aggregates might affect angularity, texture, and shape in the small portion of the lab-crushed makeup aggregates, which may also affect the overall angularity, texture, and shape of the aggregate. ACV was determined according to Tex-1xx-E, which is not yet a published standard TxDOT test procedure (unpublished). Concrete mixtures were proportioned according to the Tex-428-A (2011) suggested method. Table 3.2 presents proportioning for 0.75 ft^3 of concrete. Before mixing, coarse aggregates were regraded to meet the Tex-428-A (2011) gradation requirement, which was shown in Table 2.4. The 4-in. x 8-in. (100-mm x 200-mm) cylinders were made according to ASTM C192 (2012). The concrete was proportioned, and coarse aggregates were regraded according to Tex-428-A, because these concrete specimens were used to determine the CTE of concrete made from the aggregates. The CTE results will be presented in later chapters.

Table 3.2 Mixture proportioning for 0.75 ft^3 (0.02 m^3) concrete (Tex-428-A 2011)

Materials	Weight in lb (kg)
Cement	23.45 (10.63)
Water	11.49 (5.21)
Coarse aggregate	85.20 (38.64)
Fine aggregate	51.40 (23.31)

3.5 RESULTS AND DISCUSSION

Measured SG and absorption results for coarse aggregates are shown in Figure 3.2. The SG and absorption of the aggregates varied from 2.47 to 2.65 and 0.7 to 2.2%, respectively. RH had the highest SG of 2.65 and SS had the lowest of 2.47. Meanwhile, SS had the highest absorption (2.2%) and GR and RG2 had the lowest absorption (0.7%). Overall, SS had the lowest SG and highest absorption, potentially due to its porous structure.

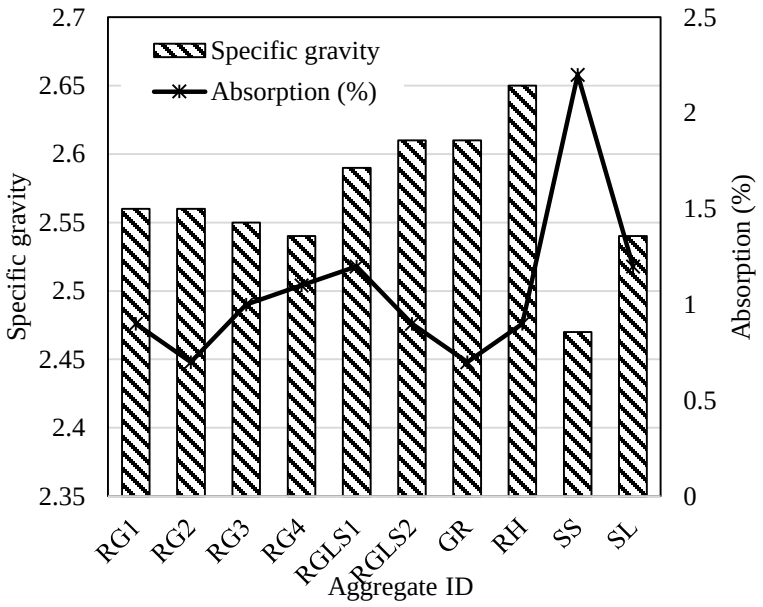

Figure 3.2 Specific gravity and absorption of aggregates

The L.A. abrasion test indicates an aggregate's toughness and abrasion resistance. This test was done according to Tex-410-A (1999) for grade B aggregate. Figure 3.3 shows the L.A. abrasion loss for the aggregates. RGLS2 showed the highest loss of 29% and RH showed the lowest loss of 11%. Both the RGLSs had higher L.A. abrasion loss than any other aggregate type, probably because of the presence of limestone, which is typically a softer aggregate. Item 421 of the TxDOT Standard Specifications for Construction and Maintenance of Highways, Streets, and Bridges (TxDOT 2004) limits the L.A. abrasion loss to a maximum of 40%, and all the specified aggregate sources satisfy this requirement.

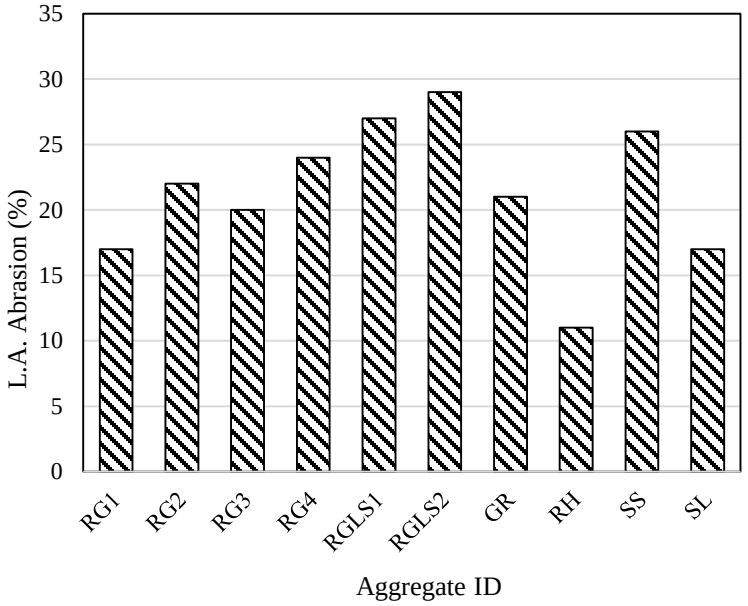

Figure 3.3 L.A. abrasion loss for aggregates

TxDOT's five-cycle magnesium sulfate soundness test was performed on all aggregate sources to determine the aggregate resistance to disintegration by weathering. Figure 3.4 illustrates magnesium sulfate soundness loss for selected aggregates. RGLS1

showed the highest loss of 12%, whereas RG2, GR, RH, and SL showed the lowest loss of 1%. According to Item 421 of the TxDOT Standard Specifications for Construction and Maintenance of Highways, Streets, and Bridges (TxDOT 2004), the allowable limit for five-cycle magnesium sulfate soundness loss is a maximum of 18%. All the aggregate sources met the soundness requirement and can be used in PCCP.

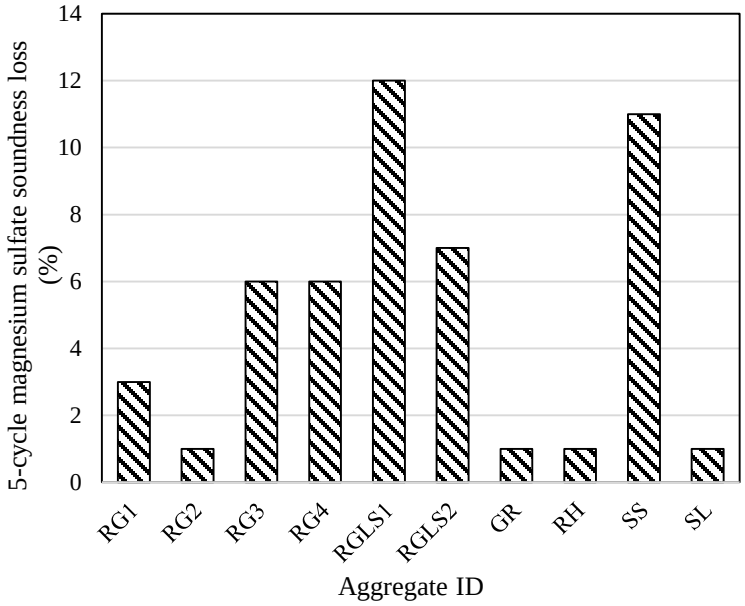

Figure 3.4 Sulfate soundness of aggregates

Figure 3.5 shows the Micro-Deval losses of selected aggregates. RGLS1 showed the highest Micro-Deval loss of 16%, and RG1 showed the lowest loss of 2%. In general, partly crushed siliceous and limestone gravel showed the maximum loss, probably due to the presence of softer limestone. SS also showed higher loss, probably due to the porous structure. Conversely, siliceous gravel and igneous rocks showed relatively lower Micro-Deval loss, potentially due to the greater hardness of these aggregates. Research done by

the Ministry of Transportation of Ontario (MTO) in Canada established that Micro-Deval is a very good indicator of field performance. The MTO adopted a Micro-Deval loss of up to 13% for concrete pavement. RGLS1 did not meet the MTO's Micro-Deval loss criterion. According to Rogers (1998), aggregate can perform well with up to a 17% Micro-Deval loss, a criterion satisfied by all the tested aggregate sources.

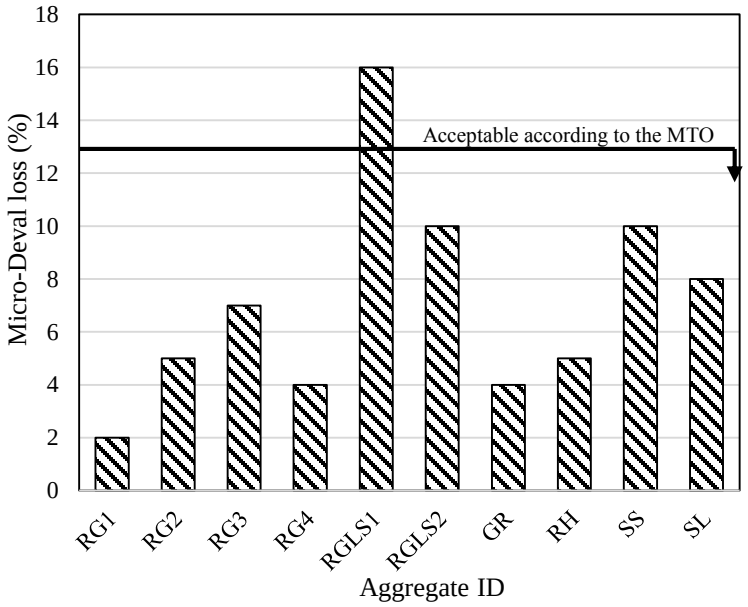

Figure 3.5 Micro-Deval loss for aggregates

Figure 3.6 shows average angularity before and after Micro-Deval. Aggregates can be divided into four groups based on their angularity: Low (≤ 2100), Moderate (2100–3975), High (3975–5400), and Extreme (5400–10000). RG2, GR, RH, and SL are in the moderate angularity range, both BMD and AMD. RG3 and SS were in the moderate range BMD and in the low range AMD. The rest of the aggregates are in the low angularity range both BMD and AMD. All the river gravels except RG2 are in the low angularity range.

The RG2 was crushed in the laboratory to produce more aggregates in the sizes that were missing in the specified grading. This might be the reason for this deviation.

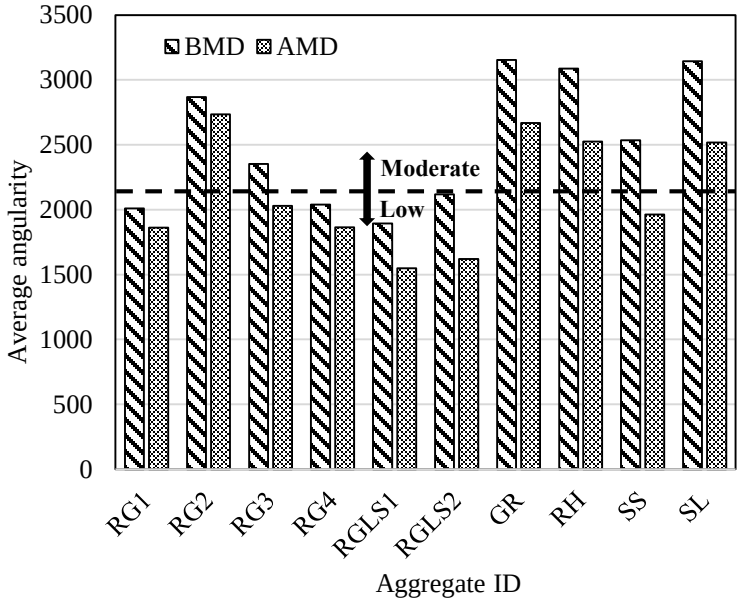

Figure 3.6 Average angularity before and after Micro-Deval

Figure 3.7 represents the percentage change in angularity BMD and AMD. Negative values represent reduction in angularity. RGLS2 showed the highest change of 23.5%, and RG2 showed the lowest of 4.3%. This change is consistent with the Micro-Deval loss, as shown in Figure 3.8. If the circled data point is considered to be an outlier, there is a good linear correlation between Micro-Deval loss and change in angularity before and after Micro-Deval. It can be noted from Figure 3.8 that change in angularity increased with the increasing Micro-Deval loss.

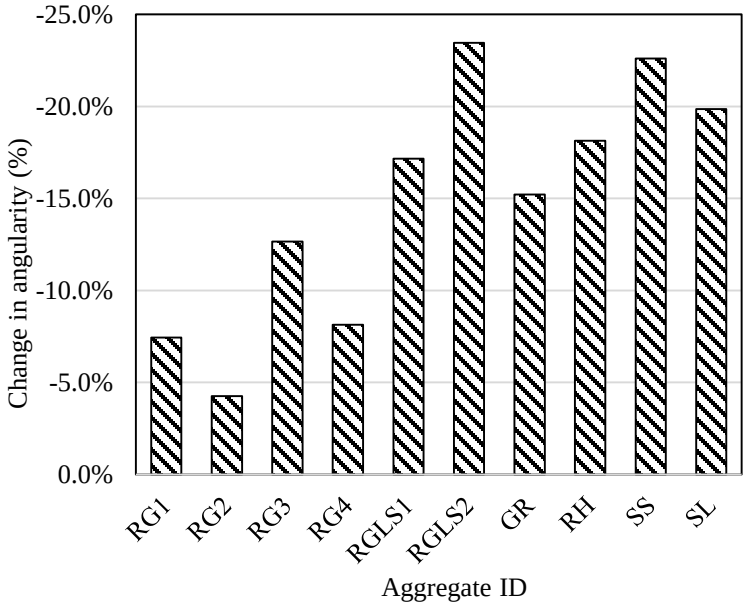

Figure 3.7 Percentage change in angularity before and after Micro-Deval

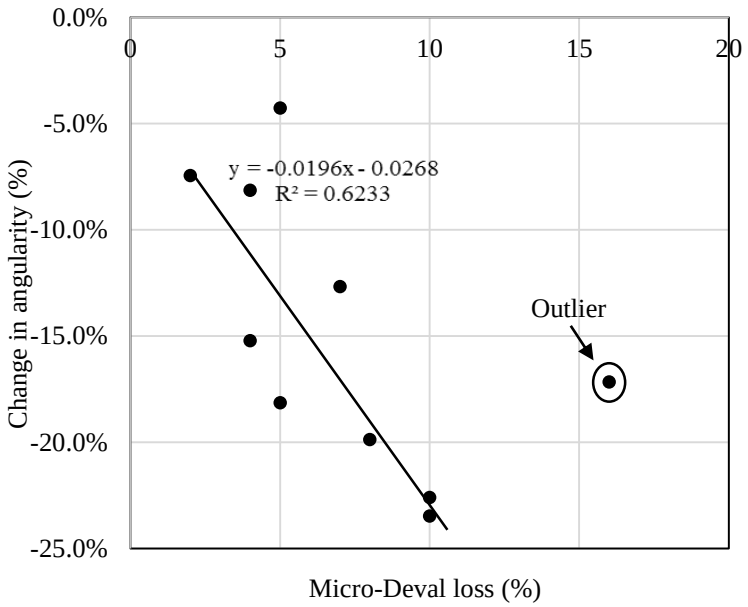

Figure 3.8 Comparison between change in angularity and Micro-Deval loss

Figure 3.9 represents the average texture value for both BMD and AMD. Aggregates are classified into four groups based on the texture: Low (≤ 200), Moderate (200–500), High (500–750), and Extreme (750–1000). RGLS2, GR, RH, and SL were in the moderate range for both BMD and AMD. The remaining aggregates were in the low texture range. Although RG2 and SS were crushed to produce unavailable aggregate sizes, they are still in the low texture range. Figure 3.10 shows the percentage change in texture for both BMD and AMD. AMD aggregate textures were supposed to decrease; however, three aggregates indicated a significant increase in texture. This may be due to the inability of AIMS to accurately measure texture for all color variations and random orientation in aggregates. Further investigation was not pursued, as it is outside the scope of this research program.

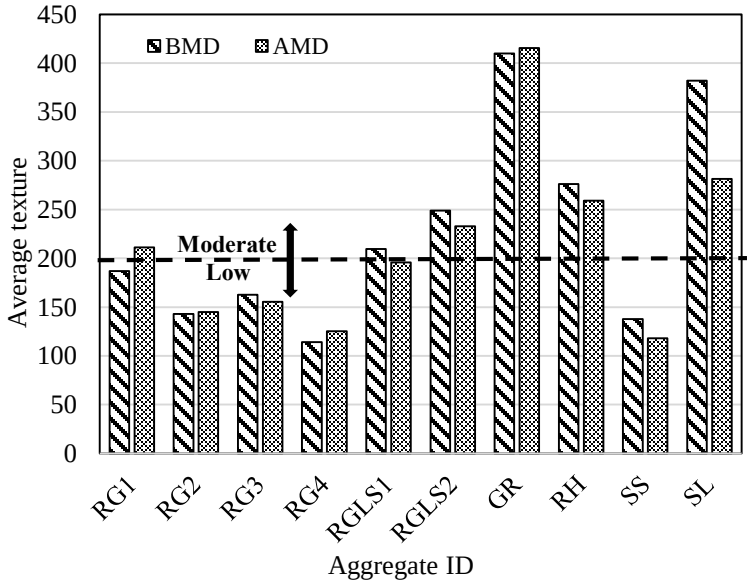

Figure 3.9 Average texture before and after Micro-Deval

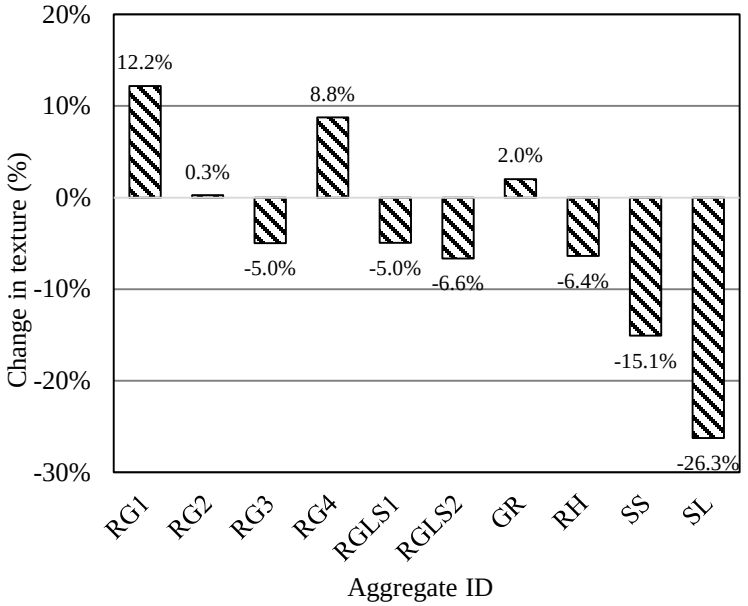

Figure 3.10 Change in texture before and after Micro-Deval

Figure 3.11 shows the particle shape distribution of the selected aggregates. A particle is considered "flaky" when the longer-to-shorter-dimension (L/S) ratio is greater than 1.66. Hence, an L/S ratio of 2:1 was selected and presented in Figure 3.11. From Figure 3.11, it can be noted that each aggregate source had at least 40% flaky particles. River gravels had highest percentage of flaky particles, including RG2 and RG3, which had about 70% flaky particles. With the exception of RG4 and RGLS2 all the aggregates showed reduction in L/S AMD. It is not clearly understood why RG4 and RGLS2 showed such deviated behavior.

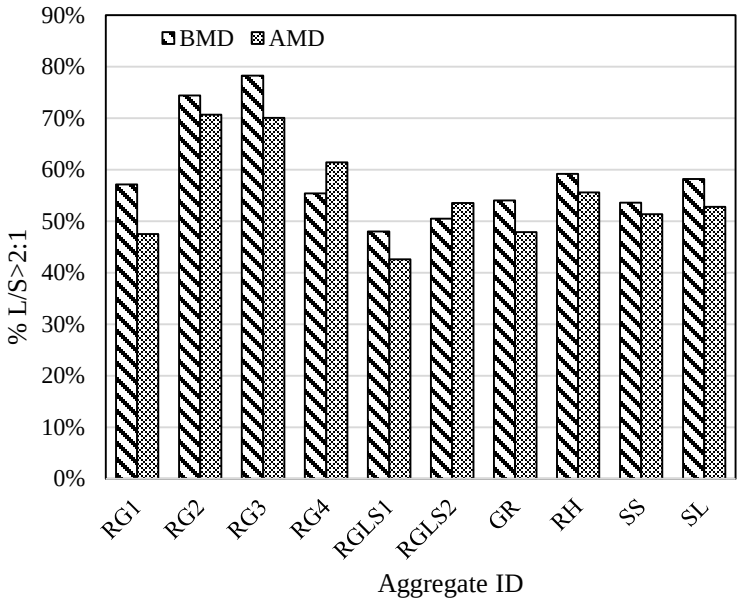

Figure 3.11 Particle shape before and after Micro-Deval

It is worthwhile to note that all the AIMS results were based on the two-dimensional black-and-white images of aggregates. Aggregates were manually placed on a tray and then images were captured. In most of the cases, the aggregate particles were oriented in a preferable position that affects the measured angularity, texture, and shape of the aggregates. Although AIMS is the only suitable method currently available for measuring the angularity, texture, and shape of coarse aggregates, efforts should be made to improve the existing method or develop a new method independent of the orientation of the aggregate particles.

Figure 3.12 presents the unconfined freezing and thawing loss of the aggregate sources. Unbound aggregates went through five cycles of freezing and thawing, and loss was determined after washing and oven-drying to constant mass. SS experienced the highest loss of 17.8%, whereas RG2 had the lowest at 1.2%. The MTO requires unconfined

loss of 6% or lower for coarse aggregates to be used in concrete pavements. Micro-Deval loss combined with unconfined freezing and thawing loss can predict field performance with 95% accuracy (Rogers et al. 2003). The unconfined loss limit proposed by the MTO might be excessively conservative for Texas since very few problems have been reported in Texas that relate to freezing and thawing. A new limit for unconfined freeze and thaw loss needs to be determined for Texas based on field performance.

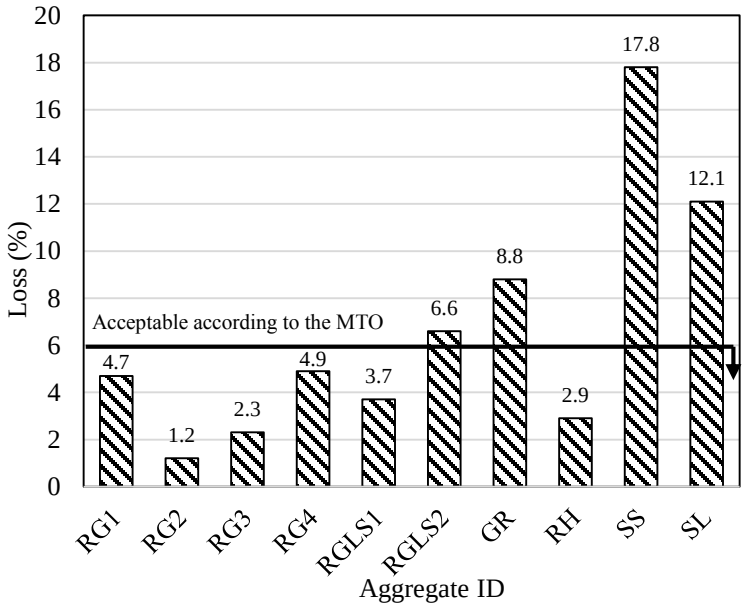

Figure 3.12 Unconfined (Canadian) freeze and thaw loss of aggregates

According to Tex-1xx-E, three ACVs—ACV4, ACD40, and ACV200— determine the percentage of ACV loss based on sieving at #4, #40, and #200, respectively. The ACV4 is presented in this chapter. Figure 3.13 shows the ACV4 for each of the aggregate sources. All the aggregates had an ACV 4 of more than 25%. RGLS2 showed the highest loss of 41% and RH showed the least at 28%. Although these test results provided for interesting

relative comparison, at this time TxDOT does not have any recommendation to consider ACV as a qualifying criterion.

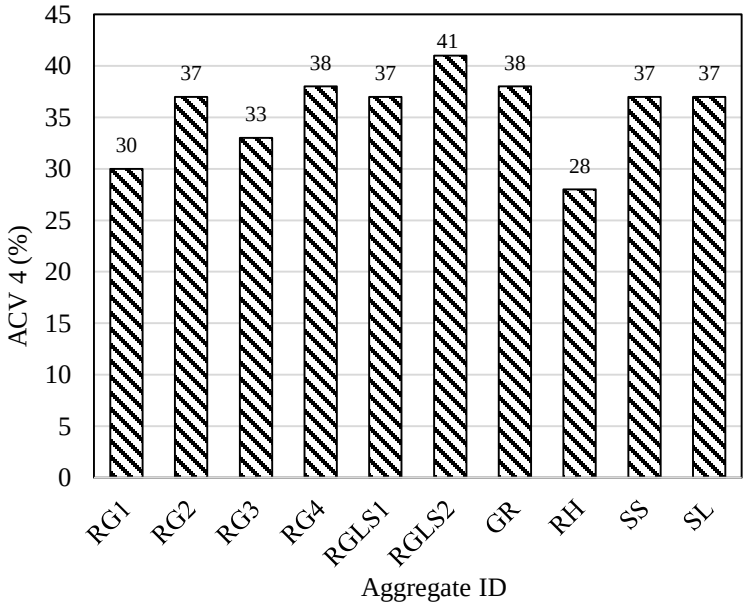

Figure 3.13 Aggregate crushing value

Seven- and 28-day concrete compressive strengths are shown in Figure 3.14. The strength of normal concrete is controlled by the strength of mortar. The strength of mortar depends on the type of cement, type of fine aggregate, and water-to-cement ratio (w/c). In this study, the mortar proportion was the same for all concrete mixtures. Similarly, the same cement, fine aggregate, and w/c were used. Therefore, the 7- and 28-day compressive strengths for concrete made with the ten aggregate sources fell into a narrow range of 4000 to 5000 psi (27.6 to 34.5 MPa) and 5500 to 7000 psi (37.9 to 48.3 MPa), respectively. All the concrete mixtures satisfied the Class P concrete strength requirements according to

Item 360 of the TxDOT Standard Specifications for Construction and Maintenance of Highways, Streets, and Bridges (TxDOT 2004).

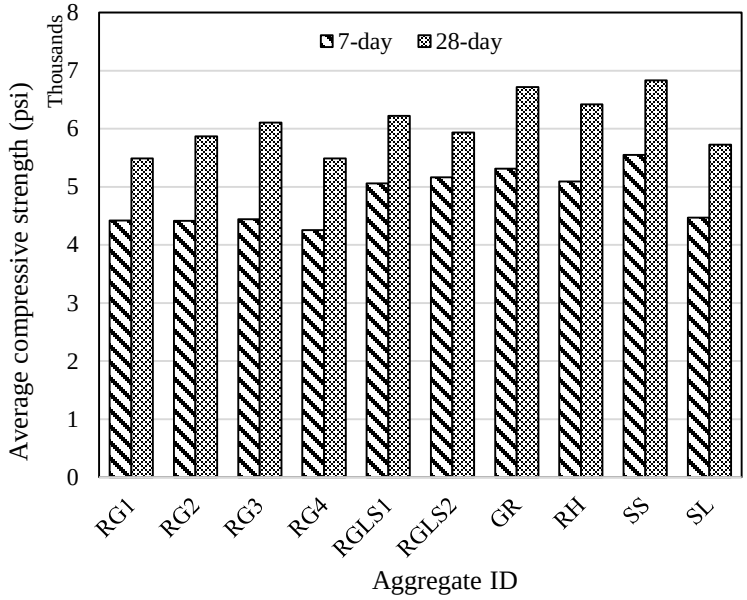

Figure 3.14 Seven-day and 28-day compressive strength of concrete

Figure 3.15 shows the 28-day modulus of elasticity (E) of the ten concrete mixtures. E varied from 5.2 to 3.5 million psi (35.8 to 24.1 GPa). RG1 had the highest E and SS had the lowest. The mortar properties for all the concrete samples were the same (the same mortar composition was used for all concrete tested); thus, the E of concrete was influenced by the properties of the aggregates. River gravels showed relatively higher E than other types of aggregates, followed by igneous rocks (GR and RH). Sand stone showed the lowest E, probably because of its porous structure.

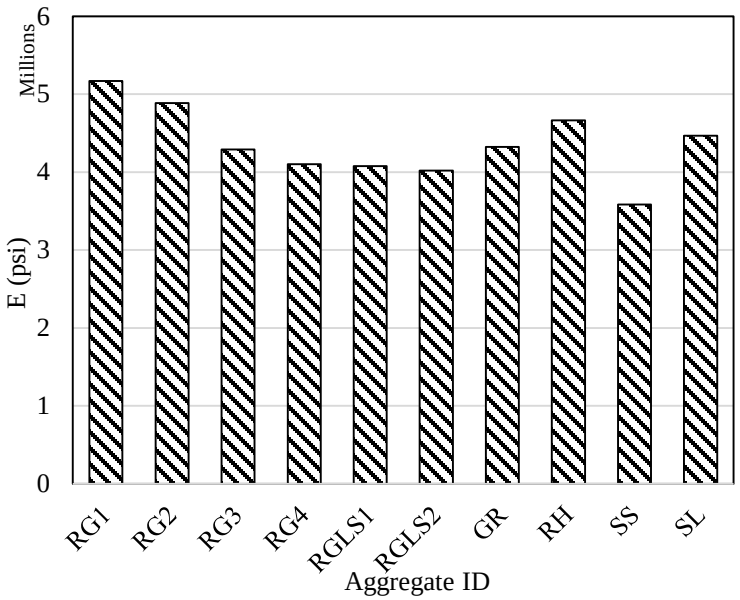

Figure 3.15 Modulus of elasticity for concrete specimens at 28 days of age

3.6 CONCLUSIONS

Ten different aggregate sources were collected from five TxDOT districts. The locations were chosen strategically, as suggested by TxDOT district personnel. Various laboratory tests were performed to determine durability and physical properties of these aggregates. The major findings are summarized as follows:

- All ten coarse aggregate sources were qualified according to Item 421 requirements of the Standard Specifications for Construction and Maintenance of Highways, Streets, and Bridges.
- Three sources failed to meet the MTO's unconfined freezing and thawing requirement, and one source did not meet MTO's Micro-Deval requirement.

- All the concrete mixes satisfied the TxDOT Class P concrete compressive strength requirement according to Item 360 of the Standard Specifications for Construction and Maintenance of Highways, Streets, and Bridges.
- River gravel showed the highest 28-day modulus of elasticity, and slate had the lowest.
- Sand stone had the highest absorption and unconfined freeze and thaw loss, as well as the lowest SG and E. This is probably due to its porous structure.
- Aggregates that were re-crushed to produce sufficient quantities of unavailable aggregate sizes showed an increase in angularity but their texture was not significantly affected.

Chapter 4: Effect of Internal Water Pressure on the Measured Coefficient of Thermal Expansion of Concrete

(This chapter was published in the Journal of Materials in Civil Engineering and was published in the dissertation with permission from the American Society of Civil Engineers (ASCE). "Siddiqui, M. S., and Fowler, D. W. (2014). "Effect of Internal Water Pressure on the Measured Coefficient of Thermal Expansion of Concrete." Journal of Materials in Civil Engineering, 04014151" (David W. Fowler was the supervisor).)

4.1 INTRODUCTION

The coefficient of thermal expansion (CTE) represents strain development due to a unit change in temperature. This property of concrete is recognized as one of the major factors responsible for pavement distresses, including cracking, faulting, punchouts, spalling, and delamination. Interest in concrete CTE is growing, since it has been included as a design parameter in the *Mechanistic-Empirical Pavement Design Guide* (MEPDG) (NCHRP and ARA 2004). A number of studies have shown that small variations in the CTE significantly affect the required thickness of portland cement concrete pavement designed to MEPDG specifications (Chung and Shin 2011; Jahangirnejad et al. 2009; Kannekanti and Harvey 2006; Kim and Won 2004; Mallela et al. 2005; Tanesi et al. 2006, 2007). Small deviations in the design input for the CTE than the actual CTE values in MEPDG can result in either unnecessarily thick pavement or inadequate thickness. Unnecessarily thick pavement increases the project cost, and inadequate thickness reduces the service life due to higher pavement distresses. The Texas Department of Transportation (TxDOT) has long recognized thermal incompatibility between aggregate and mortar as a major cause of distress in continuously reinforced concrete pavements (CRCP). Some TxDOT districts have limited the CTE of CRCP to prevent pavement distress caused by

thermal loading. Spalling has greatly diminished since the CTE of CRCP concrete in the Houston district has been limited (Naranjo 2013). Very recently TxDOT has imposed a statewide limit of 5.5×10^{-6} strain/^{o}F (9.9×10^{-6} strain/^{o}C) on CTE as an acceptance criterion for CRCP concrete aggregates. Aggregates that produce concrete specimens with CTEs higher than 5.5×10^{-6} strain/^{o}F (9.9×10^{-6} strain/^{o}C) are no longer accepted in TxDOT CRCP paving projects. As a result, it is important to accurately determine the CTE of pavement concrete for enhanced pavement design and accurate screening of coarse aggregates.

Various agencies have their own methods to determine CTE. The most widely used method is the American Association of State Highway and Transportation Officials (AASHTO) suggested method (AASHTO T 336-11 2011). All state agencies other than TxDOT use this method. Because of the inconsistency of the results obtained from the AASHTO method (Won 2005), TxDOT uses a modified version of the provisional AASHTO TP 60 (2000) method, Tex-428-A (2011). Throughout this chapter, the AASHTO T 336 and Tex-428-A methods will be referred to as the AASHTO and the TxDOT methods, respectively. Although these are the two most popular methods in the U.S., there are other CTE test methods available.

This study will compare the concrete CTE values obtained from the AASHTO and TxDOT methods and the effect of two different length-change measuring devices: the linear variable differential transducer (LVDTs) and the differential variable reluctance transducer (DVRTs). Finally, the effect of internal water pressure on the results will be discussed.

4.2 COMPARISON OF THE AASHTO AND THE TXDOT CTE METHODS

The TxDOT and AASHTO methods are modifications of the provisional AASHTO TP 60 method. As a result, there are many similarities between these two methods. However, there are also a few important differences:

- The TxDOT method specifies the concrete mixture design for the CTE samples, which includes the water-to-cement ratio (w/c), amount of cement, fraction of coarse and fine aggregates, as well as a specific sand source, while the AASHTO method does not. Specifying a mixture design is important when comparing concrete mixtures with different aggregate sources and mineralogies, since the CTE can be affected by the variation in different components of concrete mixtures (Chung and Shin 2011; Mindess et al. 2002; Won 2005).
- The TxDOT test method specifies the grading of coarse aggregate, which affects the paste requirement of concrete. Paste volume in concrete affects the CTE of concrete, because cement paste has a much higher CTE than the aggregate does (Chung and Shin 2011). Therefore, the use of similar coarse aggregate gradation is also important when comparing the CTE of concrete specimens made from different coarse aggregate sources. However, the AASHTO method does not specify coarse aggregate gradation.
- The AASHTO method uses length difference at two extreme temperatures (10 and 50ºC (50 and 122ºF)) to measure CTE. In contrast, the TxDOT method uses the length and temperature change reading from 15 to 45ºC (59 to 113ºF) and relies on regression analysis to calculate CTE. Further details on the calculation technique for both methods can be found elsewhere (AASHTO T 336-11 2011; Tex-428-A

2011). In this study, length change and temperature readings were taken at 1-minute intervals.

- The TxDOT method specifies a rate of temperature change. The time required for the temperature to change from 10 to 50°C (50 and 122°F) has to be at least two hours followed by at least one hour of isothermal state. The AASHTO method does not specify rate of heating and cooling, but requires that the length of the isothermal state has to be extended until the specimens reach a stable length, so that three consecutive readings at 10-minute intervals are same.

Both the AASHTO and TxDOT methods refer to the LVDT as a length-change measuring device, but they do not preclude the use of other devices, as long as the resolution is 0.00001 in. (0.00025 mm) and the device has a range suitable for the test. However, none of these methods considers the response of length-change measuring devices to the testing environment as an acceptance criterion.

4.3 MATERIALS

The aggregates selected for testing were acquired from five TxDOT districts: Atlanta, Houston, Amarillo, Paris, and Wichita Falls, as mentioned in Chapter 3. Four of the coarse aggregates were siliceous river gravel (RG), two were natural blends of siliceous and limestone gravel (RGLS), and one source provided granite (GR), rhyolite (RH), sand stone (SS), and slate (SL). (Table 3.1 showed the aggregate sources collected from different districts around Texas.) A limestone (LS) aggregate source was also selected from Dallas for aggregate blending. An additional nine aggregates were blends of two aggregates prepared in the laboratory. Table 4.1 presents the aggregate blends. An ASTM C150 (2012)

Type I/II cement and the TxDOT-recommended river sand source were used for all concrete mixtures. Additional information about the materials, including durability and physical properties, can be found in Section 3.3.

Table 4.1 List of aggregate blends

Aggregate ID	Blend Description
20SL-80LS	20% SL & 80% LS
50SL-50LS	50% SL & 50% LS
80SL-20LS	80% SL & 20% LS
20RG1-80LS	20% RG1 & 80% LS
50RG1-50LS	50% RG1 & 50% LS
80RG1-20LS	80% RG1 & 20% LS
20GR-80LS	20% GR & 80% LS
50GR-50LS	50% GR & 50% LS
80GR-20LS	80% GR & 20% LS

4.4 TEST PROCEDURES

Concrete was proportioned according to Tex-428-A. This method suggests a specific concrete proportioning and coarse aggregate gradation to produce comparable concrete mixtures for CTE testing by minimizing the influence of factors such as aggregate fraction, volume of paste, aggregate gradation, and w/c. Concrete proportioning techniques, coarse aggregate gradation, and mixing procedures were previously discussed in Section 3.3. Two 4-in. x 8-in. (200-mm x 400-mm) cylinders were made from each concrete mixture. The CTE was determined according to AASHTO T 336 and Tex-428-A test procedures. Each cylinder was subjected to three cycles of heating and cooling for testing purposes. A typical heating and cooling cycle is shown in Figure 4.1. Figure 4.2 illustrates a typical length-change response. LVDTs and DVRTs were used as length-

change measuring devices. Both devices were physically nulled at room temperature after the test specimen was placed in the frame. Test cylinders were preconditioned by six cycles of heating and cooling prior to the CTE testing. CTE values were measured using both LVDTs and DVRTs for each CTE test method. In this chapter, the TxDOT method measured by LVDTs and DVRTs will be referred to as TxDOT (LVDT) and TxDOT (DVRT), respectively. Similarly, the AASHTO method that used LVDTs and DVRTs will be referred to as AASHTO (LVDT) and AASHTO (DVRT), respectively. Test cylinders were first tested with a DVRT and then with a LVDT. Therefore, the LVDT results were from specimens that experienced three more cycles of heating and cooling preconditioning than those tested using the DVRT.

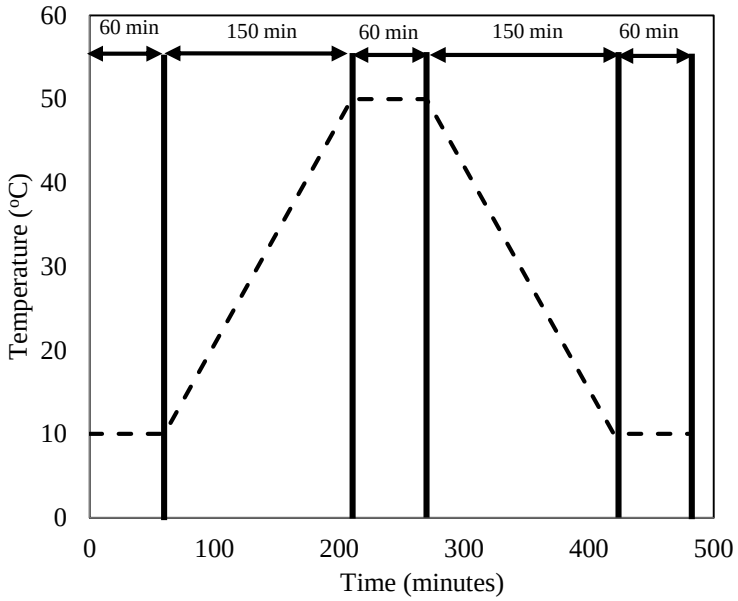

Figure 4.1 One typical cycle of heating and cooling

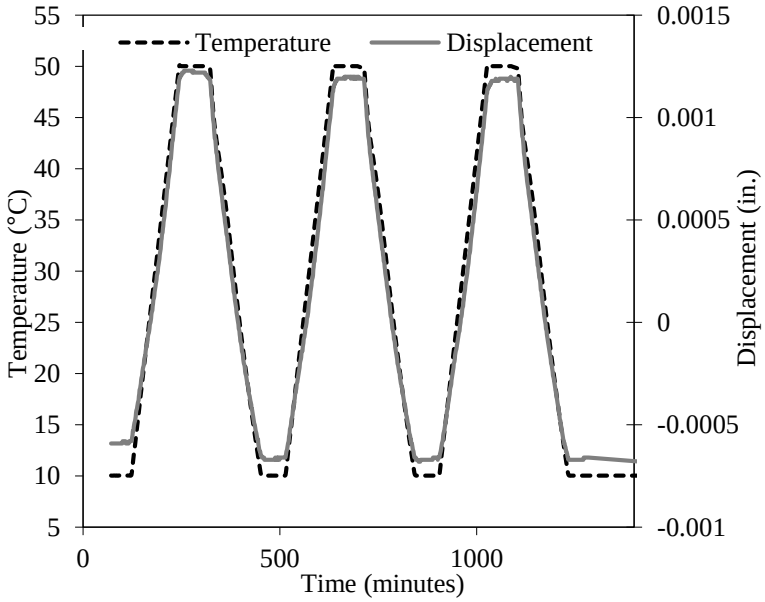

Figure 4.2 Typical response of a concrete cylinder subjected to three cycles of heating and cooling

4.5 RESULTS AND DISCUSSIONS

4.5.1 Effect of aggregate mineralogy

The CTE values obtained for concrete made with natural aggregate sources are presented in Figure 4.3. These CTE values are the average of measured CTE values obtained from two different concrete cylinders made from the same concrete mixture. Concrete made with river gravels showed the highest CTE, ranging from 5 to $6x10^{-6}$ strain/^{o}F (9 to $10.8x10^{-6}$ strain/^{o}C) for both TxDOT (LVDT) and AASHTO (LVDT), followed by SS and SL, RGLS, two igneous rocks (GR and RH), and LS. Concrete made with limestone had the lowest CTE of about $3.5x10^{-6}$ strain/^{o}F ($6.3 x10^{-6}$ strain/^{o}C) for the TxDOT (LVDT) and about $3 x10^{-6}$ strain/^{o}F ($5.4 x10^{-6}$ strain/^{o}C) for the AASHTO (LVDT) method. Obtained CTE values were consistent with the values presented in previous studies

(Jahangirnejad et al. 2009; Chung and Shin 2011; Won 2005; Naik et al. 2011; Mallela et al. 2005). The concrete made from RGLS1 and RGLS2 contained natural blends of siliceous and limestone gravels. The RGLS concrete specimens showed lower CTE than those made from river gravel and higher CTE than those made with limestone. This result supports the potential to optimize the CTE of concrete by blending low-CTE aggregates with high-CTE aggregates (Siddiqui and Fowler 2013b). Since the aggregate gradation, cement type, sand source, cement content, coarse and fine aggregate fraction, and w/c of each mixture were similar, any difference in CTE was influenced only by the mineralogy of the coarse aggregate. The CTE values suggest that coarse aggregate mineralogy has a significant effect on the CTE of concrete, as observed in previous studies (Alungbe et al. 1992; Kohler et al. 2007; Mallela et al. 2005; Won 2005). It is also notable that CTE values obtained from the TxDOT (LVDT) method are typically higher than those of the AASHTO (LVDT) method. The causes of this difference are discussed in later sections.

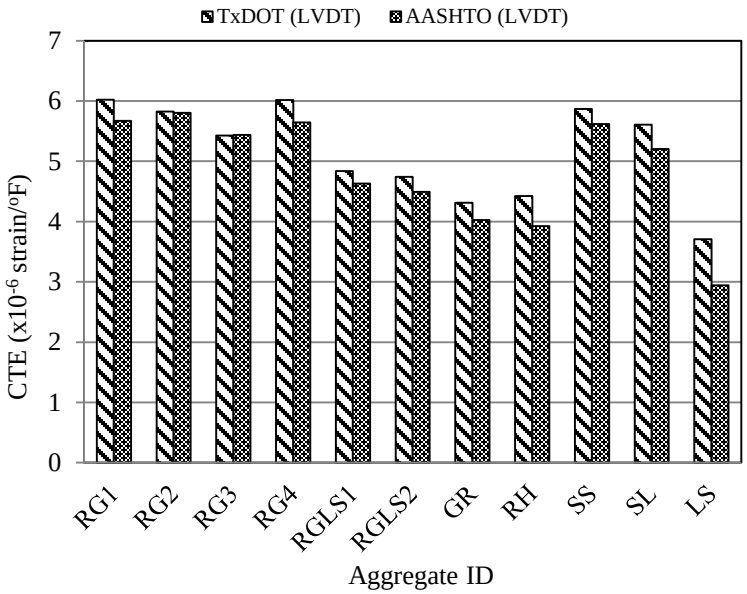

Figure 4.3 Measured CTE values for concrete cylinders for naturally occurring aggregate sources

4.5.2 Comparison of length-change measuring devices

Two different length-change measuring devices, LVDTs and DVRTs, were used in this study. Forty concrete cylinders were tested, and Figure 4.4 and Figure 4.5 show the effect of length-change measuring devices on the TxDOT and the AASHTO methods, respectively. An examination of the results obtained from the TxDOT method distributed evenly along the line of equality showed no significant effect of the length-change measuring devices on the TxDOT CTE testing process. However, the AASHTO (DVRT) showed slightly higher CTE values than did the AASHTO (LVDT). A paired t-test was performed to determine the statistical difference between the data measured by different length-change measuring devices. The assumption for null hypothesis (H_o) was "the data obtained by DVRT and LVDT are not different." A detailed analysis of the paired t-test is

presented in Table 4.2, from which it can be noted that there is no significant effect of length-change measuring devices on the TxDOT method at a significance level of 0.01 ($\alpha = 0.01$). However, the length-change measuring devices significantly affected the AASHTO method's results, and the AASHTO (DVRT) is higher than the AASHTO (LVDT) at a 99% confidence level ($\alpha = 0.01$). The reason for such behavior is not completely understood, but one reason could be the difference in the devices' calibration techniques. The DVRTs were calibrated to compensate for the effect of temperature change (a maximum offset of 0.0011% displacement/^{o}F), while the LVDTs were not.

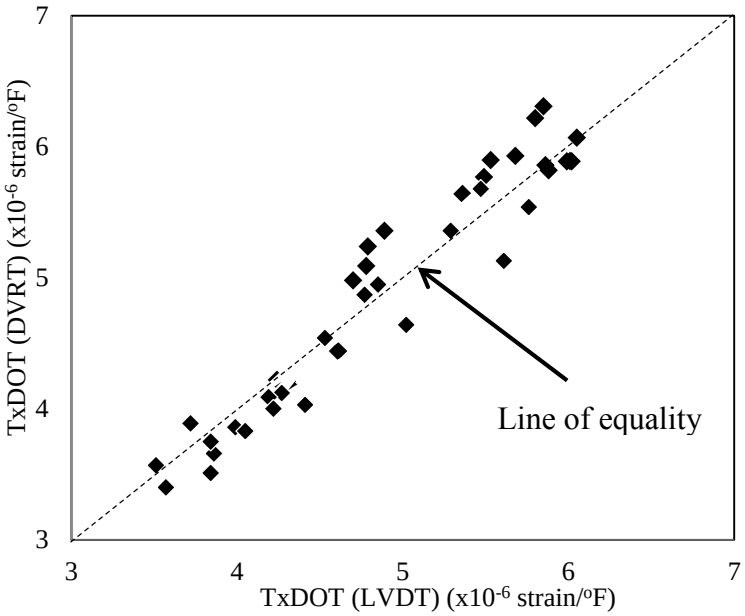

Figure 4.4 Effect of DVRT and LVDT on measured TxDOT CTE

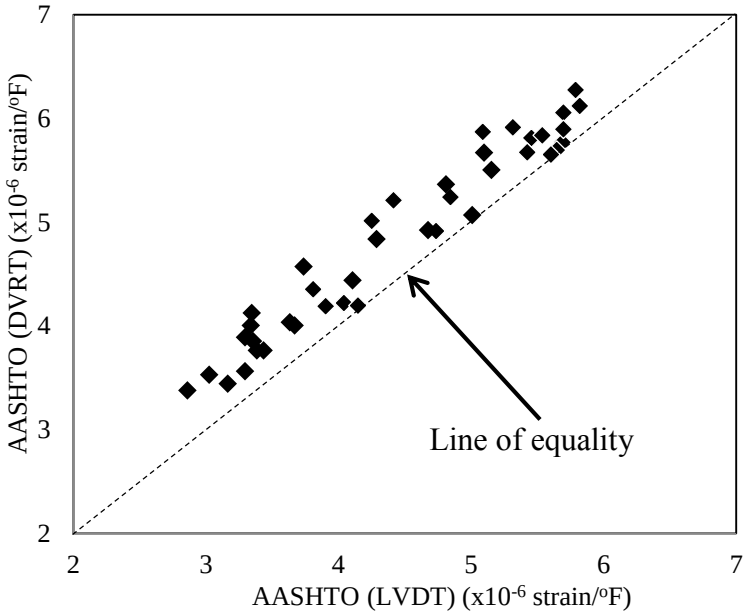

Figure 4.5 Effect of DVRT and LVDT on measured AASHTO CTE

Table 4.2 Effect of length-change measuring devices on measured CTE values

Items	TxDOT (Figure 4.4)	AASHTO (Figure 4.5)
Number of samples	40	40
Average (CTE_y - CTE_x) *	0.01	0.40
Standard deviation	0.25	0.22
t	0.25	11.49
P	0.77	0
$P<\alpha$ ($\alpha = 0.01$)	No	Yes
Null hypothesis (H_o)	Accepted	Rejected
$t_{\alpha,n-1}$ ($\alpha = 0.01$)	2.423	2.423
$CTE_y>CTE_x$**	-	Yes

** Average (CTE_y - CTE_x) is the average of differences between CTE_y and CTE_x.*

***CTE_y and CTE_x represent CTE values presented in y and x axis, respectively. For example, for Figure 4.4, CTE_y and CTE_x represent the CTE for TxDOT (DVRT) and TxDOT (LVDT), respectively.*

4.5.3 Comparison of CTE methods

Figure 4.6 and Figure 4.7 illustrate comparisons of the two CTE test methods measured by DVRTs and LVDTs, respectively. Although CTE values from the DVRT are very close to the line of equality, about 80% of the results obtained through the TxDOT method were higher than those of the AASHTO method, as shown in Figure 4.6. From Figure 4.7 it can also be observed that the TxDOT method produces higher CTE values than does the AASHTO method. Results from the paired t-test also support this conclusion at a 99% confidence level and are presented in Table 4.3. The differences in calculation techniques may explain the differences in results, but may be more likely explained by an increase in internal water pressure due to temperature change, which is discussed in later sections.

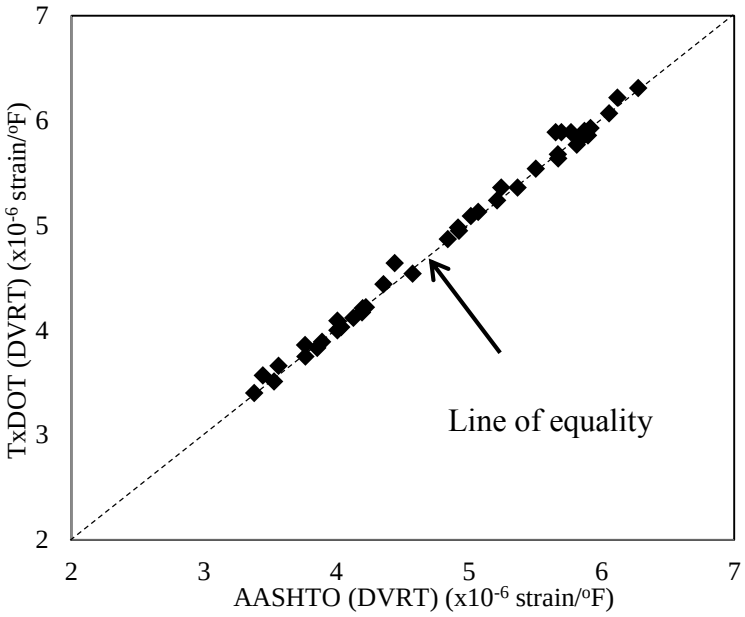

Figure 4.6 Effect of test procedures on CTE values measured by the DVRT

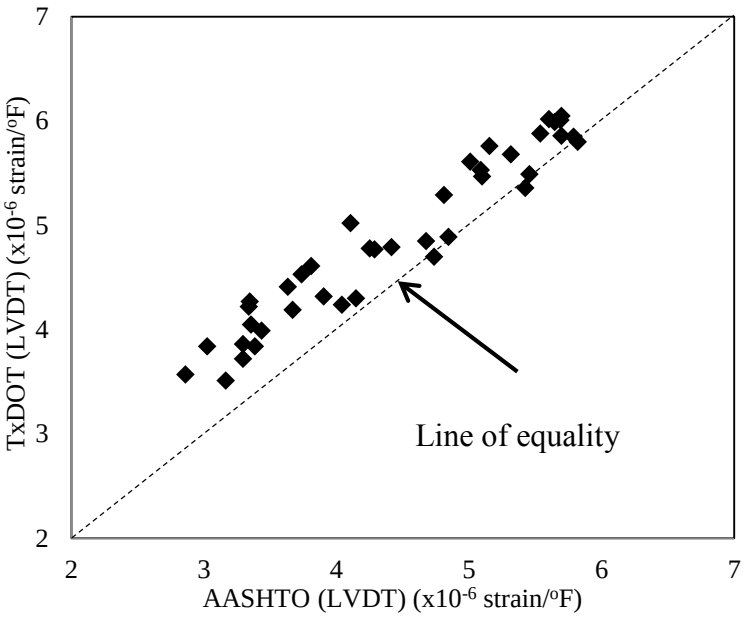

Figure 4.7 Effect of test procedures on CTE values measured by the LVDT

Table 4.3 Effect of calculation techniques on measured CTE value

	DVRT (Figure 4.6)	**LVDT (Figure 4.7)**
Number of sample	40	40
Average (CTE_y - CTE_x)	0.04	0.43
Standard deviation	0.07	0.27
t	3.79	10.03
P	0	0
$P<\alpha$ ($\alpha = 0.01$)	Yes	Yes
Null hypothesis (H_o)	Rejected	Rejected
$t_{\alpha,n-1}$ ($\alpha = 0.01$)	2.423	2.423
$CTE_y>CTE_x$	Yes	Yes

4.5.4 Explanation of the difference in the TxDOT and the AASHTO CTE

Internal water pressure and time delay to reach temperature equilibrium were identified as probable causes for the difference in measured CTE values provided by the AASHTO and TxDOT methods. To identify the effect of internal water pressure and delay in temperature equilibrium, two concrete cylinders were subjected to three cycles of heating and cooling. The rates of heating and cooling were similar to those shown in Figure 4.1, but the duration of the isothermal state was increased from 1 to 10 hours. Length-change responses for these two cylinders are shown in Figure 4.8. Deformation in the isothermal state confirms the presence of the effect of internal water pressure and delay in temperature equilibrium. To determine only the effect of delay in temperature equilibrium, the temperature of the water bath and the interior of an immersed 4-in. x 8-in. (100-mm x 200-mm) cylinder were measured. A thermocouple was placed in the middle of the cylinder during casting. Figure 4.9 shows the temperature variation of a 4-in. x 8-in. (100-mm x 200-mm) concrete cylinder while subjected to heating and cooling cycles. Times to reach temperature equilibrium after heating and cooling cycles were about 30 and 20 minutes, respectively. However, according to Figure 4.8, the length change of concrete cylinders subjected to heating and cooling cycles did not reach equilibrium even after 10 hours, and most of the length change occurred after the temperature equilibrium had been reached. Therefore, temperature equilibrium might have a short-term effect on the length change in the isothermal state, but long-term isothermal deformations are caused by internal water pressure. The mechanism and effect of internal water pressure are discussed in the next section.

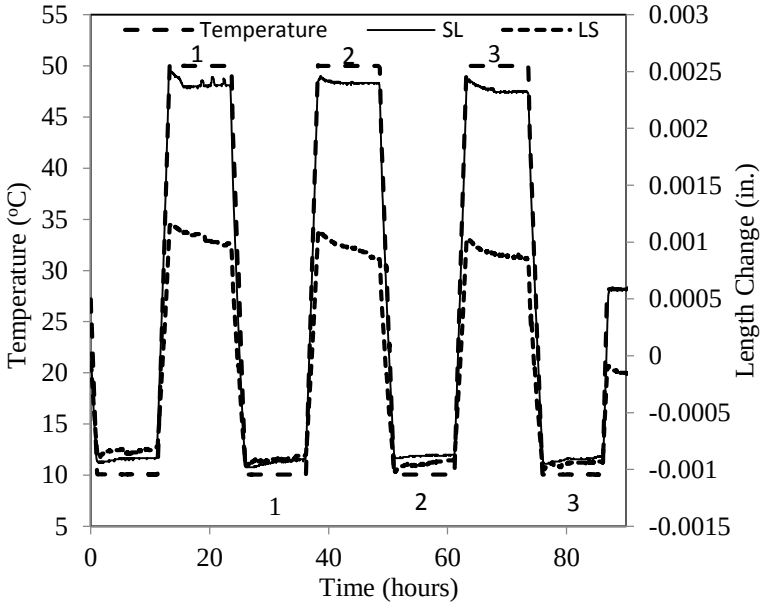

Figure 4.8 Effect of internal water pressure and delay in temperature equilibrium on the length-change response of concrete cylinders

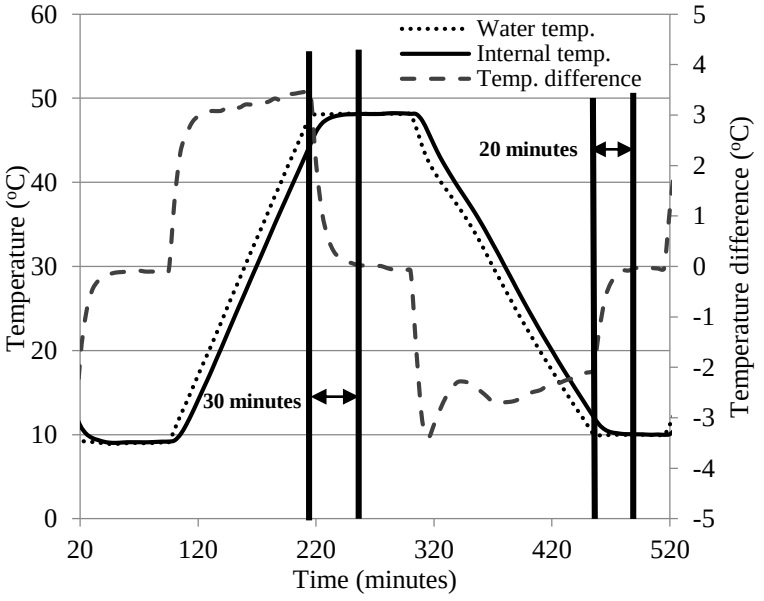

Figure 4.9 Temperature variation in a 4-in. x 8-in. concrete cylinder subjected to heating and cooling cycle. Note that the left and right vertical axes represent the measured temperature and temperature change between water (external) and internal (*r*=0) temperature, respectively.

4.5.5 Effect of internal water pressure

The effect of the internal water pressure caused by thermal changes was first identified by Bažant (Bažant 1970) and later used by Sellevold and Bjøntegaard (2006) to explain the higher CTE of cement paste before setting as compared to that of hardened cement paste. Saturated concrete can be divided into two components: solid and liquid phases. The CTE of solids is different from the CTE of liquid. This difference is responsible for two types of deformation: instantaneous deformation (ID) and time-dependent deformation (TDD). ID can be defined as deformation that occurs instantaneously with thermal changes, and TDD is the deformation due to thermal changes that continues to occur with time. When the temperature changes, ID takes place first, followed by TDD. TDD continues even after concrete reaches its thermal equilibrium. ID is a function of the rate of temperature change, the amount of interconnected pores, and the volume of internal water. TDD is a function of internal water pressure, porosity, and the size of the concrete sample.

The CTE of liquid is higher than the CTE of solids in the concrete matrix. As a result, for heating cycles, the volume of water increases more than the volume of solids. This difference in volume change increases internal water pressure, causing instantaneous expansion followed by time-dependent contraction. Time-dependent contraction takes place when excess pressure in the water-filled pores gradually reduces the flow of water to the exterior of the concrete. For cooling cycles, instantaneous contraction is followed by time-dependent expansion. A schematic diagram of the process is shown in Figure 4.10.

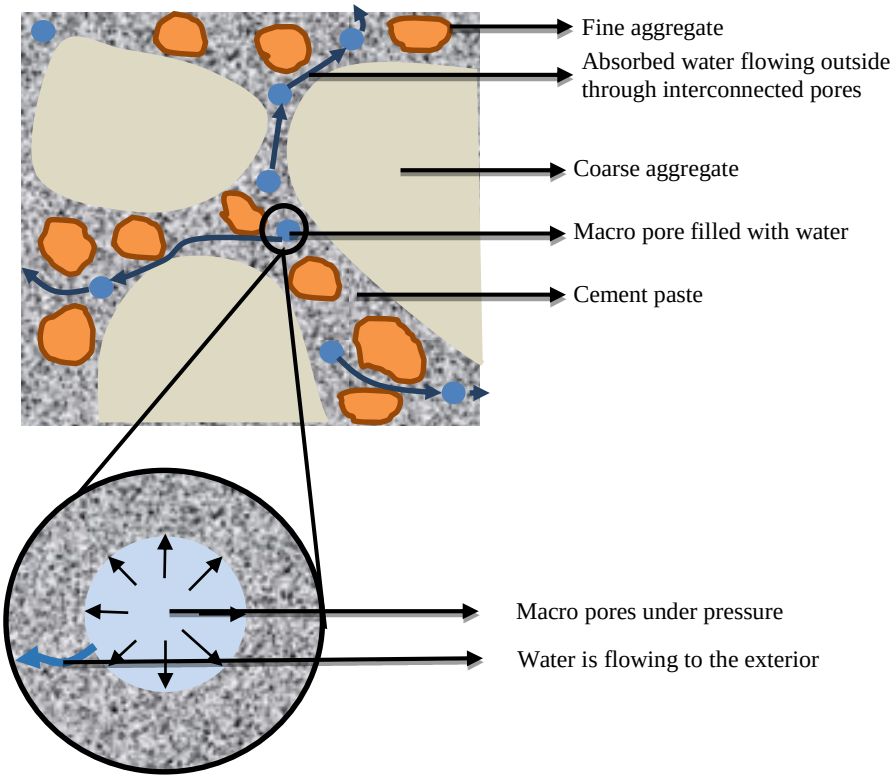

Figure 4.10 Schematic diagram of internal water pressure development during the heating cycle

The presence of ID and TDD can be observed from Figure 4.8. Deformation at the isothermal state indicates the presence of ID and TDD. At 50°C (122°F), cylinder lengths were decreasing due to time-dependent contraction at 10°C (50°F), cylinder lengths were gradually increasing due to time-dependent expansion. Relatively longer and shorter specimen lengths at the initiation of 50 and 10°C (122 and 50°F) isothermal states, respectively, indicate the presence of ID. The rate of TDD in the isothermal state decreased with time, because internal water pressure gradually dissipated due to the outer water flow. It is noteworthy, however, that even after 10 hours of isothermal condition, none of the samples seemed to reach length-change equilibrium.

Other observations can be made from the obtained results. Figure 4.11 shows total absolute length changes at the isothermal condition for LS and SL. The cycle IDs are labeled in Figure 4.8. At 50 and 10°C (122 and 50°F), sample lengths decreased and increased, respectively. Although SL had a greater length change according to Figure 4.8, LS had higher isothermal length-change recovery at both 10 and 50°C. Both concrete cylinders were made with the same proportioning; thus, the mortar properties were the same. Therefore, the difference in coarse aggregate properties must be the reason for this behavior. LS and SL had absorptions of 2.04 and 1.2%, respectively. Higher absorption means larger amounts of internal water in the concrete, which leads to higher ID followed by higher TDD recovery. The average total length change by TDD for SL and LS at the isothermal state was 7.2 and 14×10^{-5} in. (1.8 and 3.5×10^{-3} mm), respectively, which led to a CTE overestimation of about $0.12 \times^{-6}$ (2%) and 0.22×10^{-6} (6.4%) strain/°F, respectively, by current test methods. It is observed that the length change at 50°C (122°F) was higher than the length change at 10°C (50°F). The reason for this behavior cannot be readily explained.

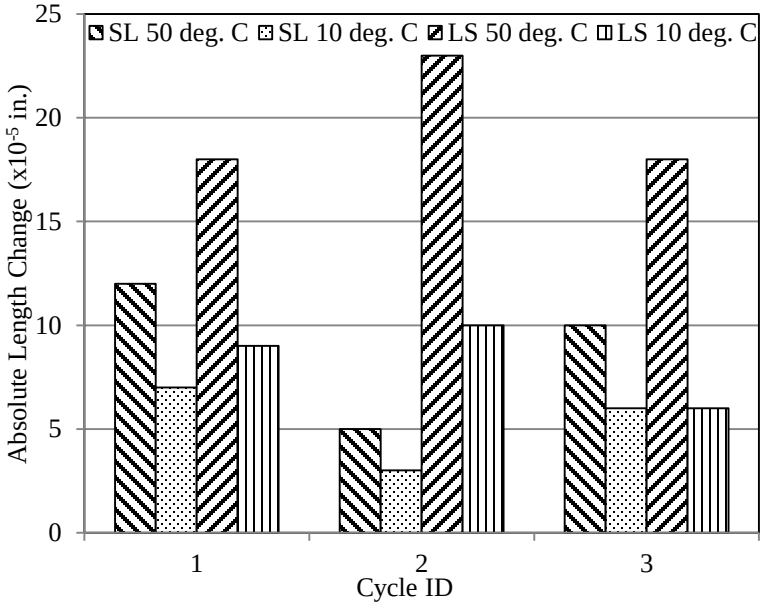

Figure 4.11 Total absolute length change at isothermal state

This phenomenon explains why the TxDOT values are higher than the AASHTO values. The AASHTO method uses length-change values at two extreme isothermal temperatures. This method specifies taking length-change readings after thermal equilibrium is reached, as indicated by consistent readings of the length-change measuring device of ±0.00001 in. (±0.00025 mm) taken every 10 minutes over a half-hour period. At that state there is no ID, and the prior effect of ID is partially recovered by TDD. In contrast, the TxDOT method uses the length-change data from 15 to 45ºC (59 to 113ºF) to calculate the CTE values. At this temperature range, ID is present due to ongoing temperature changes and decreased length-change recovery by TDD due to the shorter duration. Hence, the TxDOT method measures relatively higher length change than does the AASHTO method, which results in TxDOT's higher CTE values.

4.6 CONCLUSIONS AND RECOMMENDATIONS

The CTEs of concrete made from different aggregate sources in Texas were presented in this chapter. The effects of aggregate mineralogy, test methods, and length-

change measuring devices on measured CTE values were observed. The influence of internal water on CTE values was discussed. Based on this laboratory investigation, the following conclusions can be made:

- Both the TxDOT and AASHTO test methods confirmed the significant effects of coarse aggregate mineralogy on the CTE of concrete. The results for various aggregate mineralogies compared favorably with the earlier published data.
- Length-change measuring devices affected the AASHTO method results. Length-change measuring devices should be chosen based not only on the resolution and range, but also on the response of the device in the test environment.
- The test methods used affected the measured CTE values. Results obtained from the TxDOT test method were higher than the results obtained from the AASHTO method. Differences in calculation techniques and the effects of internal water pressure were responsible for this deviation.
- The higher absorption capacity of coarse aggregate led to higher combined effects of instantaneous deformation (ID) and time-dependent deformation (TDD).
- Length-change recovery due to TDD was greater for the heating cycles than for the cooling cycles.
- The current test procedures do not consider the effect of internal water pressure, which leads to overestimating the CTE values. Additional study is needed to improve the current test procedures to address this issue.

Chapter 5: An Analytical Model to Explain the Effect of Internal Water Pressure on the Coefficient of Thermal Expansion

5.1 INTRODUCTION

Concrete is a heterogeneous porous material, consisting of cement paste and aggregates. Typically, the porosity of aggregates and the air bubbles generated during the concrete mixing process contribute to the overall porosity of concrete. In completely saturated concrete, all the pores are filled with liquid. The coefficient of thermal expansion (CTE) of the typical liquid phase (e.g., pore fluid) is much higher than that of the solid phase comprising the concrete's skeleton. Therefore, the liquid phase changes volume in response to temperature change to a much greater extent than does the solid phase. If the rate of temperature change is slow enough, the liquid can flow into or out of the concrete body to adjust for the volume change without generating significant pressure in the pore liquid. However, during a rapid temperature change, the liquid does not have sufficient time to completely flow into or out of the concrete body, which introduces internal pore water pressure in the concrete, thus resulting in additional deformation.

Usually, the CTE of concrete is determined by measuring the length change of concrete cylinders when subjected to heating and cooling cycles. In the U.S., the two most popular CTE test methods are those proposed by the American Association of State Highway and Transportation Officials (AASHTO) and the Texas Department of Transportation (TxDOT). Chapter 4 discussed how the typical heating and cooling rates used for the TxDOT and AASHTO methods are not slow enough for water to flow into or out of saturated concrete specimens without generating internal water pressure. The

generated internal water pressure affects the length-change measurement and, consequently, affects the measured CTE of concrete. Furthermore, the pore water pressure effect results in the TxDOT method yielding higher CTE values than the AASHTO method, as shown in Chapter 4.

The objective of this chapter is to develop an analytical model to evaluate the hypothesis presented in Section 4.5.5 and to explore the effects of various parameters—including porosity, permeability, and size of concrete specimens—as well as the rate of temperature change on the axial strain and internal water pressure development. A study of these effects was undertaken to better understand the poromechanical behavior of saturated concrete cylinders being subjected to temperature changes.

5.2 BACKGROUND

The moisture content of concrete has a significant effect on the measured CTE, as confirmed by a number of studies (Chung and Shin 2011; Emanuel and Hulsey 1977; Grasley and Lange 2007; Meyers 1951; Mindess et al. 2002; Neville and Brooks 1987; Yeon et al. 2009; Zoldners 1971). Existing literature also describes the effect of moisture content in conjunction with the effect of relative humidity. In 1977, Emanuel and Hulsey (1977) presented the CTE of cement paste as a function of moisture content. According to their study, the CTE of partially saturated cement paste (65 to 75% moisture content) was the highest, about 60 and 80% higher than completely saturated and dry samples, respectively, from 0 to 18 months of age. Emanuel and Hulsey also reported that for 16-year-old cement paste, the peak CTE of concrete occurred at a much lower moisture content of about 50%. Yeon et al. (2009) and Neville and Brooks (1987) made similar observations.

Yeon et al. (2009) showed that the maximum CTE for concrete and cement paste was observed at about 80% relative humidity, whereas Neville and Brooks (1987) reported peak CTE at about 60% relative humidity. In an (unsuccessful) effort to minimize the moisture effect on measured CTE, the AASHTO T 336 (2011) and the Tex-428-A (2011) methods were developed to determine the CTE of concrete on saturated samples. In Chapter 4, it was experimentally demonstrated that the internal water pressure developed in a saturated concrete specimen subjected to heating and cooling cycles affects the measured concrete CTE.

The effect of moisture content on the CTE of concrete was first described by Meyer (1951). This effect can be explained as the result of pure thermal dilation, thermal shrinkage and swelling, and change in relative humidity. In saturated concrete, delayed thermal movement is not affected by the change in relative humidity. According to pure thermal dilation theory, internal pore water pressure occurs due to the difference in CTEs between the solid and liquid phases. This difference in CTEs is responsible for instantaneous deformation (ID), which is followed by time-dependent deformation (TDD) (Scherer 2000b; Sellevold and Bjøntegaard 2006). ID and TDD produce opposite effects. During a heating cycle, instantaneous expansion occurs, followed by a time-dependent contraction; this process is reversed during a cooling cycle. According to thermal shrinkage and swelling theory, delayed deformation occurs in concrete due to the difference in chemical potential between gel and capillary water, and the deformation is in the opposite direction of ID but in the same direction of TDD. However, it is difficult to determine how water distributes in a saturated sample. Sellevold and Bjøntegaard (2006) hypothesized that in saturated concrete, water will flow from gel to capillary pores or capillary to gel pores,

resulting in an increase in the local pressure (disjoining pressure) to reach chemical equilibrium. However, their hypothesis lacks any experimental support. Moreover, the effect of thermal shrinkage and swelling is very small compared to the total delayed deformation. Hence, thermal shrinkage and swelling were not considered while developing the analytical model.

5.3 POROELASTIC SOLUTIONS FOR CONCRETE CYLINDERS

Concrete can be considered a poroelastic material, which was demonstrated by several studies (Grasley and Leung 2011; Leung and Grasley 2012; Leung and Grasley 2012; Scherer 1994, 2006b). In order to facilitate analysis, the porosity of concrete can be approximated as invariant with respect to internal water pressure generated from temperature change. In addition, no external forces were considered during heating and cooling cycles. The solid skeleton of the concrete and the pore fluid should not be approximated as incompressible (as is sometimes done with other porous materials), because the bulk modulus of the solid and liquid phases are in the same order of magnitude. The inertia effect of the fluid flow was ignored, as the fluid flow velocity was considered to fall at the low end of the range of heating and cooling rates used in this study. The fluid from the concrete cylinders was assumed to flow in the radial direction only, which is a reasonable approximation given the aspect ratio of the cylinders considered. For the heat flow calculation, the concrete was considered to have a linear constitutive relationship between the heat flux and the temperature gradient, no sources or sinks of heat were considered, and the heat flux was assumed to occur in the radial direction only (as with the pore fluid flow, this is a reasonable assumption given the aspect ratios of the cylinders

considered). In the following section, an approximate, analytical, closed-form solution for axial strain and internal water pressure development is derived for a concrete cylinder subjected to a change in ambient temperature.

5.4 ANALYTICAL MODEL

5.4.1 Solution for axial strain and internal water pressure

Previously, Scherer (2006) derived the solution for the transformed axial stress and plane strain of an infinite uniaxial loaded cylinder. Nevertheless, the solutions are derived here for the sake of completeness. In cylindrical coordinates, the constitutive equations for an isotropic, poroelastic material experiencing infinitesimal deformation gradients may be presented as

$$\varepsilon_r = \varepsilon_f + \frac{1}{E_p}\left[\sigma_r - \nu_p(\sigma_\theta + \sigma_z)\right], \tag{5.1a}$$

$$\varepsilon_\theta = \varepsilon_f + \frac{1}{E_p}\left[\sigma_\theta - \nu_p(\sigma_r + \sigma_z)\right], \text{ and} \tag{5.1b}$$

$$\varepsilon_z = \varepsilon_f + \frac{1}{E_p}\left[\sigma_z - \nu_p(\sigma_r + \sigma_\theta)\right], \tag{5.1c}$$

where ε_r, ε_θ, and ε_z are radial, tangential, and axial strains, respectively; σ_r, σ_θ, and σ_z are radial, tangential, and axial stress, respectively; E_p is Young's modulus (modulus of elasticity), and ν_p is Poisson's ratio. The linear free strain is presented by ε_f and can be expressed as

$$\varepsilon_f = \frac{pb}{3K_p} + \frac{\alpha_p}{3}\Delta T. \tag{5.2}$$

The linear free strain is one-third of the volumetric strain that developed due to internal pore pressure and the temperature changes. The parameter p is pore fluid pressure; K_p is the bulk modulus of the porous body; α_p is volumetric thermal dilation coefficient of the porous body; b is the Biot coefficient and defined as

$$b = \left(1 - \frac{K_p}{K_s}\right), \tag{5.3}$$

where K_s is the bulk modulus of the solid phase (including the material skeleton). In a porous body, the pore fluid transportation often obeys Darcy's law,

$$J = -\frac{k}{\eta_L}\nabla p, \tag{5.4}$$

where J, k, and η_L are the volumetric fluid flux density, intrinsic permeability of the porous body, and pore fluid viscosity, respectively. Fluid continuity may be expressed in terms of pore pressure, volumetric strain of the porous body (ε), volumetric strain of the solid phase (ε_s), and volumetric strain of the pore liquid (ε_l) as (Scherer 2000b)

$$\phi\dot{\varepsilon}_l + \dot{\varepsilon} + (1-\phi)\dot{\varepsilon}_s = -\frac{k}{\eta}\nabla^2 p, \tag{5.5}$$

where ϕ is porosity and defined as $\phi = \frac{pore\ volume(V_p)}{Total\ volume\ (V)}$; ∇^2 is the Laplacian operator; and the overhead dot denotes a time derivative. Volumetric strain of the porous body, ε, can be defined as

$$\varepsilon = \varepsilon_r + \varepsilon_\theta + \varepsilon_z. \tag{5.6}$$

To determine ε, we have to solve for σ_r, σ_θ, and σ_z. For the cylinder problem, the generalized plane-strain thermoelastic solution for the stress components can be determined from Timoshenko and Goodier (1951) as

$$\sigma_r = -\frac{E_p}{r^2(1-\nu_p)}\int_0^r \varepsilon_f(r) r dr + \frac{E_p}{(1+\nu_p)}\left(\frac{C_1}{1-2\nu_p}\right), \tag{5.7a}$$

$$\sigma_\theta = \frac{E_p}{r^2(1-\nu_p)}\int_0^r \varepsilon_f(r) r dr - \frac{\varepsilon_f(r)E_p}{(1-\nu_p)} + \frac{E_p}{(1+\nu_p)}\left(\frac{C_1}{1-2\nu_p}\right), \text{ and} \tag{5.7b}$$

$$\sigma_z = C_2 - \frac{\varepsilon_f(r)E_p}{(1-\nu_p)} + \frac{2\nu E_p C_1}{(1+\nu_p)(1-2\nu_p)}, \tag{5.7c}$$

where C_1 and C_2 are constants and can be determined from the boundary conditions. The boundary conditions are

$$\sigma_r(r = R) = 0 \tag{5.8}$$

and

$$\langle \sigma_z \rangle = \sigma_{zApp} = 0, \tag{5.9}$$

where R is the radius of the concrete cylinder, $\langle \sigma_z \rangle$ is the spatially averaged axial stress, and σ_{zApp} is the applied force normalized by the cross-sectional area of the cylinder. The first condition requires that the radial stress at the radial surface of the cylinder at r=R is free from any externally applied force. The second condition satisfies the equilibrium condition. In our case, there is no applied stress, resulting in $\sigma_{zApp} = 0$. For a cylinder, the spatially averaged axial stress can be expressed as

$$\langle \sigma_z \rangle = \frac{2}{R^2} \int_0^R \sigma_z(r) r dr. \tag{5.10}$$

Eqs. (5.7a) and (5.8) are used to solve C_1 as

$$C_1 = \frac{(1+\nu_p)(2\nu_p-1)\int_0^R \varepsilon_f(r) r dr}{R^2(\nu_p-1)}, \tag{5.11}$$

whereas Eqs. (5.7c) and (5.9) are used to solve C_2 as

$$C_2 = \frac{2E_p \int_0^R r\varepsilon_f(r) dr}{R^2}. \tag{5.12}$$

Using Eqs. (5.11) and (5.12), Eq. (5.7) can be written as

$$\sigma_r = \frac{E_p}{r^2(\nu_p-1)} \int_0^r \varepsilon_f(r) r dr - \frac{E_p \int_0^R \varepsilon_f(r) r dr}{R^2(\nu_p-1)}, \tag{5.13a}$$

$$\sigma_\theta = \frac{E_p}{r^2(1-\nu_p)} \int_0^r \varepsilon_f(r) r dr - \frac{\varepsilon_f(r) E_p}{(1-\nu_p)} + \frac{E_p \int_0^R \varepsilon_f(r) r dr}{R^2(1-\nu_p)}, \text{ and} \tag{5.13b}$$

$$\sigma_z = \frac{E_p\left(R^2\varepsilon_f(\mathrm{r}) - 2\int_0^R r\varepsilon_f(r) dr\right)}{R^2(\nu_p-1)}. \tag{5.13c}$$

Young's modulus, E_p, can be expressed as

$$E_p = 3K_p(1-2\nu_p). \tag{5.14}$$

Combining Eqs. (5.6), (5.13), and (5.14) allows one to find

$$\varepsilon = \frac{4(2\nu_p-1)\int_0^R r\varepsilon_f(\mathrm{r})\,\mathrm{d}r}{R^2(\nu_p-1)} - \frac{(1+\nu_p)\varepsilon_f(r)}{(\nu_p-1)}. \tag{5.15}$$

If we consider the pore fluid and solid phase to behave linearly elastically with respect to change in pressure and temperature, we may write the constitutive equations as

$$\varepsilon_l = \frac{-p}{K_l} + \alpha_l \Delta T \text{ and} \tag{5.16}$$

$$\varepsilon_s = \frac{-p}{K_s} + \alpha_s \Delta T, \tag{5.17}$$

where α_l and α_s are the volumetric thermal dilation coefficients of the pore liquid and solid phase, respectively; K_l is the bulk modulus of the porous liquid; and ΔT is the temperature difference. Now we can rewrite Eq. (5.5) as a function of dimensionless radius *u*, where $u = r/R$:

$$\phi\dot{\varepsilon}_l + \dot{\varepsilon} + (1-\phi)\dot{\varepsilon}_s = -\frac{k}{\eta_L R^2 u}\frac{\partial}{\partial u}\left(u\frac{\partial p}{\partial u}\right) \tag{5.18}$$

To solve Eq. (5.18), we apply Laplace Transforms to eliminate the time derivative to get

$$\phi s\bar{\varepsilon}_l + s\bar{\varepsilon} + (1-\phi)s\bar{\varepsilon}_s = -\frac{k}{\eta_L R^2 u}\frac{\partial}{\partial u}\left(u\frac{\partial p}{\partial u}\right), \tag{5.19}$$

where the over-bars denote the transformed parameters and *s* is the transformation variable. Details of the Laplace Transformation process are shown in Appendix A. Solving Eq. (5.19), the transformed pore pressure can be expressed as

$$\bar{p}(u) = c_1 J_0\left(\frac{\sqrt{s}u\sqrt{-3K_fK_p+3\phi K_fK_p-3\phi K_sK_p+bK_2K_fK_s}}{\sqrt{3}\sqrt{K_6}\sqrt{K_f}\sqrt{K_p}\sqrt{K_s}}\right) + c_2 Y_0\left(\frac{\sqrt{s}u\sqrt{-3K_fK_p+3\phi K_fK_p-3\phi K_sK_p+bK_2K_fK_s}}{\sqrt{3}\sqrt{K_6}\sqrt{K_f}\sqrt{K_p}\sqrt{K_s}}\right) + \frac{3K_fK_pK_s(sK_1-sK_2K_3-s\phi K_4+s\phi K_5-sK_5)}{bsK_2K_fK_s+3s\phi K_fK_p-3sK_fK_p-3s\phi K_pK_s}\}, \tag{5.20}$$

where J_0 is the Bessel function of the first kind of order zero; Y_0 is the Bessel function of the second kind of order zero; c_1 and c_2 are solution constants that are determined from the boundary conditions; and K_1 through K_6 are constants (shown in Table 5.1).

Table 5.1 List of constants and their expressions

Coefficient	Expression
K_1	$\frac{4(2s\bar{v}_p - 1)\int_0^R r\varepsilon_f(\mathrm{r})\,\mathrm{d}r}{R^2(s\bar{v}_p - 1)}$
K_2	$\frac{(s\bar{v}_p + 1)}{(s\bar{v}_p - 1)}$
K_3	$\frac{\alpha_p}{3}\Delta T$
K_4	$\alpha_l \Delta T$
K_5	$\alpha_s \Delta T$
K_6	$\frac{k}{\eta_L R^2}$

To prevent a singularity in Eq. (5.20) at *u=0,* c_2 has to be equal to zero. The pore pressure at the radial surface of the cylinder (i.e., where $u = 1$) is zero, since the cylinder is placed in a water bath, where the surface of the bath is exposed to atmospheric (approximately zero) pressure. Hence,

$$\bar{p}(u = 1) = 0. \tag{5.21}$$

From Eqs. (5.20) and (5.21), c_1 can be obtained as

$$c_1 = -\frac{3AK_fK_pK_s}{(bK_2K_fK_s+3\phi K_fK_p-3K_fK_p-3\phi K_pK_s)\,I_0(B)}, \tag{5.22}$$

where I_0 is the modified Bessel function of the first kind of order zero. Combining Eqs. (5.20), (5.22), and c_2*=0* results in

$$\bar{p}(u) = \frac{3K_fK_pK_s\left(A-\frac{(A)I_0(uB)}{I_0(B)}\right)}{K_f(bK_2K_s+3(\phi-1)K_p))-3\phi K_pK_s}, \tag{5.23}$$

where *A* and *B* are constants that can be expressed as

$A = K_1 - K_2K_3 - \phi K_4 + (\phi - 1)K_5$ and

$$B = \frac{\sqrt{-\frac{s(K_f(bK_2K_S+3(\phi-1)K_p)-3\phi K_p K_S)}{K_6 K_f K_p K_S}}}{\sqrt{3}}.$$

Spatially average pore pressure ($\langle p \rangle$) can be defined as

$$\langle \bar{p} \rangle = 2\int_0^1 up(Ru)du, \tag{5.24}$$

and may be used to determine the axial strain. Combining Eqs. (5.1c), (5.2), and (5.24) leads to

$$\bar{\varepsilon}_z = \frac{(\nu_p-1)\left(I_0(A)\left(bK_fK_s((\phi-1)K_5-\phi K_4)+3K_3K_p\left((\phi-1)K_f-\phi K_s\right)\right)+bK_fK_s(K_2K_3+\phi K_4-(\phi-1)K_5)\,{}_0\tilde{F}_1\left(;2;-\frac{R^2A^2}{4}\right)\right)}{I_0(A)\left(Kf\left(bK_s\left((\nu_p-1)K_2-4\nu_p+2\right)+3(\nu_p-1)(\phi-1)K_p\right)-3(\nu_p-1)\phi K_pK_s\right)+2b(2\nu_p-1)K_fK_s\,{}_0\tilde{F}_1\left(;2;-\frac{R^2A^2}{4}\right)}, \tag{5.25}$$

where ${}_0\tilde{F}_1$ is the confluent hypergeometric limit function. The Stehfest algorithm was used to perform numerical Laplace Transform inversion (Mallet 2000) of Eqs. (5.23), (5.24), and (5.25) using Mathematica® (Wolfram Research, Inc., 2012) to obtain $p(u,t)$, $\langle p \rangle$, and $\varepsilon_z(t)$, respectively. Axial displacement (ΔL) can be achieved by multiplying the axial strain with the length of the concrete cylinder (L) and can be represented as

$$\Delta L = \varepsilon_z * L. \tag{5.26}$$

5.4.2 Solution for temperature gradient

The heat flow equation for a material with linear constitutive relationships between heat flux and temperature gradient and between the rate of temperature change and the rate of heat increase can be expressed as

$$\nabla^2 T(r,t) - \frac{1}{a}\frac{\partial T(r,t)}{\partial t} = 0, \tag{5.27}$$

where *T(r,t)* is temperature and a is the thermal diffusivity. The presence of any heat sources or sinks has been discounted. As previously mentioned, heat flow in a concrete

cylinder being subjected to heating and cooling cycles can be assumed to be one-dimensional for simplification. Thus, Eq. (5.27) can be written as

$$\frac{1}{r}\frac{\partial}{\partial r}\left(r\frac{T(r,t)}{\partial r}\right)-\frac{1}{a}\frac{T(r,t)}{\partial t}=0. \tag{5.28}$$

Eq. (5.28) can be solved by eliminating the time derivative using the Laplace Transformation and can be expressed as

$$\frac{1}{r}\frac{\partial}{\partial r}\left(r\frac{T(r,t)}{\partial r}\right)-\frac{1}{a}s(\bar{T}(r,s)-T(r,t=0))=0, \tag{5.29}$$

where $T(r,t=0)$ is the initial temperature and will be expressed as T_0. Thermal diffusivity a can be expressed as

$$a=\frac{k_T}{c\rho}, \tag{5.30}$$

where k_T is the thermal conductivity; ρ is the density; and c is the specific heat capacity. By solving Eq. (5.29) we find

$$\bar{T}(r)=Q_1J_0\left(200i\sqrt{30}r\sqrt{s}\right)+Q_2Y_0\left(-200i\sqrt{30}r\sqrt{s}\right)+\frac{T_0}{s}, \tag{5.31}$$

where Q_1 and Q_2 are constants and can be solved using the boundary conditions. To prevent singularity at $r=0$, Q_2 has to be zero. The Bessel function J_0 can be transformed to the Bessel function I_0 by using

$$J_0(\mathrm{x})=I_0(\tfrac{x}{i}). \tag{5.32}$$

Thus, using Eqs. (5.32) and $Q_2=0$, Eq. (5.31) becomes

$$\bar{T}(r)=Q_1I_0\left(200\sqrt{30}r\sqrt{s}\right)+\frac{T_0}{s}. \tag{5.33}$$

At the external radial surface, the concrete temperature will be equal to ambient (external) temperature (T_{ex}) and the boundary condition can be expressed as

$$\bar{T}(r=R)=\bar{T}_{ex}. \tag{5.34}$$

From Eqs. (5.33) and (5.34), Q_1 can be solved as

$$Q_1=\frac{s\bar{\mathrm{T}}_{ex}-\mathrm{T}_0}{sI_0(200\sqrt{30}R\sqrt{s})}. \tag{5.35}$$

By replacing Q_1 in Eq. (5.33), Eq. (5.33) becomes

$$\bar{T}(r) = \frac{I_0(200\sqrt{30}r\sqrt{s})(s\bar{T}_{ex} - \mathrm{T}_0)}{sI_0(200\sqrt{30}R\sqrt{s})} + \frac{\mathrm{T}_0}{s}. \quad (5.36)$$

Spatially averaged temperature ($\langle T \rangle$) for the concrete cylinder can be determined using

$$\langle \bar{T} \rangle = \frac{1}{\pi R^2} \int_0^R 2\pi r \bar{T}(r) dr. \quad (5.37)$$

Eqs. (5.36) and (5.37) were transformed using the Stehfest algorithm (Mallet 2000) in Mathematica® (Wolfram Research, Inc., 2012) to obtain $T(r,t)$ and $\langle T(t) \rangle$.

5.5 MATERIALS

An ASTM C 150 (2012) Type I/II cement and an ASTM C33 (2013) river sand were used for all concrete mixtures. Five coarse aggregates were used for concrete mixtures, including one source of granite (GR), slate (SL), river gravel (RG), a natural blend of river gravel and limestone (RGLS), and rhyolite (RH). Concrete made from these coarse aggregates will be referred to using the name of the aggregate; for example, "concrete SL" is the concrete mixture made from coarse aggregate SL.

5.6 TEST PROCEDURES

Concrete mixtures were proportioned according to the Tex-428-A method (2011). This method specifies a particular gradation for coarse aggregates. Therefore, all the coarse aggregates used in this study were regraded according to Tex-428-A. The concrete mixtures were mixed according to ASTM C192 (2012). The 4-in. x 8-in. (100-mm x 200-mm) cylinders were made with GR, SL, RGLS, and RG, while 6-in. x 12-in. (150-mm x 300-mm) cylinders were made from RH. The modulus of elasticity and porosity were

determined according to ASTM C469 (2010) and ASTM C1754 (2012), respectively. ASTM C1754 is the suggested test method to determine porosity of porous concrete. Therefore, instead of soaking and drying the concrete cylinders for the period specified by ASTM C1754, they were saturated under water and then oven-dried at 110 ± 5°C (230 ± 10°F) until the mass stabilized. Typically, 48 hours was sufficient (soaking or in the oven) to achieve completely saturated or dried concrete samples. The concrete cylinders were trimmed to 7-in. (175-mm) lengths to measure axial deformation due to temperature change. The CTE was calculated from the measured axial length change between the two isothermal states. A programmable water bath was used to change the temperature of the concrete cylinders. A differential variable reluctance transducer (DVRT) was used to measure the axial length change of the concrete cylinders. An Invar frame was used to house the concrete cylinders, with the DVRT placed at the top of the frame. A schematic diagram of the experimental setup is shown in Figure 5.1. One cylinder from each concrete mixture was used to measure the length change due to heating and cooling cycles. One temperature cycle consisted of cooling the cylinder to 10^{o}C (50^{o}F) from room temperature (typically 27^{o}C (80.6^{o}F)), followed by 10 hours of isothermal state at 10^{o}C (50^{o}F), then heating the cylinder to 50^{o}C (122^{o}F), followed by an isothermal state at 50^{o}C (122^{o}F) for 10 hours. After the 50^{o}C (122^{o}F) isothermal state, the sample was cooled to 10^{o}C (50^{o}F). The rate of heating and cooling was 0.33^{o}C/minute (0.60^{o}F/minute) for all experiments, unless otherwise stated. After the cooling ramp, the sample was kept at a 10^{o}C (50^{o}F) isothermal state for 10 hours and then heated to room temperature. Figure 5.2 shows a typical heating and cooling cycle.

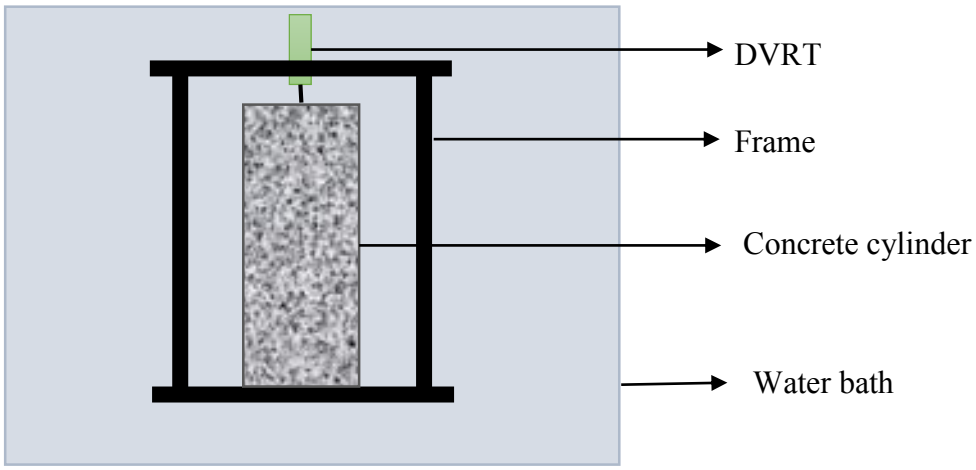

Figure 5.1 Schematic diagram of the experimental setup for measuring axial displacements of concrete cylinders associated with changes in temperature

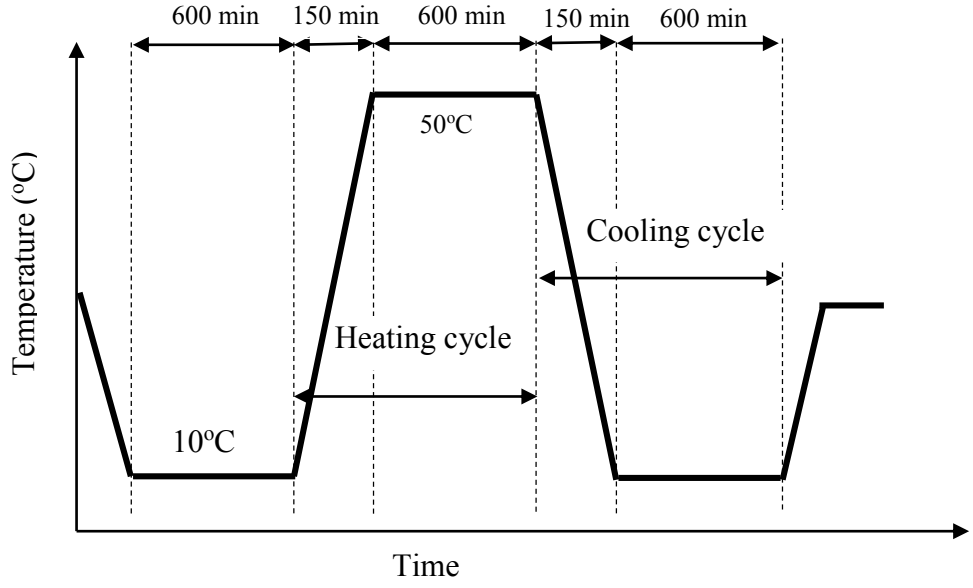

Figure 5.2 A typical heating and cooling cycle

To determine the linear CTE of concrete, length-change readings were measured at two isothermal states: 10°C (50°F) and 50°C (122°F). Concrete samples were kept in an

isothermal state for at least 10 hours prior to length-change measurement to minimize the effect of internal water pressure. The linear CTE of concrete was determined by dividing the difference in length-change reading by the length of the sample and the temperature difference between two isothermal states. This CTE was considered the linear CTE of porous body (α_{Lp}). The properties of cement paste should be same for all concrete because the same cement and concrete proportioning was used for all concrete mixtures. The linear CTE of cement paste was measured according to the method as described previously. From the known CTE of cement paste and concrete, the linear CTE of combined aggregate (coarse and fine) was determined according to the rule of mixtures proposed by Emanuel and Hulsey (1977). The linear CTE of combined aggregate was considered to be the linear CTE of the solid skeleton (α_{Ls}). The volumetric CTEs can be calculated from the linear CTE, which will be discussed in the next section

5.7 PHYSICAL PROPERTIES OF MATERIALS

Table 5.2 represents the measured physical properties of materials. Throughout this study, the Poisson's ratio (ν_p) for concrete was assumed to be 0.2. The bulk modulus of concrete can be determined from Eq. (5.14) and the bulk modulus of the solid phase can be approximated using the following equation (Vichit-Vadakan and Scherer 2002):

$$K_s = \frac{K_p}{(1-\phi)^2}. \tag{5.38}$$

Table 5.2: Experimentally determined properties of concrete samples

Concrete ID	Ep in 10^6 psi (GPa)	ϕ (%)	α_{Lp} in x10^{-6} strain/^{o}F (x10^{-6} strain/^{o}C)	α_{Ls} in x10^{-6} strain/^{o}F (x10^{-6} strain/^{o}C)
GR	4.3 (29.6)	10.4	4.51 (7.51)	4.24 (7.63)
SL	4.5 (31.0)	9.2	6.2 (11.16)	6.17 (11.11)
RGLS	4.0 (27.6)	7.0	5.12 (9.22)	4.94 (8.89)
RG	5.2 (35.6)	8.4	6.07 (10.93)	6.02 (10.84)
RH	3.9 (27.2)	7.5	5.36 (9.38)	5.21 (9.38)
Cement	-	30.0	6.4 (11.52)	-

Typically, in concrete, the pore liquid is a complex solution of water and other dissolved materials. However, in this study pore liquid was considered as water for simplicity. Therefore, the bulk modulus of pore liquid (K_l) was assumed to be 3.2 x10^5 psi (2.2 GPa). Water viscosity changes with temperature and can be represented (Al-Shemmeri 2012) as

$$\eta_L = 2.141 \times 10^{-5} \times 10^{247.8/(T(K)-140)}, \quad (5.39)$$

where $T(K)$ represents the temperature in *K*. The volumetric CTE of the pore fluid (α_l) may be considered water for a water-saturated concrete cylinder and was assumed to be 207 x10^{-6} strain/^{o}C (115x10^{-6} strain/^{o}F). For an isotropic material, the volumetric CTE is three times the linear CTE ($\alpha = 3\alpha_L$). In this study, volumetric CTEs for concrete were calculated from the linear CTEs that were presented previously.

Ai et al. (2001) documented water permeability (k_w) at a range from 4x10^{-11} to 4x10^{-15} in./s (1x10^{-12} to 1x10^{-16} m/s) for cement paste. El-Dieb and Hooton (1995) studied the water permeability of concrete. Their study concluded that concrete's water permeability can vary over a wide range from 8x10^{-11} to 8x10^{-15} in./s (2x10^{-12} to 2x10^{-16} m/s). Intrinsic permeability (k) can be determined from the density of water ρ_w, the

acceleration due to gravity (g), the viscosity of water (η_w), and k_w by using (Grasley et al. 2007):

$$k = \frac{k_w \eta_w}{\rho_w g}. \quad (5.40)$$

Therefore, $k_w(in/s) \approx 10^{10} k(in^2)$. As a result, in this chapter, k will be considered over a range from 15.5x10^{-21} to 15.5x10^{-25} in.^{2} (1x10^{-19} to 1x10^{-23} m^2).

5.8 THERMAL PROPERTIES

Calculated temperature fields depend on the thermal diffusivity (a). Thermal diffusivity in concrete is a function of ρ, k_T, and c. Concrete density (ρ) was assumed to be 150 lb/ft^3 (2400 kg/m^3), which is representative of the typical density of normal concrete. The specific heat capacity of concrete is a function of the properties of concrete constituents, the degree of hydration, and the degree of saturation (De Schutter and Taerwe 1995). The specific heat capacity of normal concrete changes from 275 Cal/kg.^{o}C (1151 J/kg. K) at 6 hours to 215 Cal/kg.^{o}C (888 J/kg.K) at 7 days (Brown and Javaid 1970). Khan et al. (1998) extensively investigated the specific heat capacity of concrete. According to their study, the specific heat capacity varies from 155 to 645 Cal/kg.^{o}C (650 to 2700 J/kg.K) for saturated and 155 to 263 Cal/kg.^{o}C (650 to 1100 J/kg.K) for dry concrete. The typical value for normal concrete ranges from 191 to 287 Cal/kg.^{o}C (800 to 1200 J/kg.K) (Mindess et al. 2002). Therefore, the concrete heat capacity was assumed to be 240 Cal/kg.^{o}C (1000 J/kg.K) throughout this study.

Campbell-Allen and Thorne (1963) experimentally measured k_T of wet concrete at a range from 1.12 to 2.54 B.t.u./ft.hr.^{o}F (1.9 to 4.4 W/m.K). The thermal conductivity of a material dictates how fast the heat flows through the material being subjected to a

temperature gradient. Throughout this chapter, the temperature at the center of the concrete cylinder (r=0) and the ambient temperature will be referred to as the internal and the external temperatures, respectively. The difference between ambient temperature and the temperature at the center of the concrete cylinder is a function of k_T. The k_T can be determined by comparing the experimentally measured and the analytically predicted internal and external temperature difference for a 4-in. (100-mm) concrete cylinder.

Type T thermocouples were used to experimentally measure the internal and external (water) temperatures of the concrete cylinders. A thermocouple was placed at the center (r=0) of a 4-in. x 8-in. (100-mm x 200-mm) concrete cylinder during casting and was later used to measure internal water temperature. Another thermocouple was used to measure the water temperature, which was considered the external temperature. Figure 5.3 shows the predicted temperature for a 4-in. (100-mm) diameter concrete cylinder during a heating cycle; k_T was assumed to be 1.2 B.t.u./(ft.hr.^{o}F) (2.0 W/m.K). The predicted internal and external temperature seemed consistent with the measured internal and external temperature, as shown in Figure 5.4. Figure 5.5 presents the predicted temperature difference between internal and external temperatures for different thermal conductivity levels. Comparing the predicted temperature difference with the measured temperature difference, a thermal conductivity of 1.2 B.t.u./(ft.hr.^{o}F) (2.0 W/m.K) seemed to be a reasonable assumption for concrete. Also, Figure 5.3 to Figure 5.6 illustrate only a small difference between internal and external temperatures, indicating that the average temperature calculated using Eq. (5.21) seemed to track very closely with the boundary condition for a typical concrete. As a result, the temperature gradient was considered

negligible and the calculated average temperature was used as the sample temperature in the analytical (pore fluid pressure) model for simplicity.

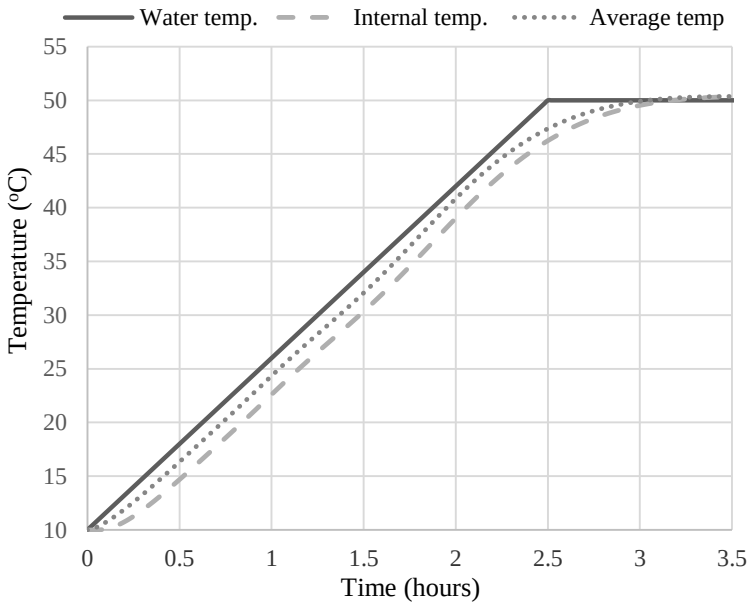

Figure 5.3 Predicted internal (i.e., at *r*=0), external, and spatially averaged temperature of a 4-in. diameter concrete cylinder for a step heating cycle

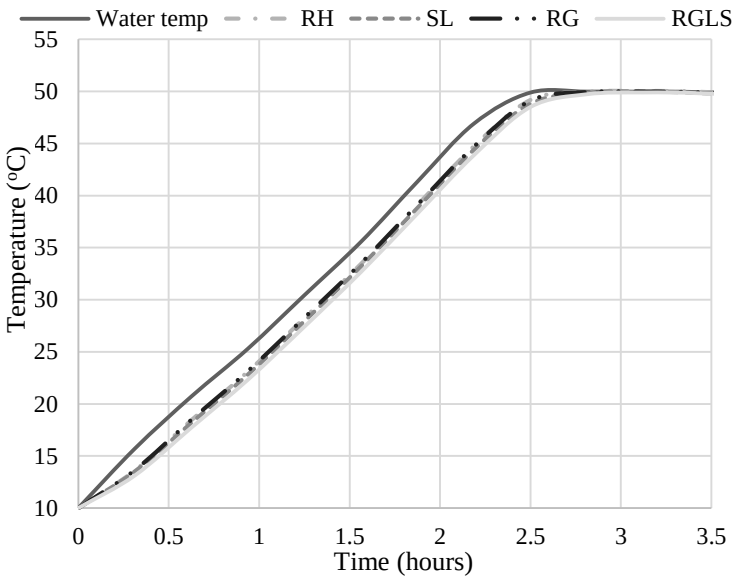

Figure 5.4 Measured internal (i.e., at *r*=0) and external (water) temperature. Note that RH, SL, RG, and RGLS represent the internal temperature of 4-in. diameter concrete cylinders made from these coarse aggregates.

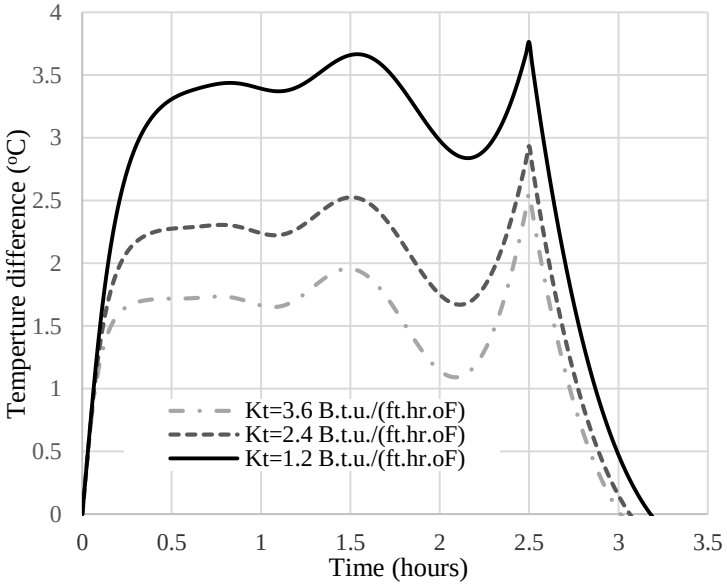

Figure 5.5 Effect of thermal conductivity on the temperature difference between internal (i.e., at *r*=0) and external temperature

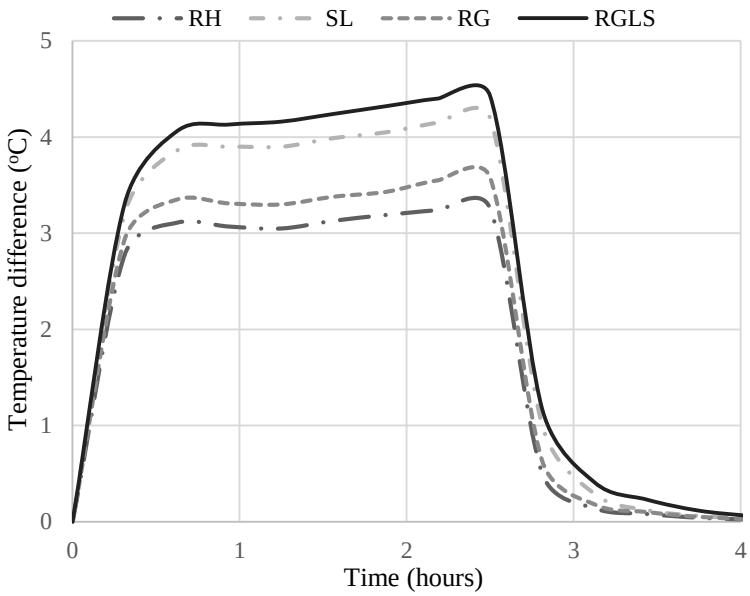

Figure 5.6 Measured temperature difference between internal (i.e., at *r*=0) and external temperature. Note that RH, SL, RG, and RGLS represent the internal and external temperature difference of 4-in. diameter concrete cylinders made from these coarse aggregates.

5.9 RESULTS AND DISCUSSION

This section will describe the robustness of the presented model to predict the axial strain and internal water pressure development of saturated concrete cylinders while subjected to temperature change. The calculated axial strain from the measured deformation will be called measured axial strain throughout this study. First, the model was validated by comparing the measured and predicted axial strains for 4-in. (100-mm) concrete cylinders while subjected to heating cycles. The effects of various parameters—including porosity, permeability, rate of temperature change, and concrete cylinder diameter—on the predicted average axial strain and internal water pressure were determined.

5.9.1 Model validation

Figure 5.7 shows the comparison between the axial stain determined from experimentally measured (M) axial deformation and analytically predicted (P) average axial strain for SL, RGLS, and GR during a heating cycle. The intrinsic permeabilities of these concrete samples were unknown and assumed to be 9.7 $x10^{-18}$, 6.45 $x10^{-18}$, and 1.3 $x10^{-19}$ $in.^2$ (1.5 $x10^{-22}$, 1 $x10^{-22}$, and 2 $x10^{-22}$ m^2) for SL, RGLS, and GR, respectively. The assumed permeability was within the typical range of permeability, as discussed previously. From the visual observation, it may be concluded that the proposed model predicted axial strain during the heating cycle with good accuracy. Moreover, the proposed model captured the time-dependent behavior of the axial strain during the isothermal state with reasonable precision.

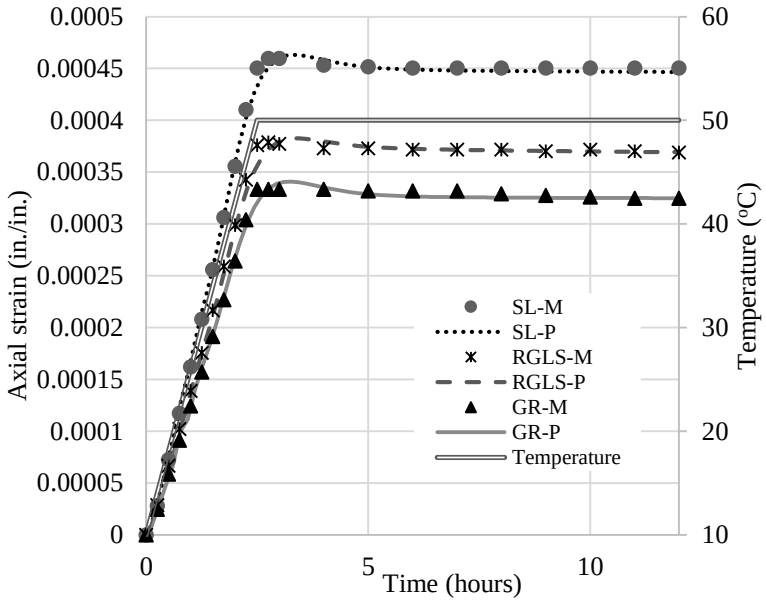

Figure 5.7 Comparison between measured and predicted axial strain for 4-in. diameter concrete cylinder during a heating cycle

Figure 5.8 presents the predicted average internal water pressure development for SL, RGLS, and GR during a heating cycle. The peak predicted average internal water pressure for SL was the highest, about 700 psi (4.8 MPa), and RGLS had the lowest: about 600 psi (4.1 MPa). The predicted average internal water pressure increased with increasing temperature and reached the peak about one hour after the initiation of the isothermal state. After reaching the peak, the pressure started to dissipate and the rate of pressure dissipation was higher for concrete with higher permeability. It should be noted from Figure 5.8 that after 10 hours of isothermal state, the internal water pressure for SL and GR completely dissipated; however, that was not the case for RGLS. The RGLS had the lowest porosity and the lowest permeability. Even though RGLS had the lowest pore water volume (i.e., lowest porosity), the internal water pressure took longer to dissipate than in other samples, thus showing the significant influence of permeability on internal water pressure dissipation. The development of internal water pressure in a concrete sample during temperature change might partially explain the inconsistent nature of the CTE test procedures. Further discussion about the effects of porosity and permeability on the predicted average pressure will be presented in later sections.

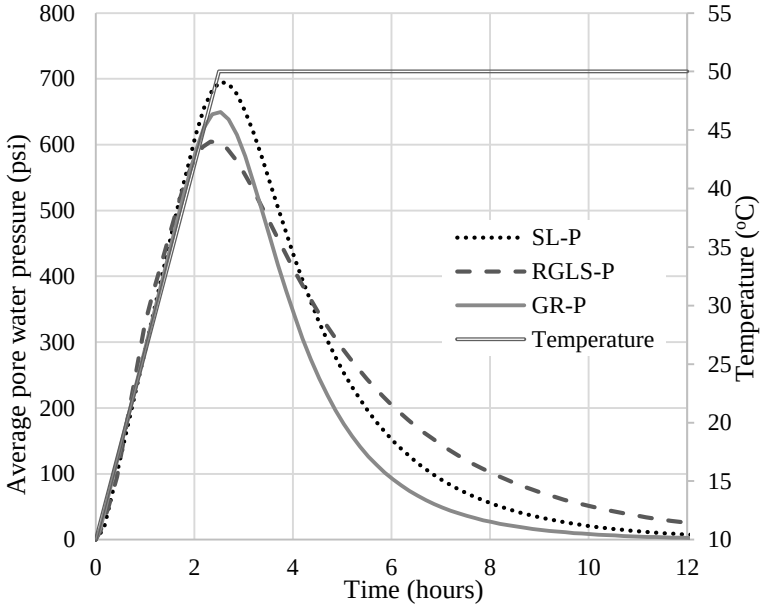

Figure 5.8 Predicted average internal water pressure development for 4-in. diameter concrete cylinders during a heating cycle

Figure 5.9 shows the predicted internal water pressure envelope for a 4-in. (100-mm) diameter concrete cylinder for RGLS during a heating cycle. There was no internal water pressure at the initiation of temperature change (i.e., temperature difference was 0°C (0°F)). The internal water pressure increased with the increasing temperature and reached the peak about one hour after the onset of the isothermal period and dissipated gradually with time. The highest internal water pressure was observed at the center of the cylinder (r/R=0) and decreased gradually to zero pressure at the outer surface of the cylinder (r/R=1), because near the outer surface water flowed out to the exterior as soon as the pressure developed.

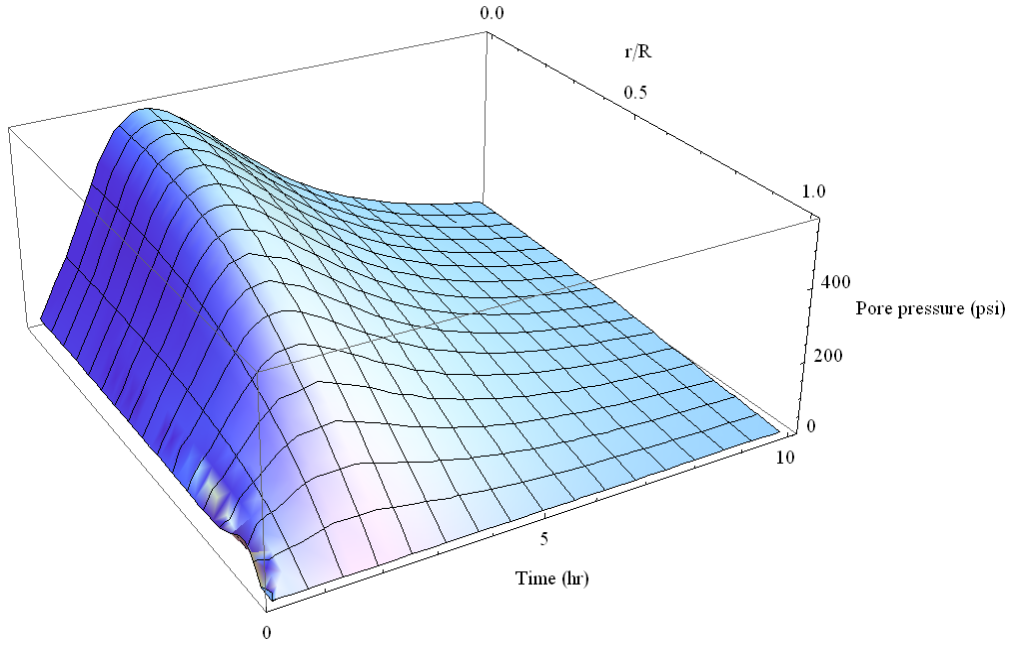

Figure 5.9 Predicted internal water pressure envelope for a 4-in. diameter RGLS concrete cylinder during a heating cycle

5.9.2 Effect of porosity

Figure 5.10 and Figure 5.11 show the effect of porosity on the predicted average axial strain and average internal water pressure, respectively, for a 4-in. (100-mm) RGLS concrete cylinder, while keeping the other parameters unchanged. The peak average axial strain and the peak average internal water pressure increased with the increasing porosity. Saturated concrete samples with higher porosity tend to have higher volumes of water. Due to the difference in CTE between liquid and solid phases, the concrete samples with high porosity developed more internal water pressure than did the concrete samples with low porosity. Consequently, higher internal water pressure resulted in higher axial strain. For 0% porosity, there was no internal water pressure development, which was also reflected in the average axial strain, as virtually no strain change was observed at the isothermal

state. The slight hump in the average axial strain at the onset of the isothermal state was due to the use of predicted spatially averaged temperature in the model instead of actual temperature, as shown in Figure 5.3. The slope of predicted axial strain vs. time for the heating ramp increased with increasing porosity, as can be seen in Figure 5.10. Higher porosity also resulted in higher average axial strain at the isothermal state at a given time. The axial strain gradually dissipated with time to equilibrium. Concrete samples with the lowest porosity reached axial strain equilibrium more rapidly than did samples with higher porosity, having the same permeability. As stated previously, higher porosity in a saturated concrete sample means a higher volume of internal water, which needs more time to flow to the exterior if the permeability remains same. Similar trends can be observed for the predicted average internal water pressure.

The average peak axial strain increased along with increasing porosity. The difference between peak average axial strain for 0 and 10% porosity was smaller than the difference between 20 and 30% porosity, and the difference between peak average axial strain for 10 and 20% porosity lies in between. The opposite trend was observed for the average predicted internal water pressure. The difference in peak average predicted internal water pressure for 0 and 10% porosity was the highest and the difference between 20 and 30% porosity was the lowest.

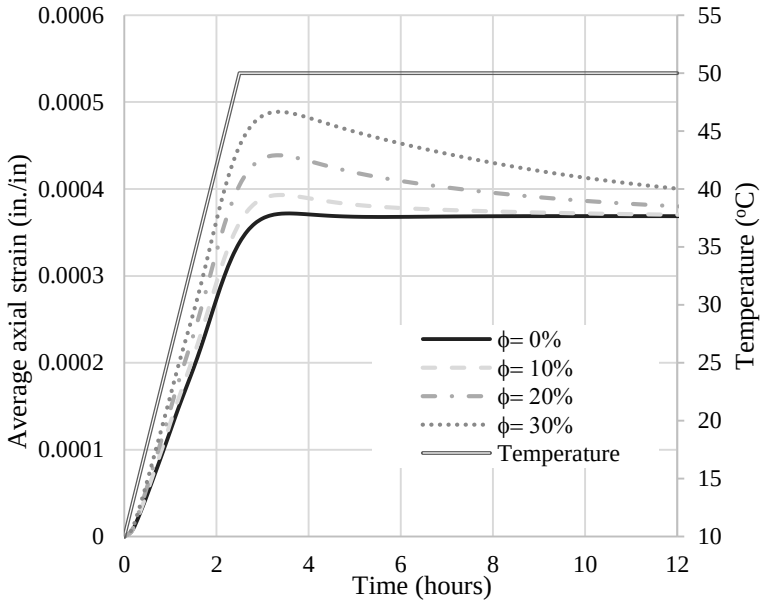

Figure 5.10 Effect of porosity on the predicted average axial strain for 4-in. RGLS concrete cylinder during a heating cycle

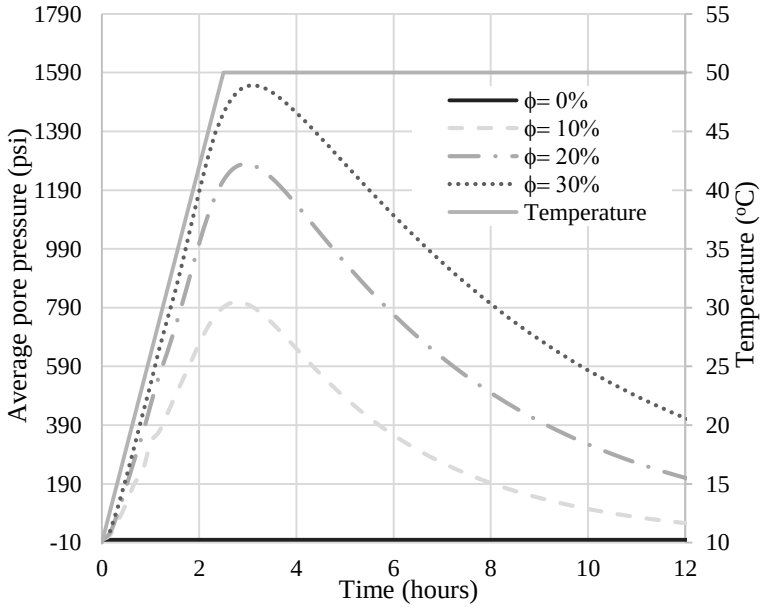

Figure 5.11 Effect of porosity on the predicted average internal water pressure for a 4-in. RGLS concrete cylinder during a heating cycle

5.9.3 Effect of permeability

Three different permeabilities for RGLS—1.55 x 10^{-18}, 1.55 x 10^{-19}, and 1.55 x 10^{-20}–in.^{2} (1.0 x10^{-21}, 1.0 x10^{-22}, and 1.0 x10^{-23} m^2)—were considered for predicting the average axial strain and the internal water pressure, while keeping other parameters unchanged. Figure 5.12 and Figure 5.13 illustrate the effect of permeability on the predicted average axial strain and internal water pressure, respectively, for a heating cycle. Similar to the porosity, the permeability affected the rate of internal water pressure increase with time during a heating ramp. However, no significant effect of permeability on the rate of axial strain increase with time was observed. The permeability had very little effect on the peak average axial strain at a range from 1.55 x10^{-19}–in.^{2} (1.0 x10^{-22} m^2) to 1.55 x10^{-20}–in.^{2} (1.0 x10^{-23} m^2); however, at a range from 1.55 x10^{-19}–in.^{2} (1.0 x10^{-22} m^2) to 1.55 x10^{-18}–in.^{2} (1.0 x10^{-21} m^2), the effect of permeability on the peak average axial strain was more significant. The effect of permeability on the peak average axial strain was not as significant as the effect of porosity. However, the permeability significantly affected the peak average internal water pressure. The peak average pressure increased from about 150 psi (1.0 MPa) for 1.55 x10^{-18}–in.^{2} (1.0 x10^{-21} m^2) to 700 psi (4.8 MPa) for 1.55 x10^{-20}–in.^{2} (1.0 x10^{-23} m^2) concrete permeability. Probably the most significant effect of permeability can be observed in the rate of the internal water pressure dissipation and the strain recovery at isothermal state. Internal water pressure for 1.55 x10^{-18}–in.^{2} (1.0 x10^{-21} m^2) dissipated to zero at about 1.5 hours after the onset of the isothermal state, whereas for 1.55 x10^{-19}–in.^{2} (1.0 x10^{-22} m^2) the internal water pressure dissipated nearly to zero after about 10 hours of isothermal state. However, no significant internal water pressure dissipation was observed for 1.55 x10^{-20}–in.^{2} (1.0 x10^{-23} m^2) even after 10 hours of isothermal state. Water can flow

into and out of concrete cylinders at a higher rate in cylinders with higher permeability, which helps to dissipate developed internal water pressure and strain recovery at a faster rate than in cylinders with low permeability.

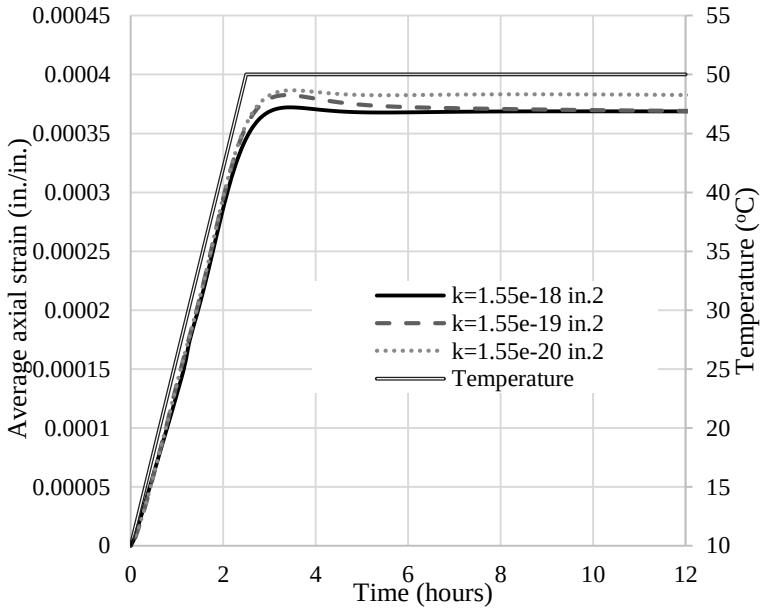

Figure 5.12 Effect of permeability on the predicted average axial strain for 4-in. RGLS concrete cylinder during a heating cycle

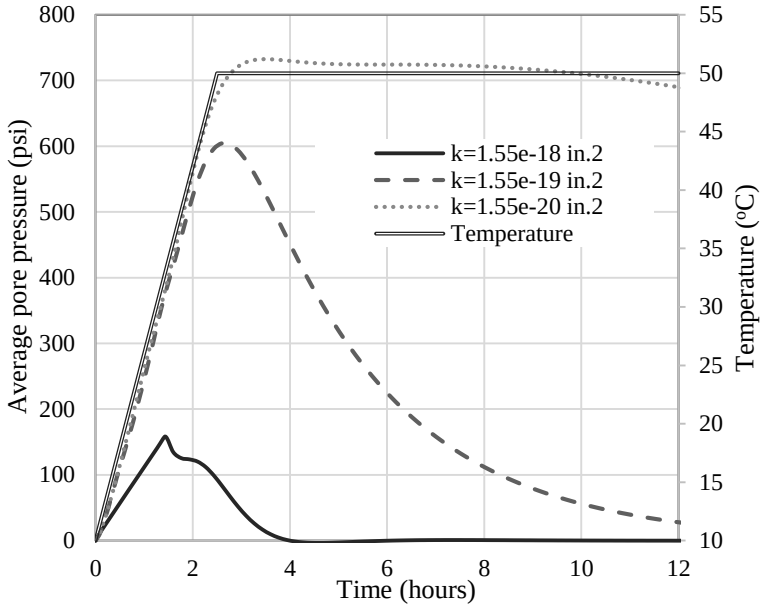

Figure 5.13 Effect of permeability on the predicted average internal water pressure for 4-in. RGLS concrete cylinder during a heating cycle

Laboratory experiments were performed on uncracked (UC) and pre-cracked (PC) samples to evaluate the effect of porosity and permeability. Three different concrete mixtures were used: RGLS, GR, and RG. Concrete cylinders were pre-cracked at 28 days by applying 75% of the 28-day ultimate compressive strength on 4-in. x 8-in. (100-mm x 200-mm) uncracked concrete cylinders. Pre-cracking introduces a new network of cracks that may increase the porosity of the concrete. The porosities of cracked concrete samples were determined experimentally. It was observed from the laboratory test results that there was a 0.5–1.0% increase in porosity for the cracked concrete samples as compared to the uncracked samples. More importantly, new cracks may establish better connections between the internal pore networks and probably connect more isolated pores to the existing pore networks. In addition, cracking may also provide more outlets for the pore water to flow into and out of the concrete cylinders. Better connection between pores and

additional outlets for the pore water flow may increase concrete's permeability. Grasley (2006) indicated that micro-cracking could easily increase the permeability by an order of magnitude. Increased porosity will increase the peak and rate of increase of both internal water pressure and average axial strain. On the other hand, higher permeability decreases the internal water pressure and the axial strain. It should be noted that the effect of porosity on the internal water pressure and the axial strain development is much more predominant than that of permeability. Therefore, a small increase in porosity might have more effect on the internal water pressure and axial stain development than would a larger increase in permeability. Figure 5.14 presents the measured axial strain for both PC and UC saturated concrete cylinders during a heating cycle. The experimental results can be explained with the help of the proposed model, as described in the previous two sections. If the effect of the increased permeability is greater than the effect of increased porosity in concrete cylinders, the overall axial strain should be lower for PC than UC concrete, as can be seen for GR in Figure 5.14. If the effects of both increased porosity and permeability are very similar and cancel out each other, the strain profile should be almost similar for both UC and PC samples, which can be explained by the axial strain development for RG, where axial strain profiles were almost the same for concrete samples both before and after pre-cracking. The RGLS concrete showed higher axial strain development for the PC sample than for the UC concrete, because the effect of increased porosity was greater than the effect of increased permeability.

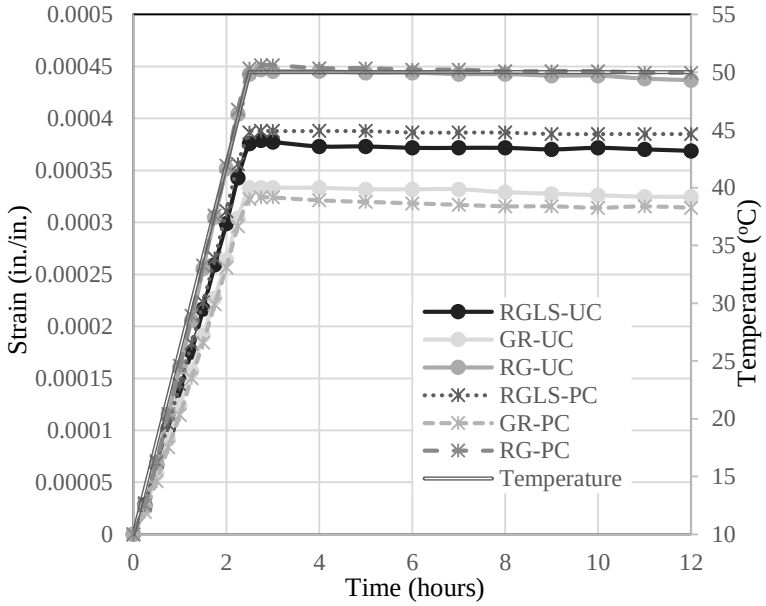

Figure 5.14: Measured axial strain for 4-in. concrete cylinders before and after pre-cracking during a heating cycle

5.9.4 Effect of rate of temperature change

Three different heating rates—0.27, 0.18, and 0.09 ºC/min. (0.49, 0.23, and 0.16 ºF/min.)—were used to predict the average axial strain and internal water pressure for RGLS. Figure 5.15 and Figure 5.16 present the effect of rate of temperature change on the predicted and measured axial strain and predicted internal water pressure development, respectively, for a 4-in. (100-mm) diameter concrete cylinder. Lower rates of heating decreased the peak average internal water pressure, but did not significantly affect the average peak axial strain. The rate of average axial strain and internal water pressure decreased with the decreasing rate of temperature change. The lower rate of temperature change reduced the rate of volume change of solid and liquid phase in a concrete system, thus reducing the rate of pressure increase and rate of axial strain development and allowing

more time for accumulated pressure to dissipate. It can also be noted from Figure 5.15 that the axial strain predicted by the proposed model matched well with the calculated axial strain from the measured axial displacement, which demonstrates the robustness of the developed model for predicting axial strain for concrete samples undergoing varying rates of temperature change.

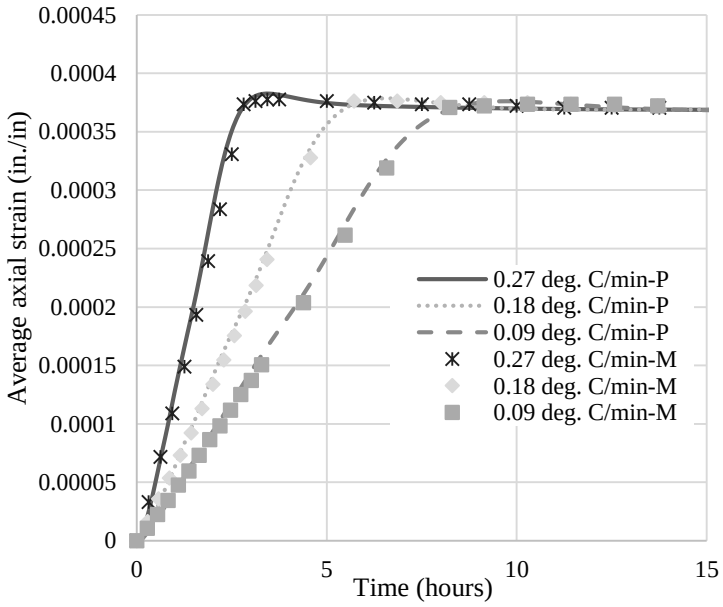

Figure 5.15 Effect of rate of temperature change on the axial strain for 4-in. RGLS concrete cylinder. In the legend, P and M represent the axial strain predicted by the proposed model and the axial strain calculated from the measured axial displacement, respectively.

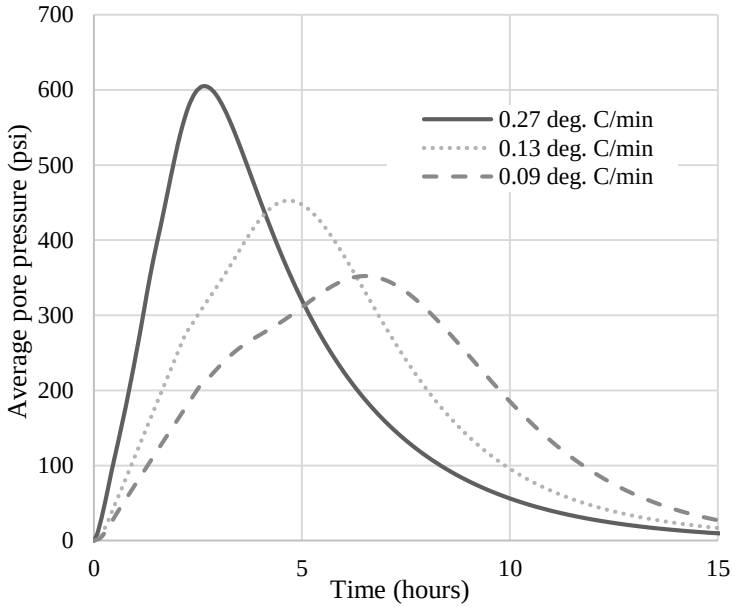

Figure 5.16 Effect of rate of temperature change on the predicted average internal water pressure for a 4-in. RGLS concrete cylinder

5.9.5 Effect of cylinder diameter

In the laboratory, both 6- and 4-in. (150- and 100-mm) diameter concrete cylinders are typically used for CTE testing, although the 4-in. (100-mm) diameter cylinders are preferable. Figure 5.17 and Figure 5.18 show the effect of concrete cylinder diameter on the predicted average axial strain and internal water pressure, respectively, during heating cycles. The rate of average axial strain and internal water pressure increase was higher for the 4-in. (100-mm) diameter cylinders than for the 6-in. (150-mm) diameter cylinders. The peak axial strains for both sizes were almost similar, but the peak average predicted internal water pressures were slightly higher for 6-in. (150-mm) diameter cylinders than for 4-in. (100-mm) diameter cylinders. The 4-in. (100-mm) concrete cylinders reached thermal equilibrium much faster than the 6-in. (150-mm) cylinders. However, it would take more

time for the pore water to move into and out of a 6-in. (150-mm) cylinder than for a 4-in. (100-mm) cylinder. As a result, more internal water pressure was developed and the axial strain at isothermal state was higher for 6-in. (150-mm) cylinders than for 4-in. (100-mm) cylinders.

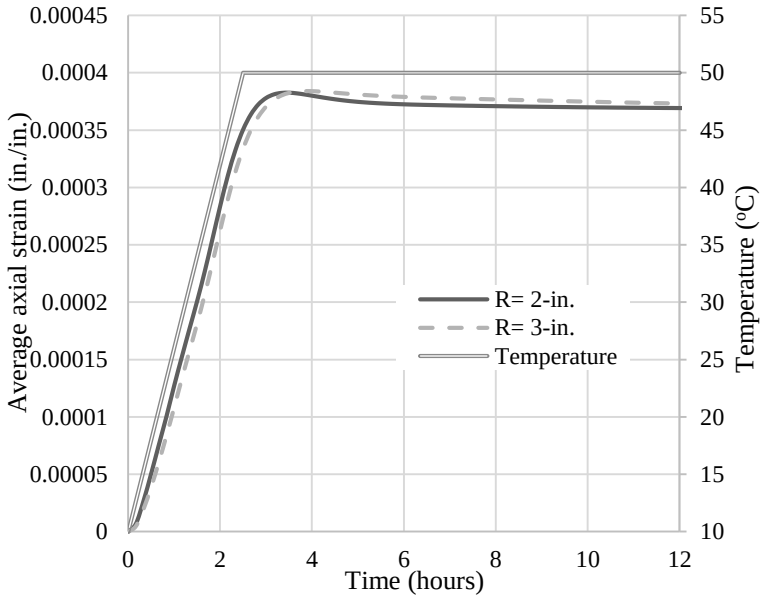

Figure 5.17 Effect of concrete cylinder diameter on the predicted average axial strain for RGLS during a heating cycle

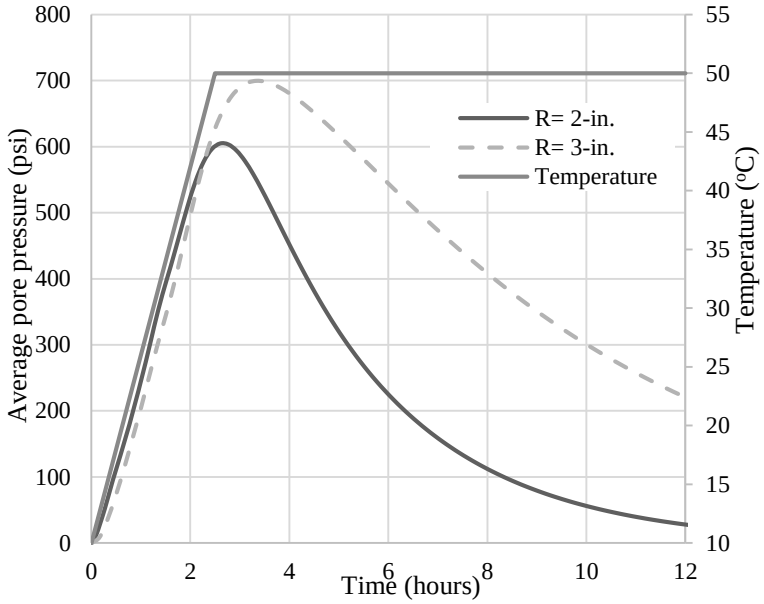

Figure 5.18 Effect of concrete cylinder diameter on the predicted average internal water pressure for RGLS during a heating cycle

Figure 5.19 presents the experimental and predicted differences in axial strain between a 6-in. (150-mm) and a 4-in. (100-mm) concrete cylinder for RH. First, the axial strain was determined from a 6-in. (150-mm) cylinder; then a 4-in. (100-mm) cylinder was cored from the 6-in. (150-mm) cylinder and later used for measuring axial strain. Permeability was assumed to be 3.10 x10^{-19}–in.^{2} (2.0 x10^{-22} m^2), which was determined via the trial-and-error method by fitting the experimental axial strain with the predicted axial strain for 4-in. (100-mm) cylinder. The predicted differences from the model matched very well with the experimental differences up to the onset of the isothermal state, except for the period from 1 to 2 hours. The deviation of the experimental values from the predicted values during the isothermal state and at the second hour cannot be readily explained. However, vibration of the water bath and/or error associated with the DVRT might be possible reasons.

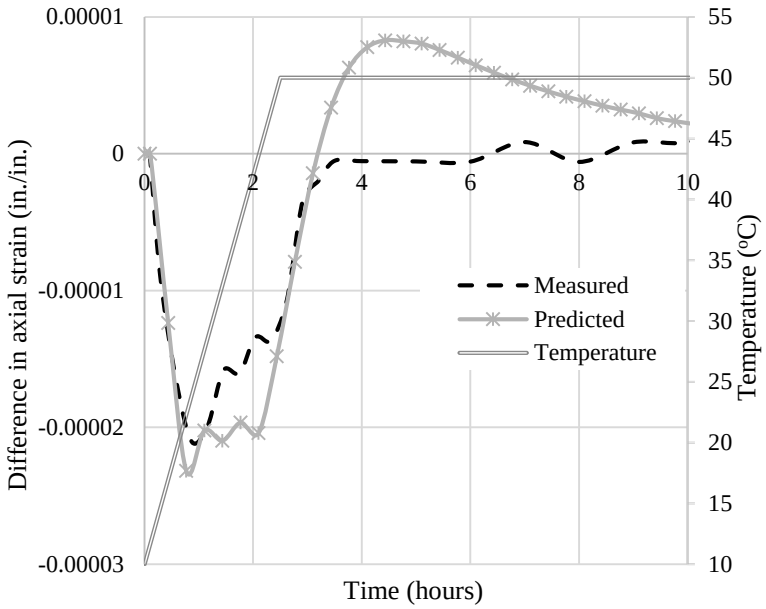

Figure 5.19 Predicted and experiment axial strain differences between 6-in. and 4-in. diameter RH concrete cylinders during a heating cycle

5.10 EXPLANATION OF INCONSISTENCY IN CTE TESTING PROCEDURE

From the above discussion, it is possible to explain the inconsistency of the CTE test procedure. The same temperature cycle was used while predicting the effect of porosity and permeability on the axial strain and internal water pressure development. Therefore, the effect of porosity and permeability as a function of time can be translated to a function of temperature. Hence, it can be concluded from Sections 5.9.2 and 5.9.3 that the slope of axial strain vs. temperature curve increased with increasing porosity for concrete with the same constituents. Moreover, higher porosity leads to higher strain development between two extreme isothermal temperatures. However, permeability had little effect on the slope of the strain vs. temperature curve, but yielded higher strain development between two

extreme isothermal temperatures. As explained in Chapter 4, the CTEs determined by the TxDOT and AASHTO methods are a function of the rate of change of axial strain and the difference in strain development at isothermal temperatures, respectively. Therefore, the TxDOT and AASHTO CTEs are affected by the change in porosity and permeability, which also explains why the TxDOT method obtains a higher CTE than does the AASHTO method. Moreover, higher porosity may lead to higher CTEs for both TxDOT and AASHTO. Conversely, higher permeability may result in the lower AASHTO CTE and might not have any effect on the TxDOT CTE. The porosity and permeability of concrete cylinders depend on the compaction of fresh concrete during casting, which typically varies from cylinder to cylinder and thus affects the CTE results. Hydration is another parameter that affects the porosity and permeability. Generally, with time, more hydration product develops and reduces the porosity and permeability, which explains why CTE values vary with the age of concrete. Degree of hydration at a given age is also dependent on the type of cementitious materials used, curing type, and curing temperature. Therefore, different cementitious materials as well as curing type and curing temperature might affect the measured CTE. As discussed in Section 5.9.5, smaller diameter concrete cylinders had higher rates of axial strain development, which might result in the higher TxDOT CTE; however, larger diameter concrete cylinders showed higher strain differences between two extreme isothermal temperatures, which might result in a higher AASHTO CTE.

5.11 ADVANTAGES AND DISADVANTAGES OF THE AASHTO AND TxDOT CTE TEST METHODS

During the study, the following advantages and disadvantages of the AASHTO and the TxDOT methods were observed:

- The TxDOT CTE was more affected by the internal water pressure than was the AASHTO CTE. Therefore, the TxDOT method yielded higher CTE values than the AASHTO method.
- Internal water pressure is dependent on the rate of temperature change. Therefore, both the TxDOT and the AASHTO CTEs are affected by the rate of temperature change. For a lower rate of temperature change, internal water pressure is lower, which yields lower overall length change and results in a lower rate of length change with respect to temperature change. Both the AASHTO and TxDOT CTEs are proportional to the overall length change and rate of length change with temperature change, respectively. As a result, the CTEs obtained from both the AASHTO and TxDOT methods should be lower given a lower rate of temperature change than for a relatively higher rate of temperature change.
- Length change at the isothermal state is time dependent due to the dissipation of internal water pressure. Therefore, the AASHTO CTE depends on the time interval between the onset of the isothermal state and the measurement of the isothermal length change. The AASHTO CTE decreases with the increasing time interval between the onset of the isothermal state and the measurement of the isothermal length change for a given concrete sample and rate of temperature change.

- The TxDOT method specifies a maximum rate of temperature change, which does not address the variability that might occur if variable rates of temperature change are used for heating and cooling cycles. Therefore, an explicit rate of temperature change is recommended to minimize the effect of internal water pressure and prevent the variability in measured CTE that might result from a variable rate of temperature change.
- The AASHTO method would benefit from a specified rate of temperature change; however, a greater benefit can be achieved by specifying the time interval between the onset of the isothermal state and the measurement of the isothermal length-change reading. A substantial time interval is recommended, which allows enough time to achieve a significant amount of TDD.
- It can be concluded that the TxDOT CTE values are more repeatable than the AASHTO CTE values because the TxDOT CTE value is affected only by the rate of temperature change, whereas the AASHTO method is affected by both rate of temperature change and time dependency of the measured length-change readings.

5.12 CONCLUSIONS

An approximate analytical model was developed for the axial strain and internal water pressure development in a concrete cylinder as a function of temperature change and material properties. Next, a brief sensitivity analysis was performed to determine the effect of various material properties on the axial strain and internal water pressure development in a concrete cylinder being subjected to temperature change. Finally, the causes of the

inconsistency of the CTE test methods were discussed in terms of material properties. Following are this study's major findings:

- The proposed analytical model can predict the axial strain development of saturated concrete specimens due to temperature change with good precision, which was confirmed by comparing the predicted axial strain with the experimental results.
- The presented analytical method can predict the internal water pressure development for concrete cylinders subjected to temperature change as a function of radial distance from the center and time.
- Significant internal water pressure can develop in saturated concrete samples due to temperature change. Concrete porosity, permeability, rate of temperature change, and sample diameter affect the axial strain and internal water pressure. Among these physical properties, porosity has the most significant effect on both the axial strain and the internal water pressure development.
- The proposed model confirmed that internal water pressure development (due to the difference in the CTEs of the liquid and solid phases) causes the TxDOT method to yield higher CTEs than the AASHTO method.
- The findings also explain the effect that the sample's age, type of cementitious materials used, and specimen size have on the measured CTE of concrete.

Chapter 6: Methods to Improve the Test Procedures for Coefficient of Thermal Expansion

6.1 INTRODUCTION

As described previously, current coefficient of thermal expansion (CTE) test techniques are sometimes noted for high variability. Internal water pressure and delay in thermal equilibrium have been identified as possible causes for this variability (Sellevold and Bjøntegaard 2006; Siddiqui and Fowler 2013a, 2014; Tanesi et al. 2013). This chapter will present techniques that have the potential to reduce the effect of internal water pressure and, as a result, improve the consistency of CTE test results.

6.2 COEFFICIENT OF THERMAL EXPANSION TEST PROCEDURES

The CTE of concrete is usually determined by measuring the length change of a water-saturated concrete cylinder over a known temperature change. The saturated concrete cylinders are subjected to heating and cooling cycles. Each temperature cycle has four segments that include an isothermal state at the lowest and highest temperatures, a heating ramp, and a cooling ramp. Figure 6.1 depicts typical heating and cooling cycles. Figure 6.1(a) presents a heating and cooling cycle that first cools concrete samples from room temperature, followed by an isothermal state at low temperature, a heating ramp, an isothermal state at high temperature, a cooling ramp, and a return to the isothermal state at low temperature. Figure 6.1(b) then presents an alternate method for heating and cooling cycles. Both these heating and cooling sequences are used in CTE testing; however, the former heating and cooling sequence is more popular.

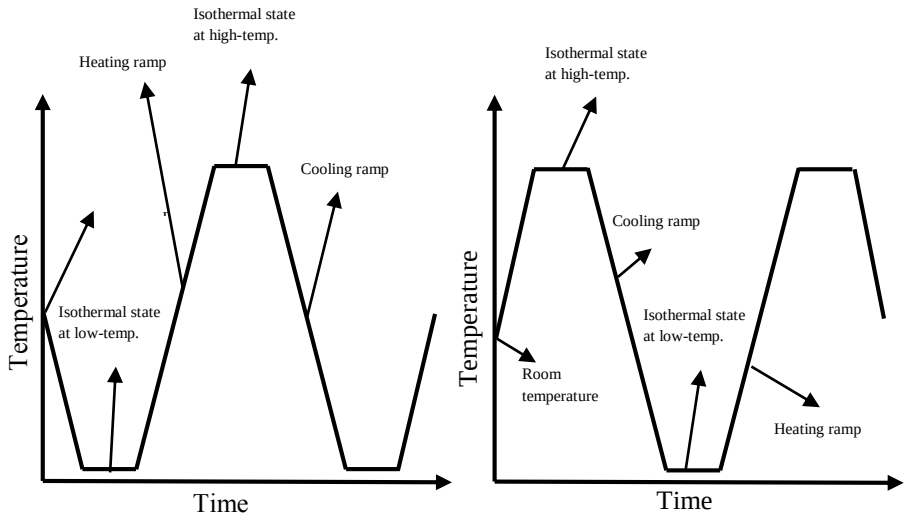

(a) Method 1 (b) Method 2

Figure 6.1 Components of heating and cooling cycles in CTE testing

Generally, length changes (one length change for the heating and one for the cooling cycle) of a concrete cylinder are measured between isothermal states at high and low temperature. The CTE is calculated by dividing the average length change by the length of the sample and the total temperature change. The American Association of State Highway and Transportation Officials (AASHTO) adopted this CTE calculation technique (AASHTO T 336-11 2011), and it is often referred to as the AASHTO method. Typically, it takes some time for the concrete samples to reach a stable length in an isothermal state. This is due both to the delay of thermal equilibrium and the effect of internal water pressure (Sellevold and Bjøntegaard 2006; Siddiqui and Fowler 2013a, 2014; Tanesi et al. 2013). According to the AASHTO method, length-change equilibrium at isothermal state is reached when three consecutive length readings at 10-minute intervals were same. However, concrete samples do not reach true length stability (zero length-change of the

concrete cylinder) in an isothermal state even after 10 hours, as shown in Section 4.5.4. Another version of this CTE calculation technique was proposed by Won (2005). According to this method, instead of taking length-change reading at two extreme isothermal states, length changes are taken as a function of temperature during the heating and cooling ramps. The CTE is calculated from the slope of the best-fit straight line for the length change vs. temperature curve. Further details on this calculation technique can be obtained elsewhere (Won 2005). This method was later adopted by the Texas Department of Transportation (TxDOT) and is known as the TxDOT method (Tex-428-A 2011). Although there are other CTE test procedures available, these two methods are the most popular for determining concrete CTE due their simplicity. In this chapter, concrete CTEs were measured using these two methods.

6.3 MATERIALS

Twenty coarse aggregate sources were tested in this study; 11 were naturally available aggregate sources, and nine of them were laboratory blends. Two aggregate sources were collected from each of five TxDOT districts: Atlanta, Houston, Amarillo, Paris, and Wichita Falls. Only one source of coarse aggregate was collected from the Dallas district. Four of the coarse aggregates were siliceous river gravel (RG), two were natural blends of siliceous and limestone gravel (RGLS), and one source each consisted of granite (GR), rhyolite (RH), sand stone (SS), slate (SL), and limestone (LS). Further details about the coarse aggregate sources can be found in Section 4.3. An ASTM C150 (2012) Type I/II cement and an ASTM C33 (2013) river sand were used for all concrete mixtures. Each coarse aggregate was regraded according to Tex-428-A (2011) to a specific gradation to

eliminate the effect of variable aggregate gradation. Concrete was proportioned according to Tex-428-A (2011). The same coarse aggregate gradation, fine aggregate, cement type, and concrete mixture design was used to eliminate the effect of other parameters (such as water-to-cement ratio, volumes of coarse and fine aggregates, and cement paste volume).

6.4 TEST PROCEDURES

Concrete was mixed and cylinders were made according to ASTM C192 (2012). Two 4-in. x 8-in. (100-mm x 200-mm) cylinders were made from each concrete mixture. The cylinders were resized to 4-in. x 7-in. (100-mm x 175-mm) for CTE testing. Resized cylinders were then submerged underwater for at least 48 hours to achieve practically complete saturation. Complete saturation is important to minimize the effect of moisture content on the CTE of concrete. The saturated samples were then placed in a metal frame for CTE testing. Differential variable reluctance transducers (DVRTs) were used as length-change measuring devices. The DVRTs were physically nulled at room temperature before being placed into the water bath. A programmable water bath was used and the cylinders were subjected to heating and cooling cycles at a range of 10 to 50^{o}C (50 to 122 ^{o}F). A typical heating and cooling cycle used for CTE testing was shown in Figure 4.1. Generally, a 60-minute isothermal state is sufficient to reach AASHTO's length-change equilibrium requirement. However, the length of the isothermal state was increased if a stable length was not achieved within the 60-minute period. Each concrete cylinder was subjected to three cycles of heating and cooling. Concrete CTEs were measured according both to the AASHTO and TxDOT methods. For the AASHTO method, CTE was measured from the second heating and cooling cycle. A correction factor was determined to account for the

thermal movement of the frame by a metal cylinder with known CTE. The difference between the known CTE and the measured CTE is the correction factor. Correction factors were re-determined at 1-month intervals to minimize the effect of any small errors that may have occurred as a result of the testing equipment. The two concrete cylinders made from each mixture were tested for CTE, and the average of the two cylinders was deemed that mixture's CTE.

6.5 RESULTS AND DISCUSSION

According to the analytical model presented in Chapter 5, porosity, permeability, sample dimensions, and the rate of temperature change affect the internal water pressure development in concrete samples subjected to temperature change. Internal water pressure can be reduced by reducing porosity, increasing permeability, using a smaller sample size, and lowering the rate of temperature change. It might not be practical to reduce the porosity of a concrete sample. Moreover, using concrete cylinders smaller than 4-in. (100-mm) in diameter is probably not suitable to produce representative samples for typical coarse aggregate gradation. Therefore, in this study, increasing permeability by pre-processing and reducing the rate of temperature change were evaluated as potential techniques to reduce the internal water pressure. Reducing the internal water pressure has the potential to improve the consistency of the CTE test methods.

Introducing micro-cracking into concrete can increase the permeability by an order of magnitude (Choinska et al. 2007; Grasley 2006; Hoseini et al. 2009). Ai et al. (2001) observed that preconditioning saturated cement paste improves the permeability. According to that study, the reason for the increase in permeability was the formation of

micro-cracking due to the internal water pressure development during temperature change. Moreover, micro-cracking can be introduced in a concrete sample by applying mechanical loading. Based on the previous discussion, three techniques were evaluated to determine their effectiveness in improving the consistency of the measured CTE results. These techniques included preconditioning the concrete samples through the use of heating and cooling cycles, pre-cracking concrete samples at 28 days, and reducing the rate of heating and cooling. Further discussion of these potential improvement techniques will be presented in subsequent sections. The following sections will compare the results obtained before and after using these techniques to determine their effectiveness. The hope is that these techniques may be incorporated into the current test method to improve the consistency of the measured results.

6.5.1 Effect of preconditioning using heating and cooling cycles

Concrete CTEs were measured before and after preconditioning concrete cylinders through the use of heating and cooling cycles. First, completely saturated concrete samples were subjected to CTE testing prior to preconditioning, which is presented in this chapter as "before preconditioning" (BPC). Next, the concrete samples were subjected to an additional six cycles of heating and cooling and then tested to measure CTE in a process referred to as "after preconditioning" (APC). Figure 6.2 and Figure 6.3 show how the preconditioning reduced the difference between the measured CTEs of two replicate concrete cylinders. After preconditioning, that difference decreased by 70 and 80% of the cases for the TxDOT and the AASHTO method, respectively. A paired t-test on the

obtained results also confirmed the claim with 90% confidence, as shown in Table 6.1. Detailed description of paired-t tests can be found in Section 4.5.2.

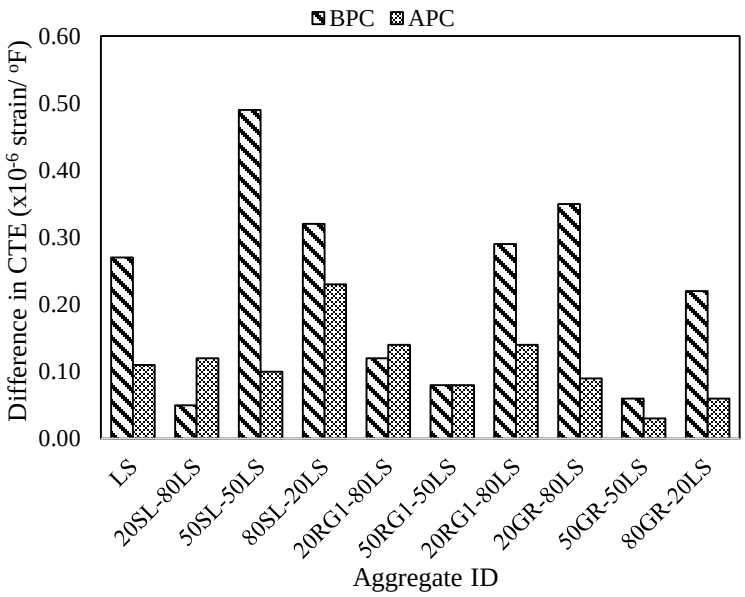

Figure 6.2 Effect of preconditioning on the consistency of the TxDOT CTE results

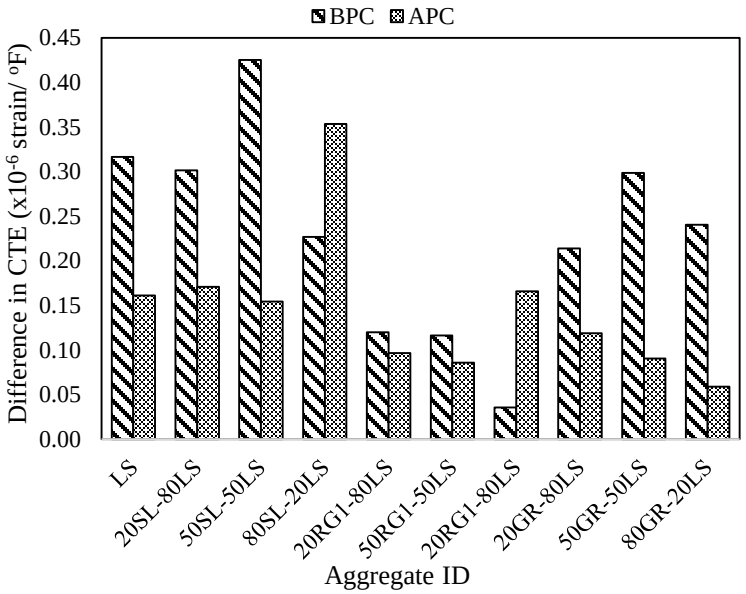

Figure 6.3 Effect of preconditioning on the consistency of the AASHTO CTE results

Table 6.1 Effect of preconditioning on the consistency of the CTE test methods calculated by paired-t testing

	TxDOT method	**AASHTO method**
Number of samples	10	10
Average (ΔCTE_{BPC} -ΔCTE_{APC})	0.08	0.11
Standard deviation	0.13	0.13
T	1.99	2.66
P (two tail)	0.03	0.048
P<α (α=0.05)	Yes	Yes
Null Hypothesis (H_o) (ΔCTE_{APC}=ΔCTE_{BPC})	Rejected	Rejected
$t_{\alpha,n-1}$	1.83	1.83
ΔCTE_{BPC} >ΔCTE_{APC}*	Yes	Yes

**ΔCTE_{BPC} and ΔCTE_{APC} represent the difference of measured CTE between two concrete samples before and after preconditioning, respectively.*

Typically, the CTE for cooling cycles (CTE_C) was higher than the CTE for heating cycles (CTE_H). Figure 6.4 shows the effect of preconditioning on the difference between

CTE_C and CTE_H (CTE_C - CTE_H) measured by the TxDOT method from the second heating and cooling cycle. The AASHTO method was not presented here, because this method calculates CTE based on the deformation at the isothermal state only and may not be a good representation of material behavior during the heating and cooling ramps. It can be observed from Figure 6.4 that after preconditioning, the difference between CTE_C and CTE_H decreased for all of the samples except limestone. Figure 6.5 compares the differences between CTE_C and CTE_H before and after preconditioning for three cycles of heating and cooling for all tested concrete samples measured by the TxDOT method. For over half (65%) of the specimens, preconditioning concrete cylinders by six cycles of heating and cooling reduced the difference between CTE_C and CTE_H. From a paired-t test, it can be concluded that preconditioning reduced the difference between heating and cooling CTEs with 99% confidence.

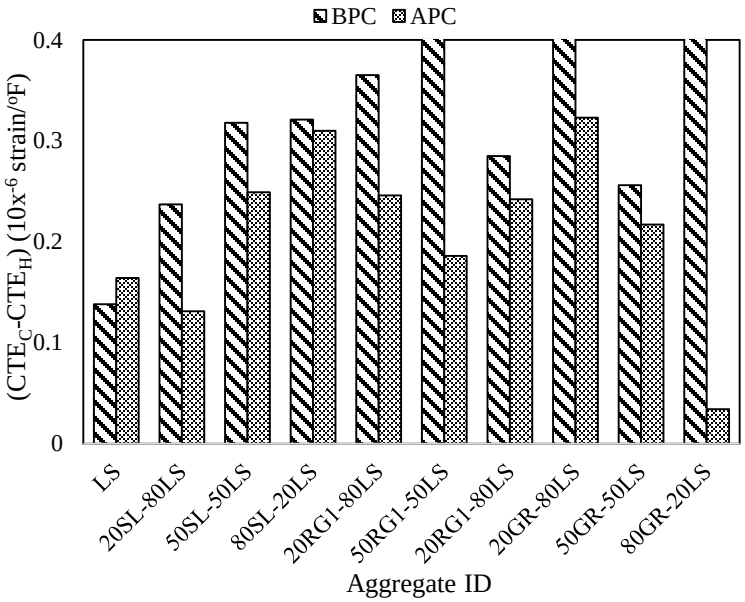

Figure 6.4 Effect of preconditioning on the difference between cooling and heating CTE measured by the TxDOT method from the second heating and cooling cycle

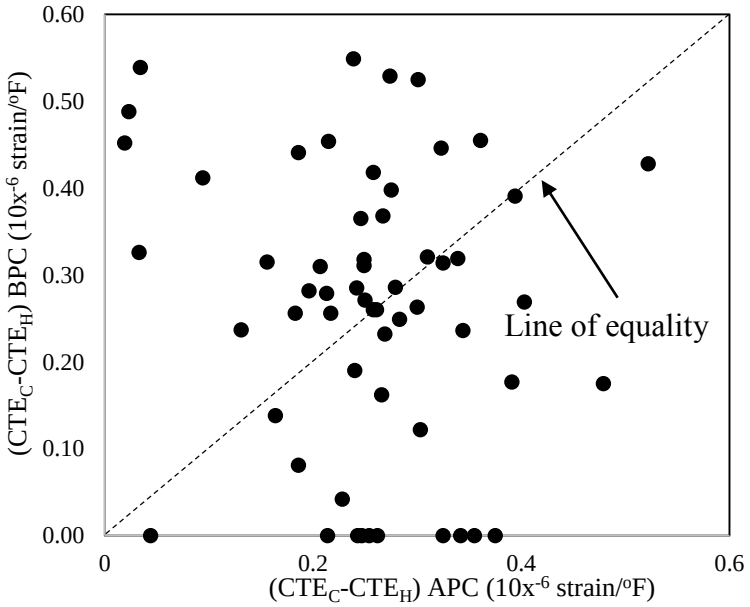

Figure 6.5 Comparison of difference in cooling and heating CTE before and after preconditioning measured by the TxDOT method for all heating and cooling cycles

The improvement in test result consistency can be explained by improved permeability. As mentioned previously, preconditioned concrete samples developed internal water pressure, which resulted in micro-cracking in the cement paste network. Micro-cracking increased the permeability of the concrete sample. Moreover, when a concrete cylinder is subjected to heating and cooling preconditioning, the pore water flows into and out of the concrete cylinders due to the difference in CTE of the liquid and solid phases of concrete. Water flows through the interconnected pores, which function as a network of tiny pipes. Water flow through this network of pipes can be hindered by debris, such as hydration products. Hydration products, such as calcium hydroxide (CH), are water soluble. Therefore, when a concrete sample is subjected to multiple cycles of heating and cooling, CH-rich pore water flows out of the concrete sample during the heating cycles and water from the exterior (with a lower concentration of CH) enters the concrete cylinder.

During the process, CH is removed from the interconnected pore network, which can be compared to removing the debris from a pipe network, eventually increasing the permeability of the concrete specimens.

Typically, the isothermal state required by the TxDOT and AASHTO methods is approximately one to two hours. As described in Section 5.8, the internal water pressure did not dissipate even after two hours of isothermal state at 50°C (122°F); the pressure at the end of the isothermal state at 50°C (122°F) acted as an offset internal water pressure for the cooling cycle. Therefore, the overall internal water pressure development during a cooling cycle was lower than for the heating cycle. If a cooling cycle is followed by a heating cycle, pressure development during the subsequent heating cycle should again be lower than during the cooling cycle. This can be attributed to the shorter length recovery during the isothermal state at 10°C (50°F) as compared to the isothermal state at 50°C (122°F), as was shown in Figure 4.11. Therefore, preconditioning helps to quickly alleviate developing internal water pressure during a temperature change and to decrease the effect of instantaneous deformation (ID), as explained in Section 4.5.5. As a result, the preconditioning improves the consistency of the test results.

The hypothesis was further reinforced by the measured displacement readings shown in Figure 6.6. Displacement readings were taken for the same cylinder before and after preconditioning by six heating and cooling cycles. The deviation between heating and cooling displacement is noticeably lower after preconditioning. This seems to support the theory that the internal pressure development after preconditioning was probably lower than before preconditioning, most likely due to increased permeability in the concrete

system. Thus, preconditioning does seem to improve the consistency of the CTE test results.

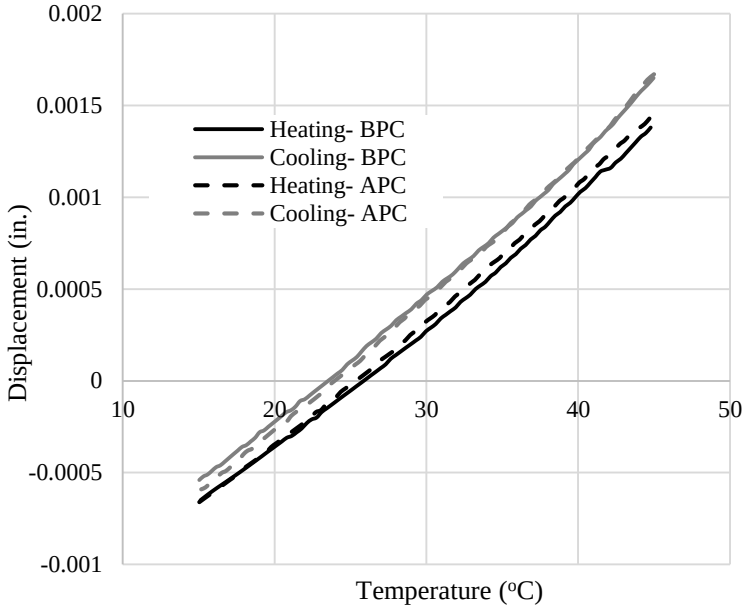

Figure 6.6 Effect of preconditioning on the measured displacement of a concrete cylinder while subjected to temperature change

6.5.2 Effect of pre-cracking

The concrete cylinders were pre-cracked at 28 days by applying 75% of the 28-day ultimate compressive strength. The CTEs were measured using uncracked (UC) and pre-cracked (PC) concrete samples. Both UC and PC samples were preconditioned by 6 cycles of heating and cooling prior to CTE measurement, because the preconditioning seems to improve the consistency of the test results, as described in the previous section. Therefore, this section will evaluate the pre-cracking as an additional improvement technique for CTE test methods, along with preconditioning. Figure 6.7 and Figure 6.8 show the difference in measured CTE between two replicates for UC and PC concrete samples. This difference in

measured CTE in the PC samples was lower than that of the UC samples in 70% of the cases for the TxDOT method, and 40% of the cases for the AASHTO method. Pre-cracking created a much better result for the TxDOT method because this method is more influenced by the internal water pressure than is the AASHTO method, as described in Section 4.5.5. However, the paired-t test confirmed that pre-cracking did not improve the consistency of either of these test methods at a 90% confidence level. Detailed analysis of the paired-t test is shown in

Table 6.2. It should be noted that both PC and UC samples were subjected to six cycles of heating and cooling prior to CTE testing. Therefore, the lack of increase in consistency might stem from the inability of the pre-cracking technique to show additional benefit along with the greater benefit of preconditioning.

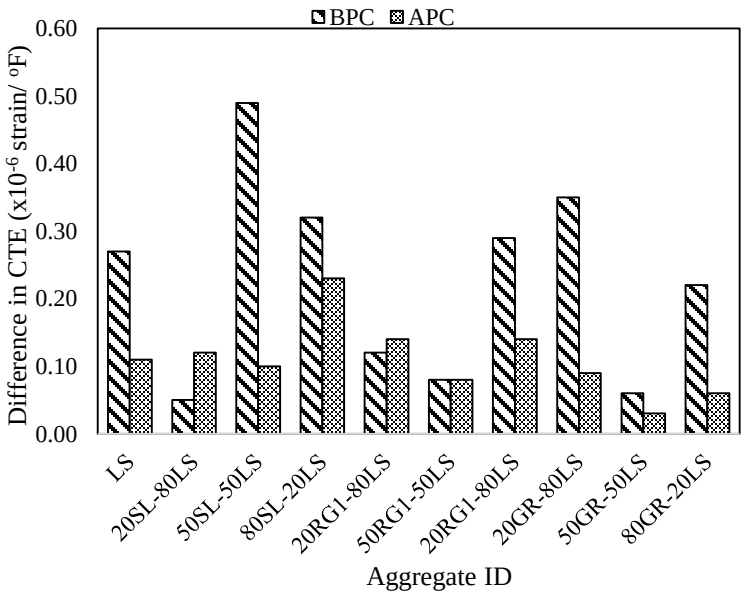

Figure 6.7 Effect of pre-cracking on the consistency of the TxDOT CTE results

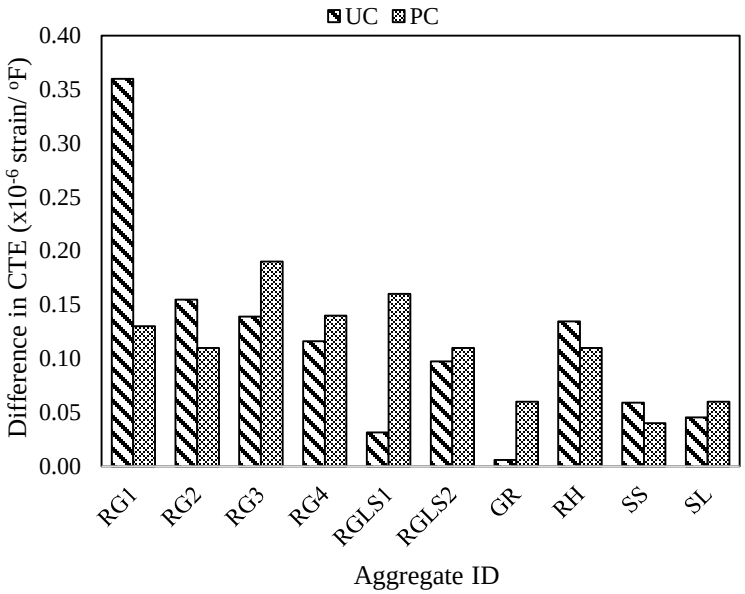

Figure 6.8 Effect of pre-cracking on the consistency of the AASHTO CTE results

Table 6.2 Effect of pre-cracking on the consistency of the CTE test methods

	TxDOT Method	**AASHTO Method**
Number of sample	10	10
Average (ΔCTE_{PC}-ΔCTE_{UC})	0.001	0.003
Standard deviation	0.05	0.09
T	0.07	0.11
P (two tail)	0.96	0.90
P<α (α=0.05)	No	No
Null Hypothesis (H_o) ($\Delta CTE_{PC}=\Delta CTE_{UC}$)	Accepted	Accepted

**ΔCTE_{UC} and ΔCTE_{PC} represent difference of measured CTE between two concrete samples before and after pre-cracking, respectively.*

Figure 6.9 shows the apparent differences between CTE_C and CTE_H during the second heating and cooling cycle measured by the TxDOT method. It can be concluded from Figure 6.9 that 90% of the time, differences between CTE_C and CTE_H were smaller in the PC samples than in the UC samples. Figure 6.10 presents the difference between the

heating and cooling CTE for all the heating and cooling cycles for concrete samples measured according to the TxDOT method. In about 90% of the cases the difference between CTE_C and CTE_H was smaller for PC samples than for UC samples. The paired-t test also confirms this claim with 99% confidence.

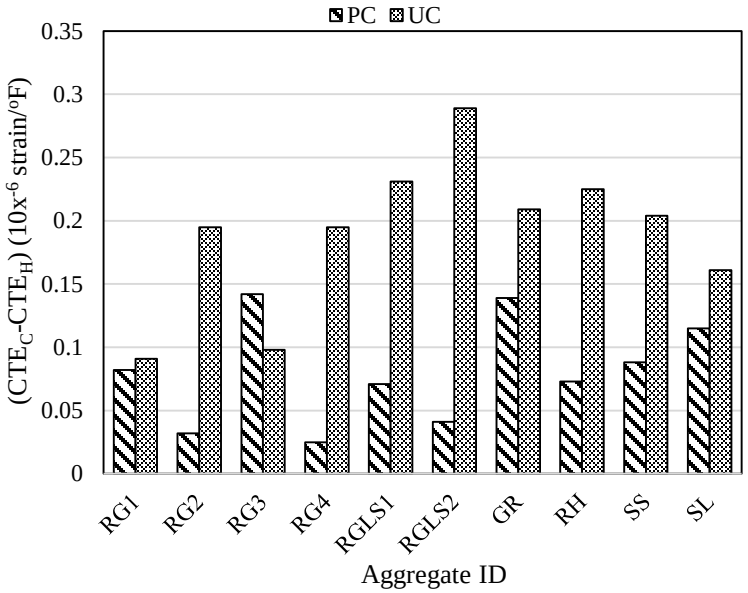

Figure 6.9 Effect of pre-cracking on the difference between cooling and heating CTE measured by the TxDOT method for the second heating and cooling cycle

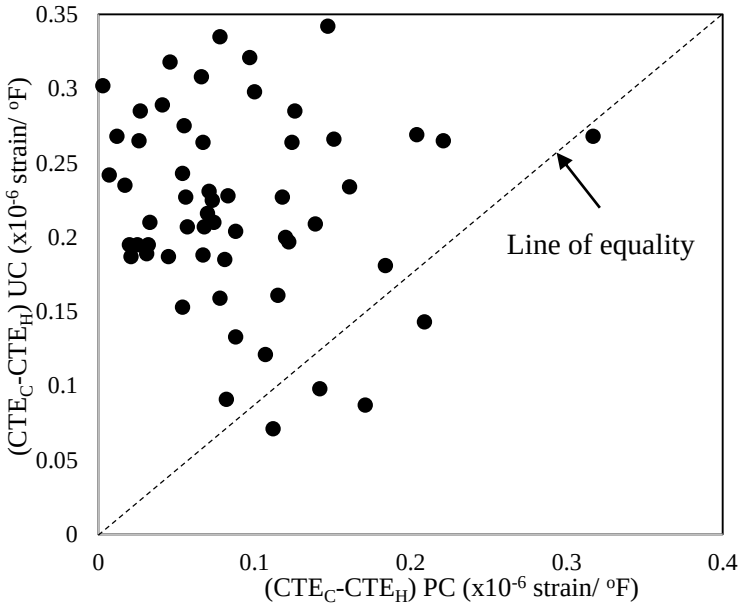

Figure 6.10 Comparison of difference in cooling and heating CTE before and after pre-cracking measured by the TxDOT method

Pre-cracking a concrete cylinder introduces microfractures in the concrete system. This may lead to two scenarios. First, pre-cracking can increase the permeability of the concrete by establishing more connections among the interconnected pores; also, more isolated pores might connect to the existing continuous pore networks, consequently introducing more paths for the movement of the pore water. Second, additional cracking can increase porosity, thus introducing more liquid into the concrete. This increases the internal water pressure and leads to higher ID. Therefore, if the benefit from the increase in permeability is more than the increased porosity in the concrete system, the ID should be lessened and the CTE test result consistency might increase. However, if the opposite case happens, overall internal water pressure might be higher for the PC sample than for the UC sample and the sample will experience more ID that might adversely affect the consistency of the CTE test results.

Figure 6.11 and Figure 6.12 show the average measured CTE for UC and PC samples. For the AASHTO method, it seems UC and PC samples give similar CTE values. However, CTE values measured by the TxDOT method showed higher CTE for PC samples than for UC samples. This observation is also supported by the paired-t test at the 90% confidence level. Two important observations can be made from the results. First, pre-cracking introduced additional water into the saturated concrete samples and increased the ID. This affected the CTE measured by the TxDOT method and resulted in a higher PC CTE, because the TxDOT method readings are affected more by the ID than are the AASHTO method readings, as described in Section 4.5.5. Second, pre-cracking also increased the permeability, which helped to alleviate the internal water pressure quickly and resulted in a similar PC and UC CTE for specimens tested with the AASHTO method.

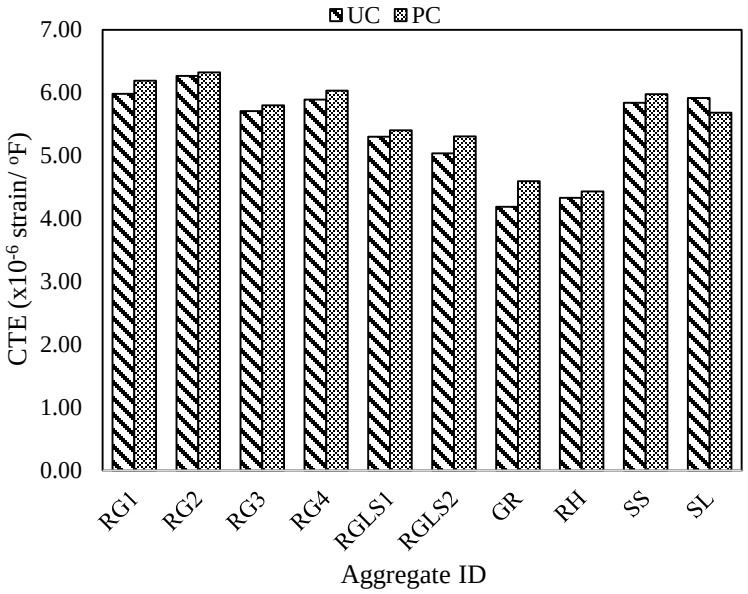

Figure 6.11 Effect of pre-cracking on the measured TxDOT CTE

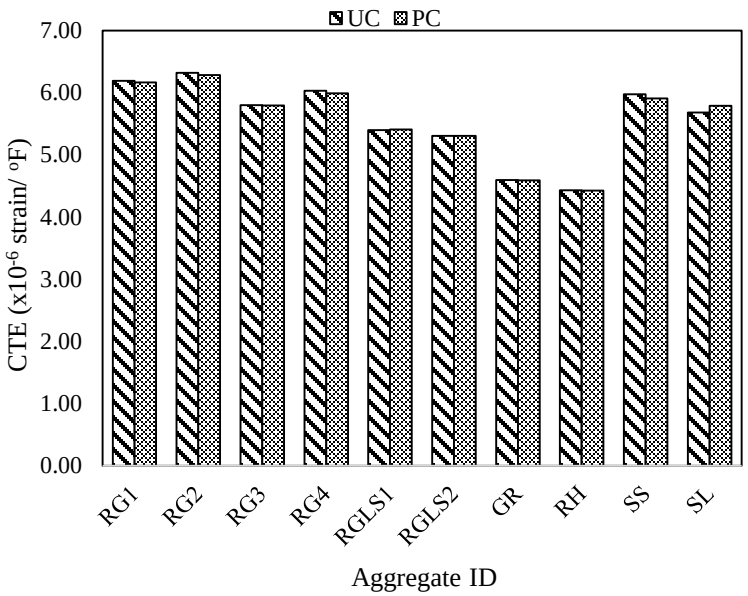

Figure 6.12 Effect of pre-cracking on the measured AASHTO CTE

Figure 6.13 shows the measured displacements of a concrete cylinder being subjected to heating and cooling cycles before and after pre-cracking. Pre-cracking did not show any additional reduction in deviations between heating and cooling displacements when used along with preconditioning. This outcome attests to the uncertain nature of pre-cracking as a mean of improving the consistency of CTE test results.

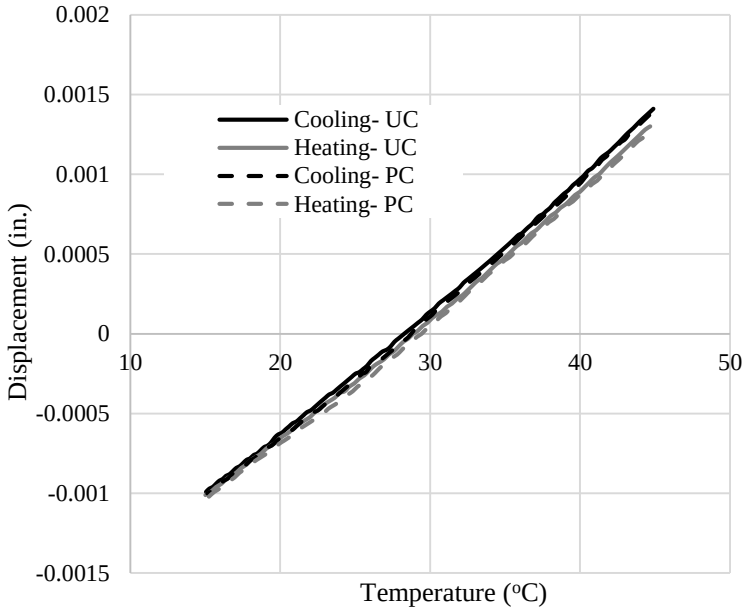

Figure 6.13 Effect of pre-cracking on the measured displacement of a concrete cylinder while subjected to temperature change

6.5.3 Effect of rate of temperature change

Two different temperature change rates were used in this study. The first was 0.3°C/minute (0.6°F/minute) and the second was 0.1°C/minute (0.18°F/minute). The 0.3°C/minute rate of temperature change will be expressed as a higher (H) rate of heating and cooling and the 0.1°C/minute rate will be presented as lower (L) rate, respectively. Concrete samples were subjected to six cycles of heating and cooling preconditioning prior to CTE testing at H and L temperature change rates. Figure 6.14 and Figure 6.15 show the differences in CTE subjected to H and L rates of temperature change for both the TxDOT and AASHTO methods. The CTE differences between the two replicate cylinders were reduced by 80 and 60% of the cases for the TxDOT and the AASHTO method, respectively, when L was used instead of H. However, the paired-t test showed that no

significant improvement was achieved at the 90% confidence level. The detailed results are shown in Table 6.3. Thus, reducing the rate of temperature change did not confer any additional benefit (beyond the greater benefit of preconditioning) in reducing the CTE differences between two replicates.

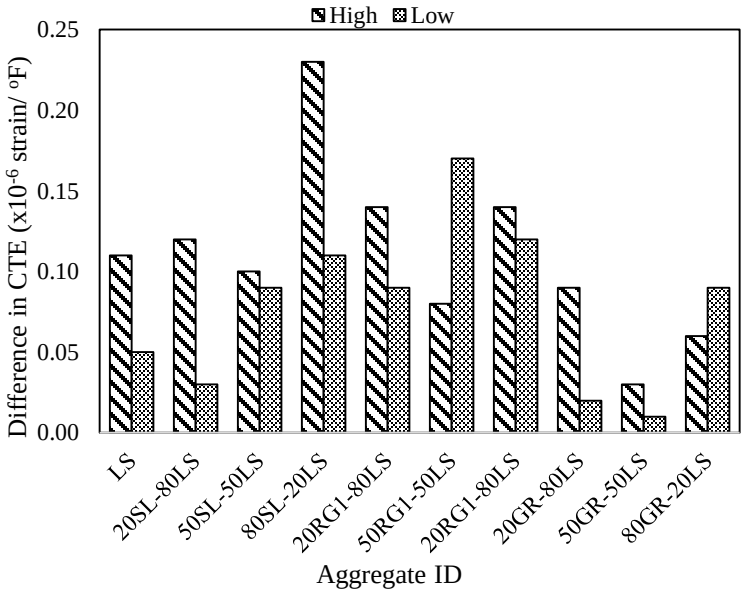

Figure 6.14 Effect of rate of temperature change on the consistency of the TxDOT CTE results

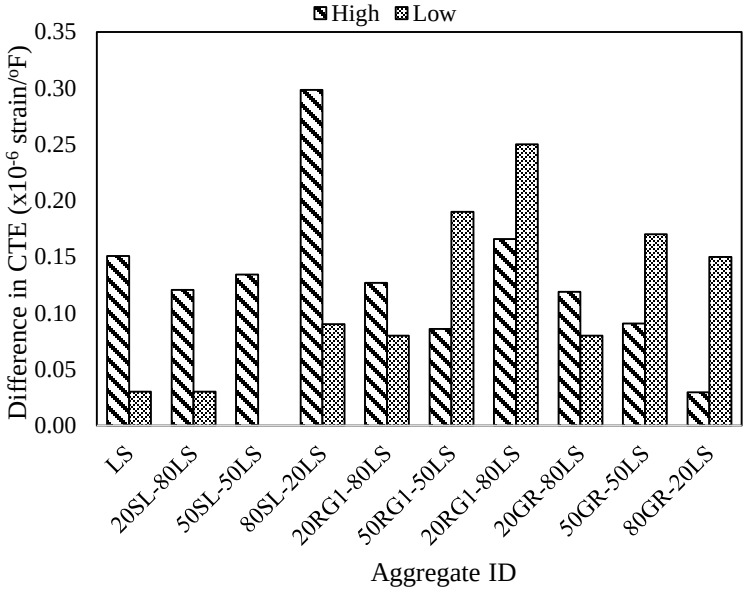

Figure 6.15 Effect of rate of temperature change on the consistency of the AASHTO CTE results

Table 6.3 Effect of rate of temperature change on the consistency of the CTE test methods

	TxDOT method	**AASHTO method**
Number of sample	10	10
Average (ΔCTE_H-ΔCTE_L)	0.025	0.03
Standard deviation	0.12	0.06
T	0.69	1.67
P (two tail)	0.11	0.13
P<α (α=0.05)	No	No
Null Hypothesis (H_o) (ΔCTE_H=ΔCTE_L)	Accepted	Accepted

**ΔCTE_H and ΔCTE_L represent the difference of measured CTE between two concrete samples for high and low rate of temperature change, respectively.*

Figure 6.16 shows the differences between the apparent CTE for heating and cooling cycles while subjected to the second cycle of temperature change as measured by the TxDOT method. In about 90% of the cases, the use of L rate of temperature change

reduced the differences between CTE_C and CTE_H. Figure 6.17 presents the comparison between differences in CTE_C and CTE_H for all the cycles for both the L and the H rate of temperature change. It can be concluded that the L rate of temperature change reduces the differences between the heating and cooling CTEs, and the pair-t test at 99% confidence supported this conclusion.

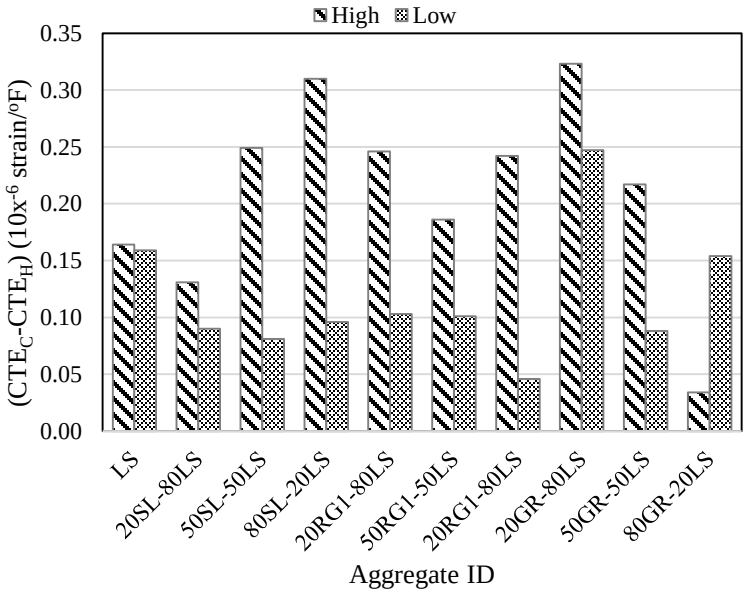

Figure 6.16 Effect of rate of temperature change on the difference between cooling and heating CTE as measured by the TxDOT method

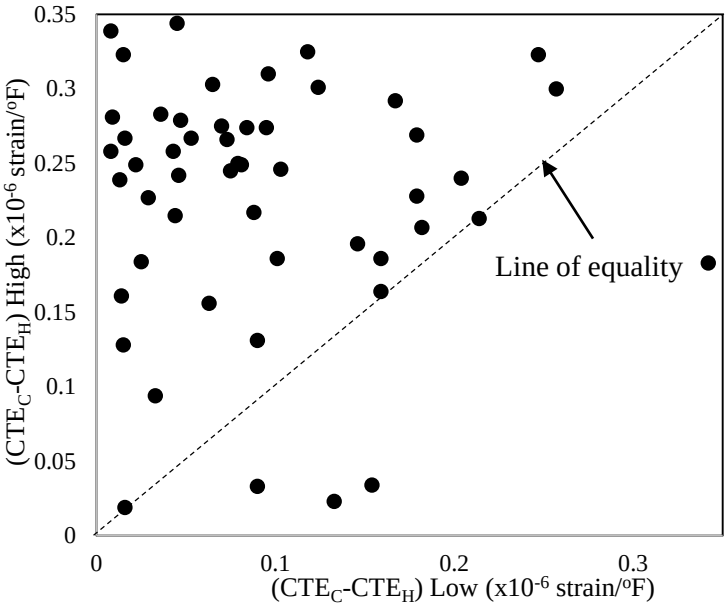

Figure 6.17 Comparison of differences between the cooling and heating TxDOT CTE at different rates of temperature change

The lower rate of temperature change reduced the rate of volume change of the liquid and solid phases. This reduced the pore pressure development and also allowed more time for the pore water to move into and out of the saturated concrete mass. Thus, it reduced the pore pressure, and thereby improved the consistency of the CTE test results. This hypothesis was supported by the displacement reading of concrete samples being subjected to heating and cooling cycles. Figure 6.18 shows the displacement of a concrete cylinder at both the H and the L rates of temperature change. A visual observation indicates that the deviation between heating and cooling displacement was almost negligible for the L rate of temperature change. This indicates that the L rate reduces the internal water pressure and, as a result, reduces the deviation between heating and cooling displacements.

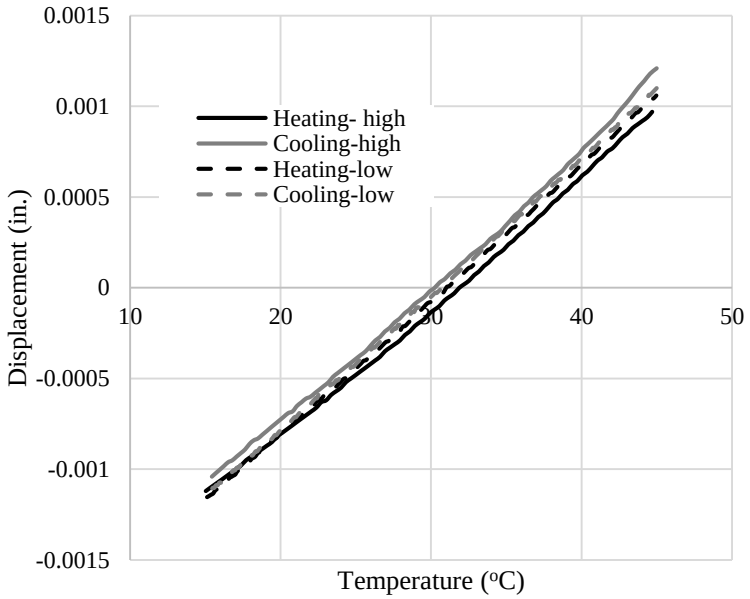

Figure 6.18 Effect of rate of temperature change on the measured displacement of a concrete cylinder during heating and cooling cycles

6.6 CONCLUSIONS

Three methods were studied to improve the consistency of results obtained from the TxDOT and AASHTO CTE test methods: preconditioning concrete specimens using heating and cooling cycles, pre-cracking, and reducing the rate of temperature change. Two parameters were considered as the indicators of test result consistency: i) the difference in CTE between the two replicate concrete specimens for each aggregate type and ii) the difference in apparent CTE between the heating and cooling ramp portions of the temperature cycle. A summary of the findings is as follows:

- Preconditioning concrete specimens using heating and cooling cycles reduced the difference of measured CTE between the two replicate concrete samples as well as the difference between heating and cooling CTEs.

- Pre-cracking the specimens and using a lower rate of temperature change—when used along with preconditioning—did not significantly reduce the difference in measured CTE between two tested replicate concrete samples. However, these two techniques did reduce the difference between the measured heating and cooling CTEs. Thus, they might slightly improve the consistency of the CTE test results.
- Preconditioning concrete samples through the use of heating and cooling cycles prior to CTE testing, along with a lower rate of temperature change, reduced the deviation between heating and cooling displacements. This indicates that these two methods can reduce the internal water pressure development. Pre-cracking was unable to reduce the deviations between heating and cooling displacements.
- To improve the consistency of the existing CTE test results, preconditioning seems to be the most effective among the studied techniques, followed by reducing the rate of temperature change, and, finally, pre-cracking.
- Based on the experimental results, both preconditioning and reducing the rate of temperature change can readily be incorporated into the existing CTE test methods to improve the consistency of the results.
- Lower rates of temperature change increase the test duration. Therefore, further study is needed to determine an optimum rate of temperature change to achieve both reasonable accuracy and test duration.
- The effect of pre-cracking is unreliable, and therefore is not recommended for incorporation as an improvement technique. However, further study can be done by cracking concrete samples at a higher load (greater than 75% of the ultimate

strength) to determine the possibility of achieving more benefit from additional crack formation that might improve the permeability of concrete sample.

Chapter 7: Concrete Mixture Design Method for Coefficient of Thermal Expansion Optimization

(Part of this chapter was presented at the 93rd Annual Meeting of the Transportation Research Board, January 2014, Washington, D.C., "Siddiqui, M. S., Rached, M., and Fowler, D. W. (2014), A Rational Mixture Design for Pavement Concrete, 93rd Annual Meeting of the Transportation Research Board, National Research Council, Washington, DC." (Marc Rached helped in developing the research idea, laboratory experiments, and reviewing the article and David W. Fowler was the supervisor). This article was also accepted for publication in the 2014 series of the Transportation Research Record: Journal of the Transportation Research Board (forthcoming) and published in the dissertation with permission from Transportation Research Board.)

7.1 INTRODUCTION

The coefficient of thermal expansion (CTE) of concrete contributes to distress in concrete structures. Reducing the CTE of concrete, therefore, can reduce the distress potential of concrete structures. Concrete's CTE is influenced by the CTE of its constituents. Thus, using low-CTE aggregate is probably the most effective method to reduce the overall CTE of concrete. However, some Texas Department of Transportation (TxDOT) districts, such as Houston and Beaumont, do not have locally available low-CTE aggregate sources. Therefore, in those areas where low-CTE aggregate sources are not locally available, one potential way to reduce the CTE of concrete to meet the previously mentioned TxDOT limit is to blend low-CTE imported aggregate (coarse and fine aggregates) with high-CTE local aggregate. This will promote the use of locally available aggregate sources and minimize the demand of imported aggregate. Typically, manufactured sand has a lower CTE than natural river sand. Manufactured sands generally have poor shape and texture, are too fine or too coarse compared to natural sand, and are not suitable for paving concrete mixtures without additional adjustments, according to

currently available mixture design methods. In addition, reducing the cement paste volume might help to reduce the CTE of concrete.

The concrete industry is also promoting more economical and sustainable concrete mixtures. Since cement is the most expensive component of concrete, as well as the component with the largest carbon footprint, reducing cement content by using more aggregate is an ideal way to achieve this goal. Conversely, sources of quality aggregate are being depleted and the industry is being forced to use less desirable sources, such as manufactured fine aggregates. Compared to natural sand, manufactured fine aggregate generally has poor grading, shape, and texture, and thus requires higher cement contents to achieve the desired concrete properties. While crushed stone has been extensively used by the concrete industry, manufactured sand has not. Fine aggregates have a higher impact on workability than do coarse aggregates (Quiroga and Fowler 2004), and this is one of the reasons why the use of manufactured sand has been minimal when compared to crushed stone.

Methods commonly used for proportioning concrete, such as ACI 211, select the cement content of a mixture based on slump, strength, and durability requirements (ACI Committee 211 1991). However, these methods do not provide guidance on minimizing cement. Various research projects performed by the International Center for Aggregate Research (ICAR) have shown that cement can be reduced in concrete while maintaining the strength and improving the durability (Quiroga and Fowler 2004; Koehler and Fowler 2007; Rached et al. 2009). ICAR research has also shown that the minimum cement content is a function of the desired workability, which is dependent on the type and combination of aggregate being used. This chapter presents a method for minimizing the cement content

of paving concrete mixtures using any source or combination of aggregate and allowing multiple aggregate blending—techniques that might be useful for reducing CTE without affecting performance. Test results are presented in this chapter to support the benefit of this proposed method.

7.2 BACKGROUND

In the 1970s, an aggregate manufacturer in North Carolina began promoting the use of manufactured sands in pavement concrete. A test section was made with manufactured sand containing a maximum of 3% microfines (aggregates passing the No. 200 sieve). The performance of this manufactured sand was a nightmare for the paving contractor (Saunders 1995). The concrete workability was unacceptable. There was excessive bleeding, edge slump, and edge shearing (Saunders 1995). Following this incident, a 50/50 blend of manufactured sand and natural sand was used instead to improve performance.

In 2008, three sections made with 100% manufactured sand were constructed in Texas as part of an implementation project. The goal of the implementation project was to compare the performance of concrete made with 100% manufactured sand to the performance of the typical blended sand mixture commonly used in that area. The three sections containing manufactured sand were made with the same source of limestone sand but with varying microfine content. The mixture proportions used for all mixtures were the same as the mixture proportions used for the 50/50 blended sand mixture (the control section). The mixture proportions used for the 100% manufactured sand sections were not optimized for the fine aggregates being used, which created concrete that was not easy to work or to finish, as shown in Figure 7.1.

Figure 7.1 Placement of 100% manufactured sand sections (from personal collection)

Concrete mixture design involves specifying the various concrete ingredients, such as cement, aggregates, water, chemical admixture, and mineral admixtures. The goal of a successful mixture design is to achieve the desired fresh and hardened concrete properties in the most economical way. The ACI 211 (1991) is an empirical method that is most commonly used for proportioning concrete mixtures. It was intended for aggregates that meet ASTM C33 (2013) grading requirements, since those aggregates were exclusively used in concrete at the time the method was developed. ASTM C33 defines a band of acceptable grading, and it limits the microfine content of sands to 5% for concrete subject

to abrasion. Manufactured sands often do not meet grading requirements set by ASTM C33. They can either be too fine or even too coarse depending on the mineralogy of the aggregate and the type of crusher used. Research has shown that shape, texture, and the combined aggregate grading (fine + coarse aggregate) are the major factors affecting concrete workability (Quiroga and Fowler 2004; Koehler and Fowler 2007; Rached et al. 2009). The ACI 211 method does not consider all these factors in estimating the mixture's water and cement content requirements; rather, it only suggests making water adjustments based on the shape of the coarse aggregate (rounded vs. crushed). Moreover, the required volume of coarse aggregate is determined based on the fineness modulus (FM) of the fine aggregate. Very different aggregate grading can yield the same FM value (Hudson 2003); FM is an unreliable method for measuring fine aggregate grading. Such a difference in grading might not be significant for natural sands that meet ASTM C33 standards, but this difference can be critical for manufactured sands with high microfine content. The ACI 211 method considers the combined effect of size, shape, and texture of coarse aggregate by means of dry-rodded unit weight (DRUW). However, the effect of these properties is not considered for fine aggregates or for the combination of aggregates being used. Furthermore, the method described by ACI 211 is intended for only two aggregate fractions: one fine and one coarse aggregate. No guidance is provided for blends of three or more aggregates. Studies have shown that the combined grading of coarse and fine aggregate obtained using the ACI 211 method has a high potential of being gap graded (Shilstone Sr. 1990). Uniformly distributed aggregates are desirable for concrete mixtures, because they produce a higher packing density, and thus better workability, when compared to gap-graded aggregate (Andersen and Johansen 1993; Glavind et al. 1993;

Goltermann and Johansen 1997; Johansson 1979). Uniformly distributed mixtures also need less paste to fill the voids, thus decreasing problems in fresh concrete such as bleeding, creep, and shrinkage (Dobrowolski 1998; Shilstone 1999).

Other available concrete mixture design methods—including band grading, Shilstone's optimized concrete mixture design, the Europack system of mixture design, the theory of particle mixtures, and the compressible packing model method—aim to improve the grading of aggregates to achieve better packing density. The "8-18" band grading method recommends having the total percentage of coarse and fine aggregate retained on any sieve to be between 8 to 18%. Band grading does not address issues relating to fine aggregates and is, therefore, not suitable for differentiating between natural and manufactured sands. Quiroga and Fowler found that poor workability and gap-graded particle distribution can occur when using the "8-18" band (Quiroga and Fowler 2004). Shilstone (Shilstone Sr. 1990) proposed using a coarseness chart, as well as a power 0.45 chart, for analyzing the size and uniformity of the combined aggregate particle distribution. Unlike other methods, Shilstone's method considers the grading of the whole aggregate combination but does not take into account aggregate shape or texture. The Europack (G.M.Idorn Consult A/S 1995) software can develop binary or ternary blends of aggregates. The software uses the packing density and characteristics of each aggregate to achieve the maximum packing density for any combination of aggregates. However, to determine the paste requirement of the combined grading, Europack requires the use of another method such as ACI 211. The theory of particle mixtures is based on the mathematical model that developed particle grading with the lowest voids (Dewar 1999). It combines the finest fraction first and then continues to combine coarser fractions. A

Vicat test is used to determine the packing density of the cement paste. De Larrard (De Larrard 1999) proposed a compressible packing model that considers the packing density as a function of shape, texture, and grading. The compressible packing model also allows the use of multiple fractions of aggregate.

The problem with most of the methods presented in this section is that they do not take into account the effect of the combined aggregate grading, nor do they provide a method for calculating the cement content, or else they are too complex. Moreover, these methods are general proportioning methods that could be used for any type of concrete; thus, results obtained are dependent on the knowledge of the designer. Koehler and Fowler (Koehler and Fowler 2007) proposed a mixture design for optimizing self-consolidating concrete known as the ICAR mixture design. The method presented in this chapter uses the same philosophy of proportioning but is modified for the design of slip-form paving concrete mixtures.

7.3 MATERIALS

Six different sands and five different coarse aggregates were used in this study. Two of the sands are natural river sands (RS) and the rest are manufactured sands (MS). Figure 7.2 shows the particle size distribution of the sands. Both river sands (RS1 and RS2) and one of the manufactured sands (MS4) met ASTM C33 requirements, but the other manufactured sands (MS1, MS2, and MS3) did not. MS1 and MS3 had high microfine contents, about 8 and 22%, respectively, while MS2 was too coarse. The particle size distribution of the coarse aggregates used is presented in Figure 7.3. Three coarse aggregates (CA1, CA2, and CA5) conformed to TxDOT grade 4 (ASTM grade 57)

requirements, while the fourth coarse aggregate (CA4) met the TxDOT grade 2 (ASTM grade 467) requirements. CA3 met the TxDOT grade 3 but did not meet any ASTM C33 grading. The aggregates chosen for this research are suitable to recreate several of the grading problems often encountered when designing paving concrete mixtures. Table 7.1 shows important physical properties of coarse and fine aggregates, including mineralogy, saturated surface-dry specific gravity (SG_{SSD}), absorption, and fineness modulus. An ASTM C150 (2012) Type I/II and an ASTM C494 (2013) Type A water-reducing admixture (WRA) was used for concrete mixtures. No supplementary cementitious material was used. The recommended range of WRA dosage is 3 to 10 fl oz/100 lbs (195 to 652 mL/100 kg). A water-to-cement ratio (w/c) of 0.45, typically used for concrete pavement, was used for all laboratory concrete mixtures.

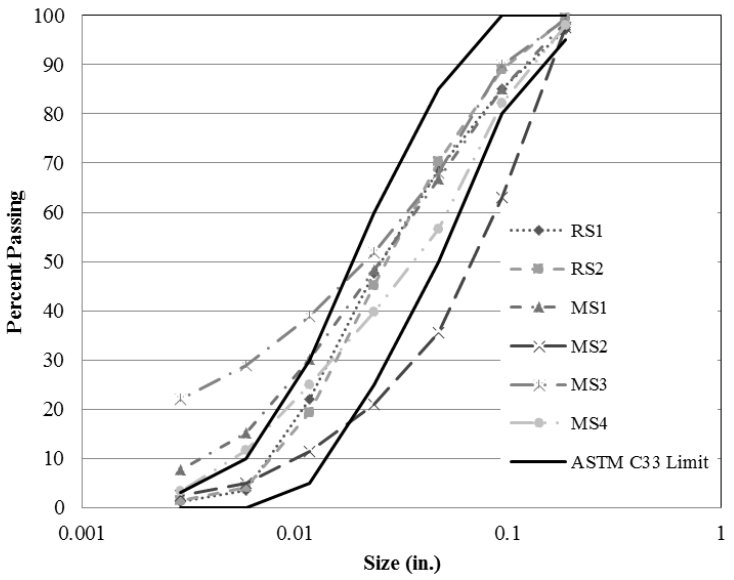

Figure 7.2 Particle size distributions of fine aggregates

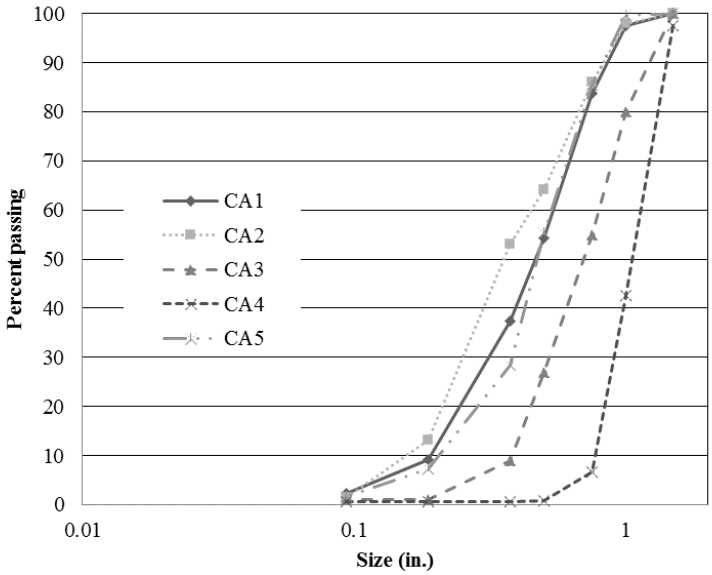

Figure 7.3 Particle size distributions of coarse aggregates

Table 7.1 Physical properties of coarse and fine aggregates

	Aggregate ID	Mineralogy	SG_{SSD}	Absorption (%)	FM
Fine Aggregates	RS1	River Sand	2.6	0.45	2.76
	RS2	River Sand	2.62	0.6	2.73
	MS1	Limestone	2.57	2.29	2.56
	MS2	Slate	2.54	0.84	3.67
	MS3	Limestone	2.55	2.57	2.24
	MS4	Dolomite	2.78	0.38	2.87
Coarse Aggregates	CA1	Limestone	2.65	1.09	-
	CA2	Limestone	2.67	0.69	-
	CA3	Limestone	2.58	1.6	-
	CA4	Limestone	2.625	0.88	-
	CA5	Limestone	2.561	0.94	-

7.4 MIXTURE PROPORTIONING AND TEST METHODS

Eleven different aggregate blends were used for concrete mixtures. Blends 1 to 10 were composed of one coarse and one fine aggregate, while blend 11 was composed of two coarse and two fine aggregates. Table 7.2 shows aggregate blends and the percentages of each aggregate used, as well as the DRUW measured void content. The percentage of each aggregate in a blend was obtained using a power 0.45 curve. The DRUW of each blend was measured (combined DRUW), and the void content was then calculated. The void content could be considered the minimum paste volume needed to fill the voids between aggregates.

Table 7.2 Aggregate blends showing aggregate fractions and optimized paste volume

	Coarse Aggregate					Fine Aggregate						
Blend ID	CA1 %	CA2 %	CA3 %	CA4 %	CA5 %	RS1 %	RS2 %	MS1 %	MS2 %	MS3 %	MS4 %	Void content %
1	60	-	-	-	-	40	-	-	-	-	-	25.0
2	60	-	-	-	-	-	-	40	-	-	-	24.8
3	55	-	-	-	-	-	-	-	45	-	-	25.3
4	62	-	-	-	-	-	-	-	-	38	-	25.6
5	58	-	-	-	-	-	-	-	-	-	42	27.9
6	-	65	-	-	-	-	35		-	-	-	29.5
7	-	64	-	-	-	-	-	36	-	-	-	30.0
8	-	58	-	-	-	-	-	-	42	-	-	28.4
9	-	-	60	-	-	-	40	-	-	-	-	26.3
10	-	-	62	-	-	-	-	38	-	-	-	25.9
11	-	-	-	18	50	-	20	-	-	12	-	25.7

The combined DRUW is a function of grading, shape, and texture of combined aggregates. Combined aggregate grading was chosen based on the 0.45 power curve to

obtain the highest packing density. Selected volume fractions of fine and coarse aggregate were then hand-mixed until the blended aggregates achieved visual homogeneity. The DRUW was then measured according to ASTM C29 (2009). Poorly shaped and poorly textured aggregates will have a lower DRUW, because the particles move with greater difficulty in the blended aggregate matrix. In contrast, well-shaped and well-textured aggregates can move more easily and achieve a higher DRUW. Therefore, poor aggregate shape and texture result in higher void contents in the blended aggregates and require a higher volume of cement paste to fill the voids. For well-shaped and textured aggregates, the cement paste volume required to fill the voids will be lower.

Two to four mixtures were batched and tested for each blend of aggregate, while varying the paste volume. The water-reducer dosage was selected by trial and error and adjusted to obtain a slump greater than 1 in. (25 mm). The procedures used for mixing concrete were based on ASTM C192 (2012). To better distribute the admixture, the WRA was added to the water prior to mixing, and no additional admixture was added after all the ingredients were mixed (no post-dosing). Concrete workability was measured using the slump test described in ASTM C143 (2012). Concrete cylinders were cast to determine the 28-day compressive strength and elastic modulus (E) according to ASTM C39 (2012) and C469 (2010), respectively. For aggregate blends 1 to 8, 4-in. x 8-in. (100- mm x 200-mm) cylinders were used; for blends 8 to 11, 6-in. x 12-in. (150-mm x 300-mm) concrete cylinders were used.

7.5 PROPOSED MIXTURE DESIGN STEPS

Based on the results presented in the previous sections, it can be concluded that the optimum paste volume required to achieve a slump of 1 to 3 in. (25 to 75 mm) and an adequate compressive strength can be determined by computing the void content measured by the DRUW. This optimum volume could then be adjusted after trial batches are poured. The suggested proportioning method can be summarized as follows:

1. Evaluate aggregate properties, including sieve analysis, specific gravity, absorption, and the presence of deleterious material in the microfines.

2. Determine the optimum combination of aggregates. Use of a 0.45 power chart is recommended to obtain a dense combined aggregate grading.

3. Determine the void content for the aggregate combination obtained in step 2 using a combined DRUW test. The void content (percent void) is equal to the paste content required for the mixture.

$$\%voids_{compacted\_agg} = \left(1 - \frac{DRUW\,(lb/ft^3)}{\left(62.4\ {}^{lb}/_{ft^3}\right)\sum_{i=1}^{n}(p_i(SG_{OD})_i)}\right) * 100\%$$

where p_i and $(SG_{OD})_i$ are the volume fraction and oven-dry specific gravity of the i^{th} aggregate, respectively.

4. Choose paste quality: w/c, percentage air, SCM, admixture, etc.

5. Perform trial batches and adjust the mixture proportions accordingly. If the desired workability is not achieved, paste can be added to the mixture. On the other hand, if the trial batch shows that it is possible, then reduce the paste content.

Figure 7.4 to Figure 7.8 represent different steps of the proposed mixture design. This is a pictorial representation of a concrete mixture consisting of two coarse and two fine aggregates.

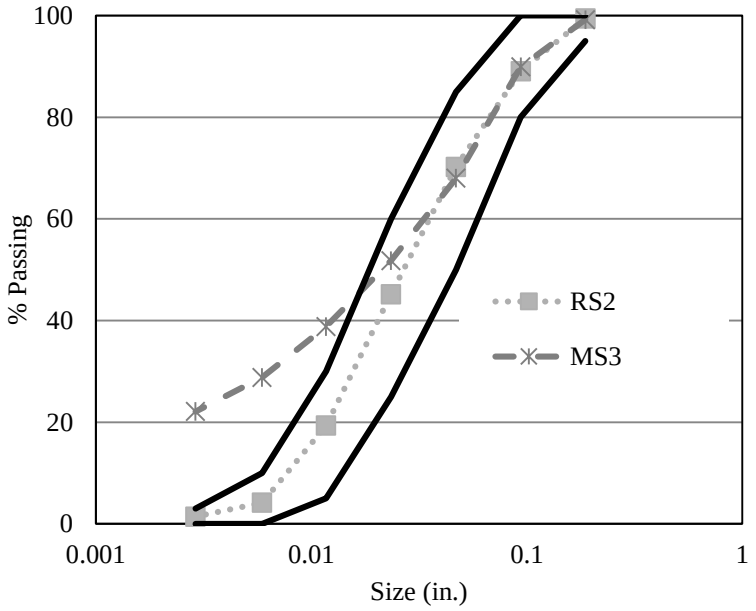

Figure 7.4 Fine aggregate grading

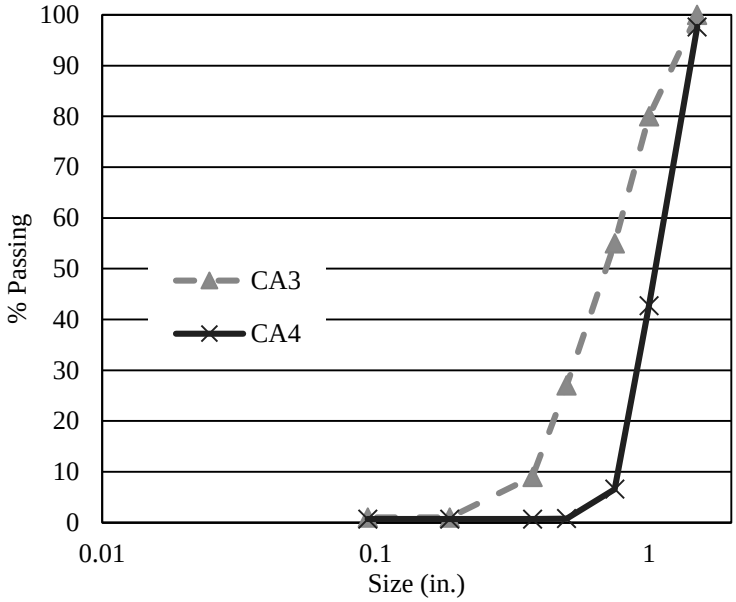

Figure 7.5 Coarse aggregate grading

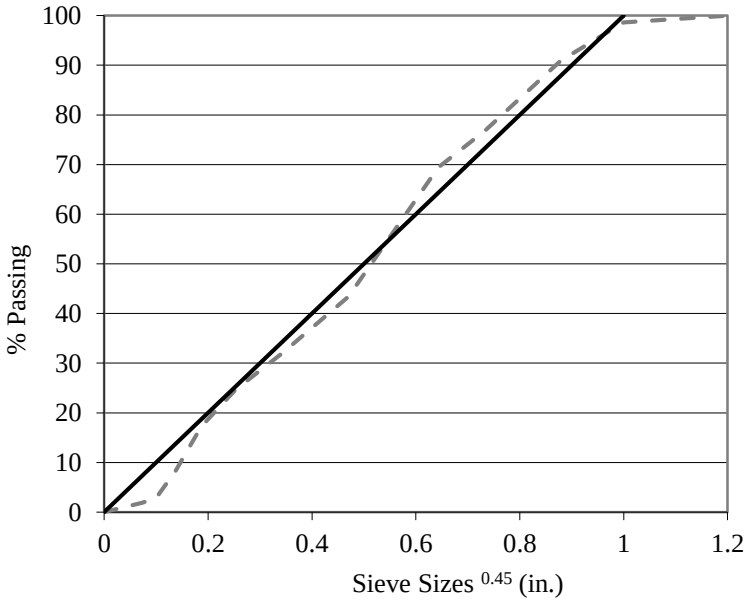

Figure 7.6 Selection of aggregate proportion to achieve highest packing density. In this mixture design, 18, 50, 20, and 12% of CA4, CA5, RS2 and MS3 was used, respectively. The solid line is the power 0.45 curve and the dotted line shows the combined aggregate gradation.

Figure 7.7 Coarse and fine aggregates before blending (left) and after blending (right) to determine DRUW. Theoretical cement paste volume was equal to the void content calculated from DRUW.

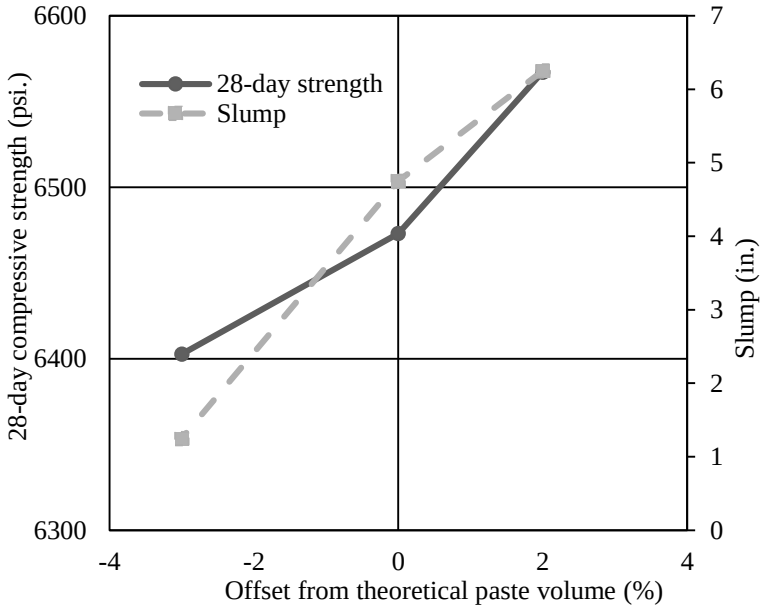

Figure 7.8 Optimum paste volume based on strength and workability requirement

7.6 RESULTS AND DISCUSSIONS

7.6.1 Physical properties of concrete mixtures made with the theoretical paste volume

Mixtures 1–11 presented in this chapter were made with paste contents equal to the void contents (theoretical paste volume) for blends 1–11 as determined by DRUW. The accepted slump range for slip-form concrete by most state agencies varies from 0.5 to 3 in., with 1 to 1.5 in. (25 to 38 mm) considered desirable. Figure 7.9 shows that eight out of eleven mixtures made with the minimum paste content had slump values higher than 1 in. (25 mm). By reducing the WRA dosage, mixtures with slump values higher than 3 in. (75 mm) could easily be adjusted to obtain a slump value lower than 3 in. (75 mm). Mixtures 2, 4, and 8 had slumps lower than 1 in. (25 mm); Mixtures 2 and 8 could have possibly reached a higher slump value if the WRA dosage had been increased. Although the maximum dosage of WRA was used, Mixture 4 had a slump of ¼ in. (6.25 mm) and yielded a 'sticky' mix. This was attributed to the presence of a very high microfine content of around 22%.

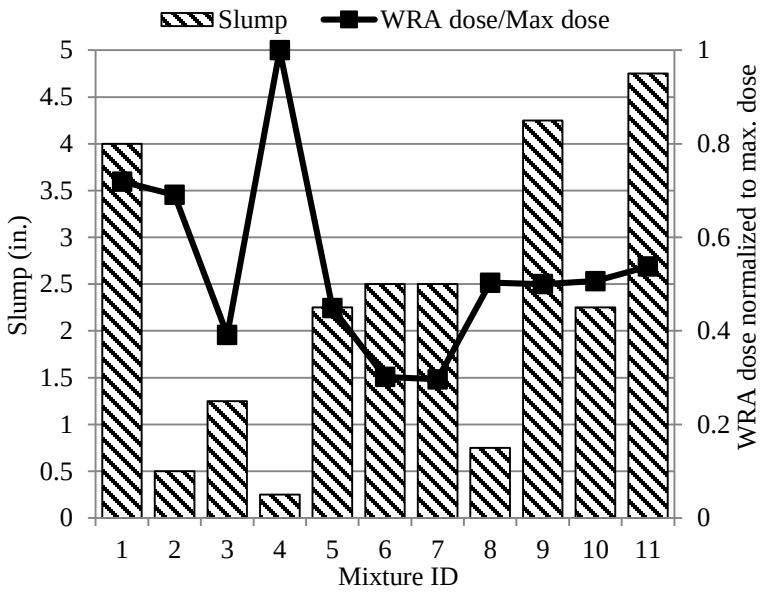

Figure 7.9 Slump and WRA dosage of concrete mixtures with minimal paste volume

Figure 7.10 shows the results of the 28-day compressive strength and the modulus of elasticity of concrete mixtures made with the DRUW-determined minimum paste content. All the concrete mixtures had a minimum compressive strength requirement of more than 4400 psi (30.3 MPa), which is typically what is required by state agencies such as TxDOT. The 28-day modulus of elasticity varies from 3.5 to 5 million psi. (24.1 to 34.5 GPa). Mixtures 3 and 8 contained MS2 sand and had the lowest modulus of elasticity. The MS2 sand is a slate that is very poorly shaped, which can explain why such low moduli of elasticity values were obtained. Poor grading and particle shape of fine aggregate may generate weaker interfacial transition zones and can cause lower modulus of elasticity values.

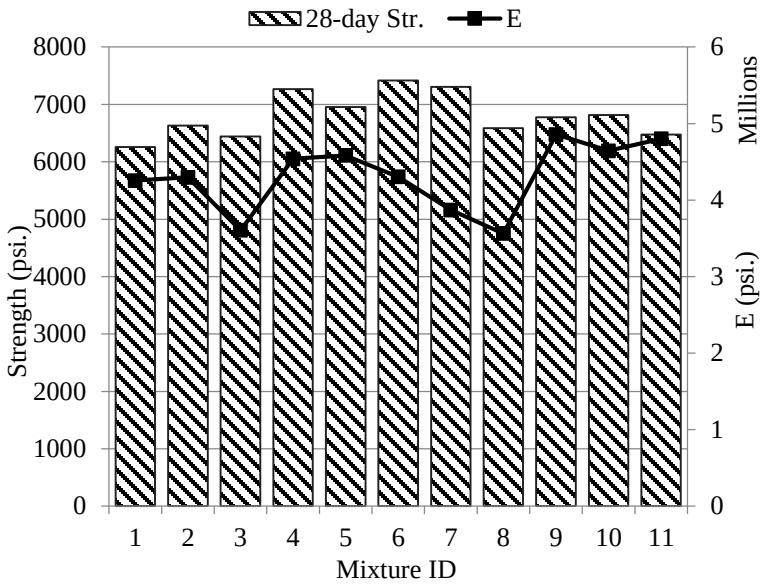

Figure 7.10 28-day compressive strength and modulus of elasticity of concrete mixtures with minimal paste volume. The solid horizontal line shows the TxDOT 28-day strength limit of 4400 psi.

7.6.2 Effect of paste volume on the physical properties of concrete

As previously discussed, paste volumes of the concrete mixtures were varied to evaluate the effect of paste volume on the properties of concrete. Figure 7.11 shows that even though higher dosages of WRA were used for lower paste mixtures, the workability of the mixtures decreased as the paste volume decreased.

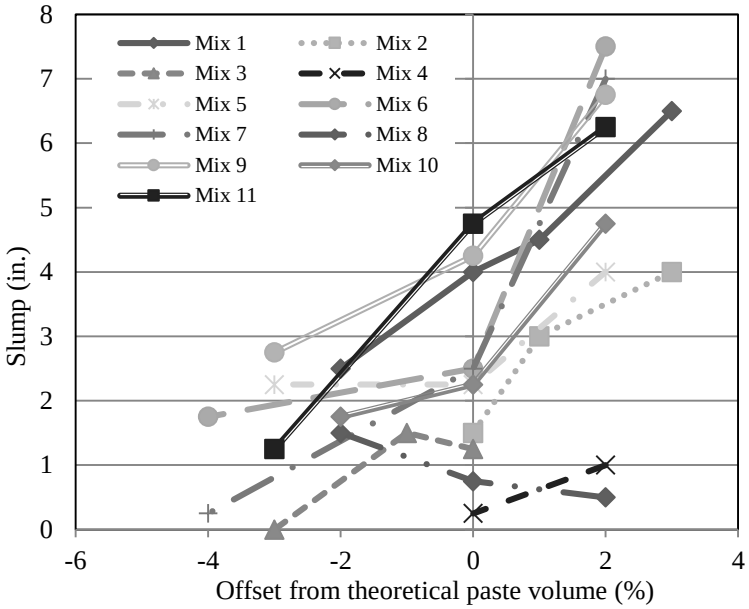

Figure 7.11 Effect of paste volume on the workability of concrete mixtures

Figure 7.12 and Figure 7.13 show the effect of paste volume on the 28-day strength and the concrete's modulus of elasticity. All the concrete mixtures tested had a compressive strength higher than 4400 psi (30.3 MPa). Mixtures made with blends 3, 5, and 8 showed a reduction in strength as the paste volume decreased beyond the theoretical minimum determined by the DRUW. These mixtures did not have sufficient paste to coat all the aggregates. Mixtures made with blends 3 and 8 contained MS2 sand. MS2 sand had the worst grading and shape; this increased paste demand and most probably contributed to the strength reduction. Mixtures made with blends 6 and 7 showed reductions in strength with increases in paste volume. This was not expected and cannot be readily explained. The variation in modulus of elasticity due to the variation in paste volume is not significant and may fall within the expected variability of the test results.

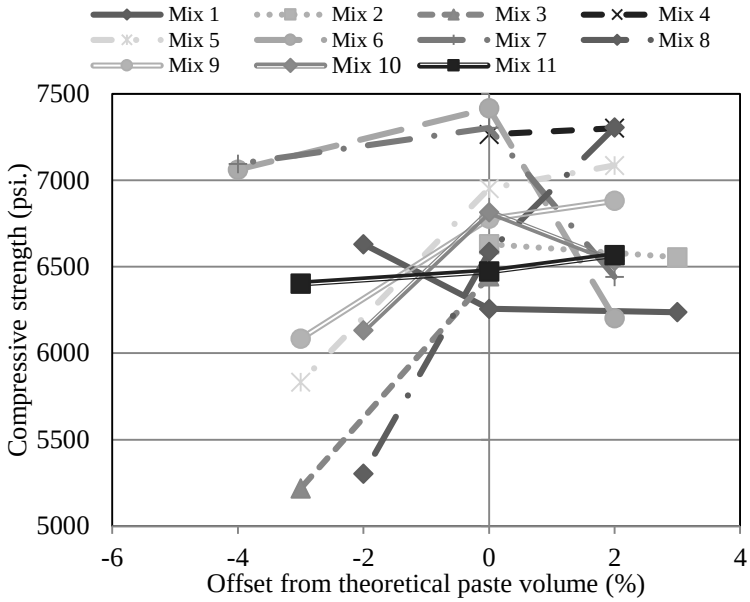

Figure 7.12 Effect of paste volume on the 28-day strength of concrete

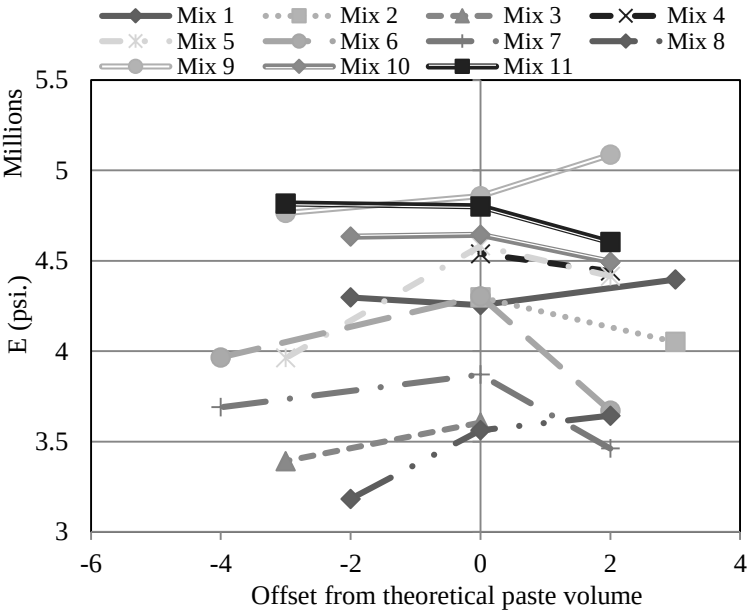

Figure 7.13 Effect of paste volume on the modulus of concrete

7.7 COMPARISON OF THE ACI 211 METHOD AND THE PROPOSED MIXTURE DESIGN

Trial concrete mixtures were proportioned according to ACI 211 for aggregate blends 1, 2, 5, 6, and 7 to compare with mixtures designed according to the proposed method (made with a paste content equal to the void content calculated from the DRUW of blends). Aggregates used in these blends met ASTM C33 requirements, except MS1, which did not satisfy ASTM C33 by a small margin. While proportioning concrete by ACI 211, 5000 and 6000 psi (34.5 and 41.4 MPa) 28-day compressive strengths were selected. Although 6000 psi (41.4 MPa) was a better match for the 28-day strength of the tested concrete, 5000 psi (34.5 MPa) was also chosen, due to the over-design nature of the ACI 211 design method.

Table 7.3 presents cement content and aggregate fractions for the selected mixtures. The percentages of coarse aggregate and fine aggregate were calculated as percentage fraction of total aggregate. According to ACI 211, total cement content was 583 and 683 lb/yd^3 (346 and 405 kg/m^3) for 5000 and 6000 psi (34.5 and 41.4 MPa) concrete, respectively. This is higher than the cement content obtained using the proposed method. Furthermore, the cement contents of concrete mixtures designed according to the proposed method were different for each blend, while ACI 211 had the same cement content for different blends with the same 28-day compressive strength. The probable reason for this difference lies in the way these two methods determine paste volume. The proposed method has the potential to produce economical and sustainable concrete, while maintaining desired durability and strength. Although some ACI 211 concrete mixtures were able to achieve similar percentages of aggregate fractions, the cement contents were

still higher than those of the proposed method, because ACI 211 does not select cement content based on the compacted void contents of combined aggregates. Figure 7.14 shows the cement requirement for concrete mixtures proportioned by the proposed method and by the ACI 211 method. The proposed mixture design required 150 and 80 lb/yd^3 (89 and 47.5 kg/m^3) less cement for the 6000 and 5000 psi (34.5 and 41.4 MPa) design strengths, respectively, compared to the ACI 211 designs. Reduction of cement not only saves money, but also reduces the carbon footprint of concrete, making it a more sustainable construction material.

Table 7.3 Comparison of proposed method and ACI 211 mixture design method

	Proposed Mixture Design			**ACI 211**					
				5000 psi			**6000 psi**		
Mixture ID	Cement (lb/yd^3)	%CA	%FA	Cement (lb/yd^3)	%CA	%FA	Cement (lb/yd^3)	%CA	%FA
Mix 1	506	60	40	583	61	39	683	63	37
Mix 2	500	60	40	583	65	35	683	65	35
Mix 5	568	58	42	583	58	42	683	60	40
Mix 6	516	65	35	583	60	40	683	62	38
Mix 7	527	64	36	583	63	37	683	64	36

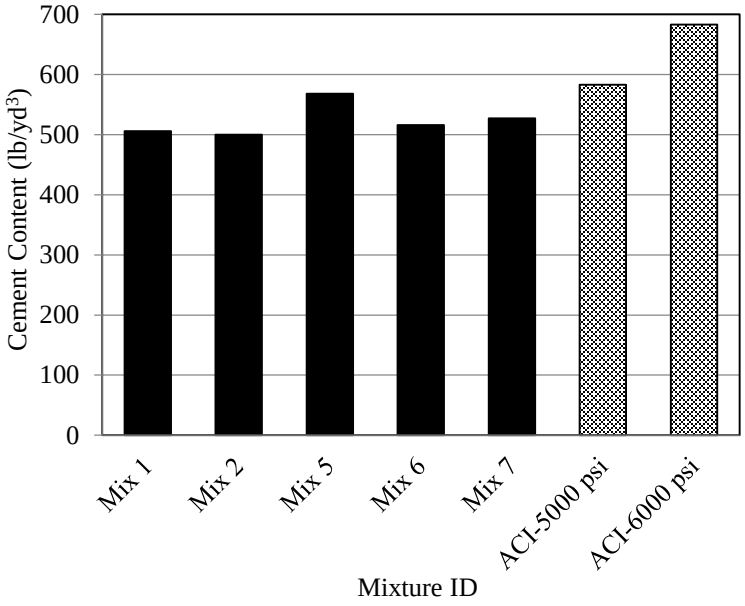

Figure 7.14 Comparison of proposed method and ACI 211 mixture design method

7.8 CONCLUSIONS

A mixture-proportioning method for pavement concrete is proposed in this chapter. Compared to other proportioning methods, this method has the following advantages:

- Paste requirements are computed based on the volume of paste needed to achieve fresh and hardened properties. This is why the proposed proportioning method has the potential to minimize the cement content of paving concrete mixtures using any source or combination of aggregate.
- The method presented is simple and does not require complicated calculations or expensive equipment.
- Concrete mixtures proportioned according to the proposed mixture design method yielded about 3 to 14% and 17 to 27% savings in cement compared to the ACI 211

5000 and 6000 psi (34.5 and 41.4 MPa) concrete, respectively, and the strengths were higher in every case.

- It is use-specific and thus tailored for pavement concrete.
- Though this study is focused on pavement concrete, this mixture design generally can be used for any type of concrete. Further study is needed to verify the suitability of this mixture design method for all types of concrete.

Chapter 8: Optimizing Concrete's Coefficient of Thermal Expansion and Its Importance in Concrete Structures

8.1 INTRODUCTION

The coefficient of thermal expansion (CTE) of concrete is responsible for deformations in unrestrained concrete structures whenever concrete is subjected to temperature change. Thermal stresses occur when the deformations are restrained. The magnitude of thermal stress depends on change in temperature, CTE, modulus of elasticity of the materials, and degree of restraint of the concrete member. If the developed thermal stress is greater than the tensile strength of the concrete, cracks occur. At early age, concrete is more prone to thermal cracking due to low strength (Schindler and McCullough 2002). In addition, a high amount of early-age relaxation may occur. Higher CTE generates higher thermal stress at a given temperature difference. Reducing the CTE of concrete is likely to reduce the distress potential of concrete structures. According to Mallela et al. (2005), it might not be cost-effective to reduce concrete CTE by changing the constituents of concrete mixture. However, optimizing the CTE of concrete according to the need of a given structure can result in a significant savings in repair and rehabilitation costs and increase the durability and longevity of concrete structures.

Concrete CTE is a function of the CTE of its constituents. The CTE of concrete can be reduced by reducing the CTE of its individual components, such as using low-CTE aggregate, blending low-CTE aggregates with high-CTE aggregates, and reducing the cement paste volume. Concrete mixture design techniques presented in Chapter 7 provide

guidelines for multiple aggregate blending and minimizing cement content. This mixture design method was used to produce concrete with different cement paste volumes.

This chapter will present the potential to reduce concrete CTE by blending low-CTE aggregates with high-CTE aggregates and reducing cement paste volume. Finally, a CTE optimization technique will be presented.

8.2 BACKGROUND

It can be concluded from the previous discussions that thermal stress plays a major role in the durability and longevity of concrete structures. Optimizing the CTE of concrete can diminish these unwanted thermal distresses and improve the service life of the structures, as well as reduce repair costs. Emanuel and Hulsey (1977) presented a model based on the rule of mixture to predict the CTE of concrete from its constituents, which can be presented as

$$\alpha_c = f_T\left(f_M f_A \beta_p \alpha_s + \beta_{FA}\alpha_{FA} + \beta_{CA}\alpha_{CA}\right), \tag{8.1}$$

where α_c, α_s, α_{FA}, and α_{CA} are the linear CTE of concrete, saturated hardened cement paste, fine aggregate, and coarse aggregate, respectively; f_T is the correction factor for temperature alteration; f_M is the correction factor for moisture; f_A is the correction factor for age; β_p, β_{FA}, and β_{CA} are proportions by volume of hardened cement paste, fine aggregate, and coarse aggregate respectively. Thus,

$$\beta_p + \beta_{FA} + \beta_{CA} = 1. \tag{8.2}$$

In this study, the CTE was measured for saturated samples in a controlled environment at an age between 2 to 3 months. As a result, $f_T = f_M = f_A = 1$ and Eq. (8.1) becomes

$$\alpha_c = \beta_p \alpha_s + \beta_{FA} \alpha_{FA} + \beta_{CA} \alpha_{CA}. \quad (8.3)$$

From Eq. (8.3) it is evident that the CTE of concrete can be reduced by reducing the CTE of coarse and fine aggregate. Typically the CTE of cement paste is much higher than the CTE of most aggregate types. Therefore, concrete CTE can also be reduced by reducing the cement paste volume. Eq. (8.3) was developed based on the assumption that there is only one type of cement, one fine aggregate, and one coarse aggregate in a concrete mixture. It was a valid assumption at that time, because there was no need to blend multiple aggregates and/or multiple cement sources. However, blending aggregate from multiple sources is gaining acceptance due to depletion of good quality aggregate sources and the unavailability of acceptable aggregates in or near the construction site. Moreover, blending aggregate from multiple sources is necessary to reduce the CTE of concrete. Therefore, for concrete with one type of cement and multiple coarse and fine aggregates, Eq. (8.3) can be written as

$$\alpha_c = \beta_p \alpha_s + \sum_{i=1}^{n} \beta_{FAi} \alpha_{FAi} + \sum_{j=1}^{m} \beta_{CAj} \alpha_{CAj}, \quad (8.4)$$

where $\sum$ is the operator for summation; n and m are the number of fine and coarse aggregates in concrete, respectively; α_{FAi} and α_{CAj} are the linear CTE of i^{th} fine aggregate and j^{th} coarse aggregate, respectively; β_{FAi} and β_{CAj} are proportion by volume of i^{th} fine aggregate and j^{th} coarse aggregate, respectively.

8.3 NUMERICAL MODEL FOR THERMAL STRESS DEVELOPMENT

This section will develop a basic model for the thermal stress development in a fully restrained concrete member. Thermal strain developed in a concrete body can be expressed as follows:

$$\varepsilon_T = CTE \times \Delta T, \quad (8.5)$$

where ε_T is thermal strain, *CTE* is coefficient of thermal expansion, and ΔT is temperature change. Thus, the thermal stress can be expressed as

$$\sigma_T = \varepsilon_T \times E_{c,} \quad (8.6)$$

where σ_T *is* thermal stress and E_c is modulus of elasticity of concrete. According to ACI 318 (ACI Committee 318 2011), the modulus of elasticity of concrete, E_c, can be expressed as

$$E_c = 57{,}000\sqrt{f_c'} \text{ (psi)}, \quad (8.7)$$

where f_c' is the compressive strength of concrete. From Eqs. (8.5), (8.6), and (8.7) it becomes

$$\sigma_T = CTE \times \Delta T \times 57{,}000\sqrt{f_c'} \text{ (psi)} \quad (8.8)$$

Eq. (8.8) was used to develop Figure 8.1 and Figure 8.2. Figure 8.1 shows the influence of concrete CTE on the stress development in a fully restrained concrete member subjected to temperature change. Concrete compressive strength was assumed to be 5 ksi (34.5 MPa), which is a typical compressive strength for normal concrete. Thermal stress was determined for temperature changes (ΔT) of 10, 20, 30, and 50°F (5.5, 11, 16.7, and 27.8°C). The thermal stress vs. CTE lines are not parallel and the slopes of line are increasing with the increased temperature change. This represents that at higher temperature, the CTE has a larger influence on thermal stress development, which can be explained by Eq. (8.8). It can be noted from Eq. (8.8) that, for a given concrete strength, the rate of change in thermal stress as a function of CTE is proportional to temperature difference. Therefore, a greater temperature change results in a higher rate of thermal stress increase, thus increasing concrete CTE.

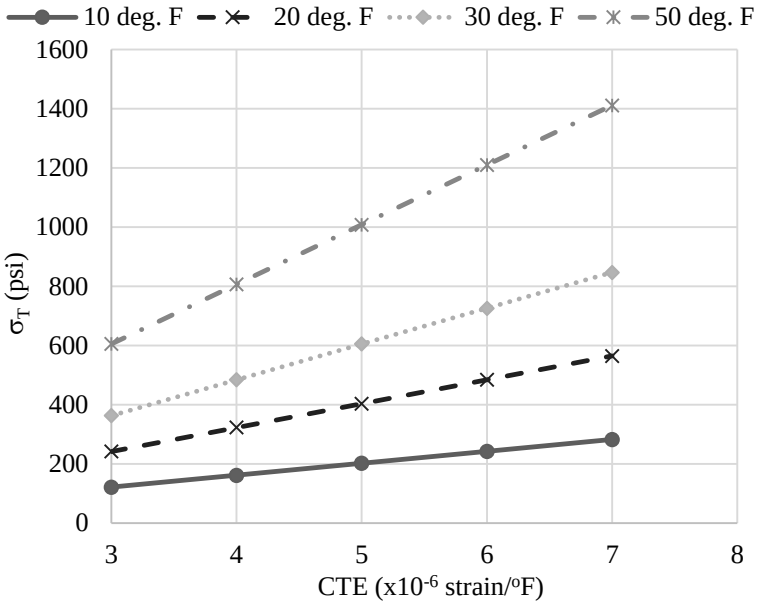

Figure 8.1 Effect of CTE on thermal stress development at 10, 20, 30, and 50ºF (5.5, 11, 16.7, and 27.8ºC) temperature change for 5 ksi (34.5 MPa) fully restrained concrete

Figure 8.2 represents the influence of CTE on thermal stress development in concrete for different compressive strengths (f_c'). Temperature change was assumed to be 30ºF (16.7ºC). Thermal stress development in higher strength concrete is more influenced by the CTE than is low strength concrete, which can be explained by Eq. (8.8). For a given temperature change, the rate of change in thermal stress is proportional to the modulus of elasticity, which is proportional to the square root of concrete strength. This results in higher thermal stress increases for high strength concrete than for low strength concrete with increasing CTE.

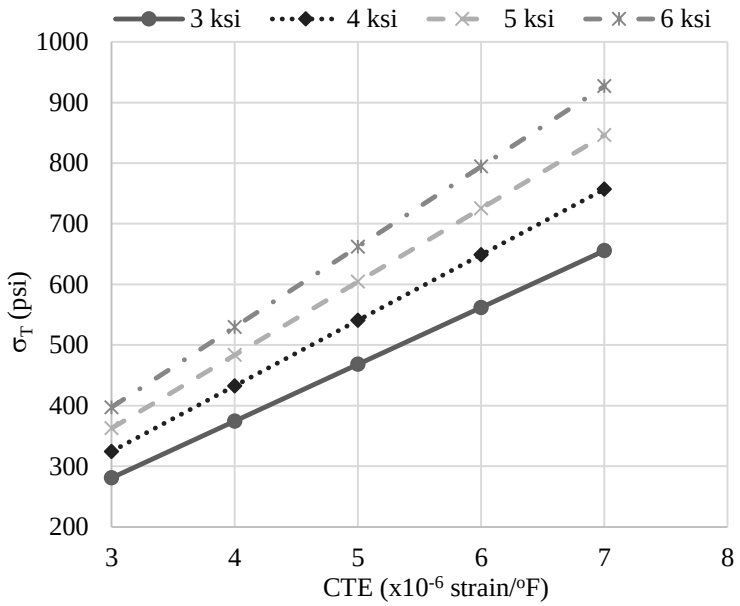

Figure 8.2 Effect of CTE on thermal stress development for 3, 4, 5, and 6 ksi (20.5, 27.5, 34.5, and 41.5 MPa) concrete, while subjected to 30°F (16.7°C) temperature change

From the previous discussion it can be concluded that CTE has a significant effect on the thermal stress development in concrete structures. Reducing the concrete CTE can significantly reduce the thermal distress.

8.4 OPTIMIZING CONCRETE CTE

Concrete consists of cement paste and aggregates that can be divided into two components: coarse and fine. The CTEs of concrete constituents affect the CTE of concrete. Reducing the CTE of each component will reduce concrete CTE. This section will discuss laboratory observation regarding the influence of each constituent's CTE on the overall CTE of concrete.

8.4.1. Materials

An ASTM C 150 (2012) Type I/II cement was used for all concrete mixtures. Coarse and fine aggregates were collected from various locations around Texas. Four coarse and four fine aggregates were used in this study. Table 8.1 presents the mineralogy, specific gravity (SG), and absorption of these coarse and fine aggregates. To determine the effect of cement content on the CTE of concrete, aggregate blends 1 to 3 and 5 to 8 were used. Further details on blends 1 to 3 and 5 to 8 can be found in Section 7.3 and 7.4.

Table 8.1 Physical properties of coarse and fine aggregates

	Aggregate ID	Mineralogy	SG	Absorption (%)
Coarse aggregate	RG	River gravel	2.56	0.7
	GR	Granite	2.61	0.7
	SL	Slate	2.54	1.2
	LS	Limestone	2.67	0.69
Sand	RS	River sand	2.62	0.6
	DLS	Dolomite	2.78	0.38
	SLS	Slate	2.54	0.84
	LSS	Limestone	2.57	2.29

8.4.2. Test procedures

Three optimization techniques were evaluated in this study: blending low-CTE coarse aggregate with high-CTE aggregate, blending low-CTE fine aggregate with high-CTE fine aggregate, and reducing cement content. For the first two observations, concrete mixtures were proportioned with a cement, fine aggregate, and coarse aggregate volume ratio of 1:2.65:4.5. Mortar samples were also prepared with a mixture of multiple fine aggregates to better understand the effect of blending low-CTE and high-CTE fine

aggregate. The sand-to-cement ratio for mortar was 2.65, which was the same sand-to-cement ratio used for concrete mixtures. To evaluate the effect of cement paste volume on the concrete's CTE, concrete mixtures were proportioned for aggregate blends 1 to 3 and 5 to 8 according to the mixture design method presented in Chapter 7. This proportioning technique was used because it presented a rational procedure to reduce cement content. Concrete and mortar were mixed according to ASTM C192 (2012) and ASTM C305 (2013), respectively. A water-to-cement ratio (w/c) of 0.45 was used for all concrete and mortar mixtures. Two 4-in. x 8-in. (100-mm x 200-mm) cylinders were made for each mixture. The CTE was determined according to Tex-428-A (2011) test procedures. Each cylinder was trimmed to a 7-in. (350-mm) length for the CTE testing. Cylinders were submerged under water for at least 48 hours to achieve complete saturation. Each cylinder was subjected to three cycles of heating and cooling for the CTE testing. A heating and cooling cycle started with cooling to 10°C (50°F) and maintaining that isothermal state for at least one hour, then heating to 50°C (122°F), followed by a 1-hour isothermal state at 50°C (122°F), and then again cooling to 10°C (50°F). The cooling and heating rate was adjusted so that it took at least two hours to reach 10°C (50°F) to 50°C (122°F) and vice versa. Typical heating and cooling cycles used for CTE testing were presented in Figure 4.1.

8.4.3 Results and discussions

Three different CTE optimization techniques are presented in this chapter. The findings are presented in the following sections.

8.4.3.1 Effect of coarse aggregate blending on the CTE of concrete

Coarse aggregate occupies about 40 to 50% of concrete volume and has significant influence on the CTE of concrete. Concrete CTE can be significantly reduced by reducing the CTE of the coarse aggregate. Only RS was used as the fine aggregate source for all the concrete mixtures presented in this section. Figure 8.3 shows the measured CTE of concrete prepared using RG, SL, GR, and LS coarse aggregates. RG has the highest CTE of about 6.5 $x10^{-6}$ strain/^{o}F (11.7 $x10^{-6}$ strain/^{o}C), followed by SL, GR, and LS. The properties of the mortar portion for all the concrete mixtures were the same, because the same cement, sand, and w/c were used. Therefore, the difference in the CTE of the concrete cylinders is only a function of the coarse aggregate CTEs. Two mortar cylinders were made using the same sand, cement, sand-to-cement ratio, and w/c ratio that were used for the concrete mixtures. The measured CTE of the mortar was 6.3 $x10^{-6}$ strain/^{o}F (11.34 $x10^{-6}$ strain/^{o}C). The CTEs of coarse aggregates were calculated from the known CTE of concrete and mortar using Eq. (8.4). Figure 8.4 presents the calculated CTE of coarse aggregates. RG had the highest CTE of about 6.5 $x10^{-6}$ strain/^{o}F (11.7 $x10^{-6}$ strain/^{o}C) and LS had the lowest of about 1.5 $x10^{-6}$ strain/^{o}F (2.7 $x10^{-6}$ strain/^{o}C). The obtained aggregate CTE is consistent with the coarse aggregate CTE presented in literature (Chung and Shin 2011; Emanuel and Hulsey 1977).

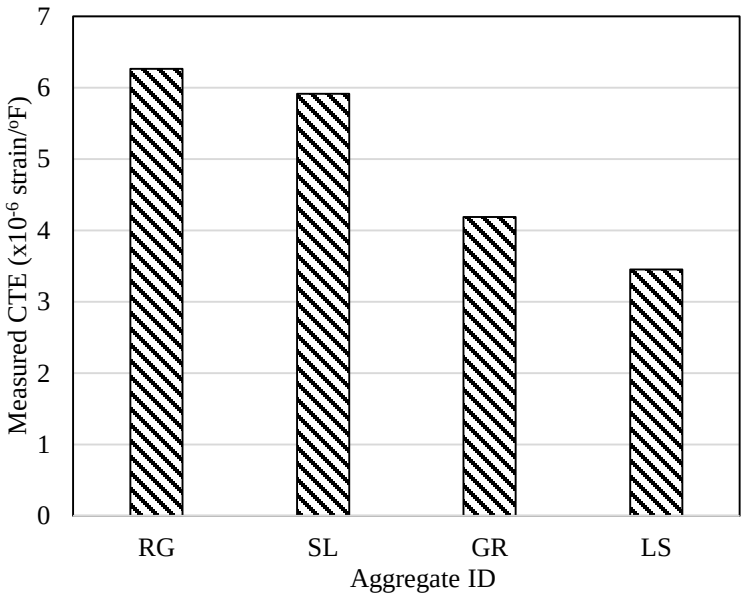

Figure 8.3 Measured CTE of concrete containing different coarse aggregates

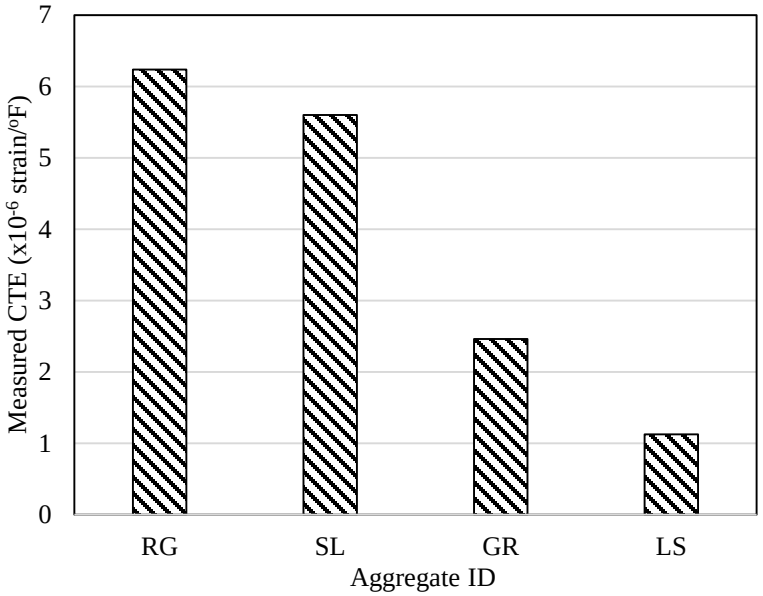

Figure 8.4 Calculated CTE of coarse aggregates

To determine the effect of replacing high-CTE coarse aggregate with low-CTE coarse aggregate on the reduction of concrete CTE, RG, SL, and GR were replaced by LS at 0, 20, 50, 80, and 100% by volume. Figure 8.5 shows the effect of coarse aggregate blending on the CTE of concrete. Note that RG-LS, SL-LS, and GR-LS represent concretes made from coarse aggregate blends of river gravel-limestone, slate-limestone, and granite-limestone, respectively. It can be concluded from Figure 8.5 that the concrete CTE decreased as the volume of limestone increased. The relationship between concrete CTE and the volume of limestone is linear with a coefficient of determination (R^2) of 0.99 for all three coarse aggregate blends. Therefore, a crude estimation of the required volume replacement by low-CTE coarse aggregate to achieve a target concrete CTE can be determined by knowing only the CTE of concrete made from 100% high-CTE and 100% low-CTE coarse aggregates and using straight line interpolation.

Another important fact that should be considered when choosing a low-CTE coarse aggregate source is that the CTE of blended aggregate concrete can never be less than the CTE of 100% low-CTE coarse aggregate concrete. Figure 8.6 presents the slope of the best-fit straight line as a function of difference between the CTE of two blended coarse aggregates. A best-fit straight line passing through the origin was chosen as a trend line for Figure 8.6. It can be concluded that there is a good linear correlation between the rate of CTE reduction and the difference between the CTE of two blended coarse aggregates with a coefficient of determination of 0.99. Therefore, the difference in CTE between high- and low-CTE aggregate determines the required volume replacement of high-CTE coarse aggregate to achieve a target concrete CTE. Thus, to achieve a target CTE reduction for a

given high-CTE coarse aggregate, required volume replacement with a low-CTE coarse aggregate decreases with the decreasing CTE of the low-CTE coarse aggregate.

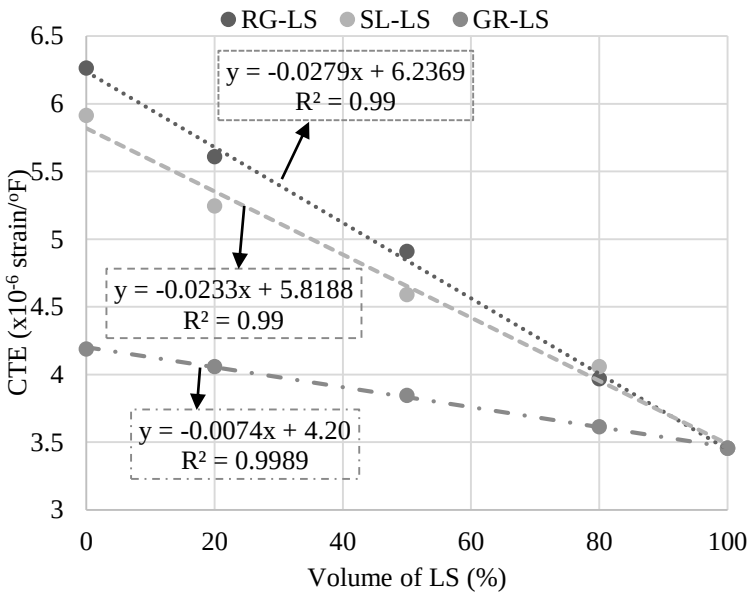

Figure 8.5 Benefit of blending low-CTE coarse aggregate with high-CTE coarse aggregate to reduce the CTE of concrete

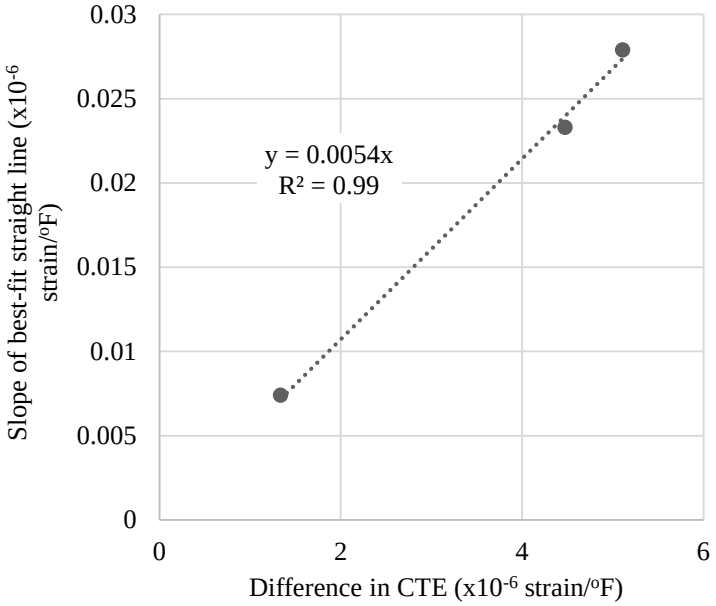

Figure 8.6 Effect of difference in CTE between two coarse aggregates on the rate of concrete CTE reduction

8.4.3.2 Effect of fine aggregate blending on the CTE of concrete

Mortar occupies about 50 to 60% of concrete by volume. Concrete CTE can be reduced by reducing the CTE of mortar. Figure 8.7 shows the measured CTE of mortars made from RS, SLS, DLS, and LSS. RS showed the highest CTE of about 6.5 x10^{-6} strain/ºF (11.7 x10^{-6} strain/ºC), followed by SLS and DLS. LSS had the lowest CTE of about 3.5 x10^{-6} strain/ºF (6.3 x10^{-6} strain/ºC). Two cement paste samples (4-in. x 8-in. (100-mm x 200-mm) cylinders) were prepared with the same type of cement and w/c that were used in the mortar mixtures. The CTE of cement paste was measured according to Tex-428-A. The measured cement paste CTE was 6.5 x10^{-6} strain/ºF (11.79 x10^{-6} strain/ºC). The CTEs of fine aggregates were calculated using Eq. (8.4) based on the known CTE of cement paste and mortar. Figure 8.8 presents the calculated CTE of fine aggregates. RS

had the highest CTE of about 6.5 x10^{-6} strain/^{o}F (11.7 x10^{-6} strain/^{o}C), followed by SLS, DLS, and LSS. Therefore, high-CTE fine aggregate results in high-CTE mortar when other parameters remain the same.

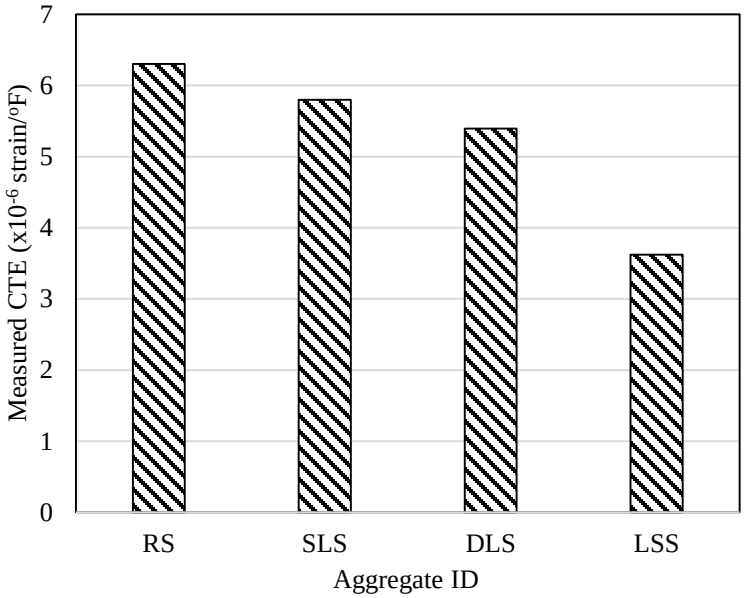

Figure 8.7 Measured CTE of mortar made from different fine aggregates

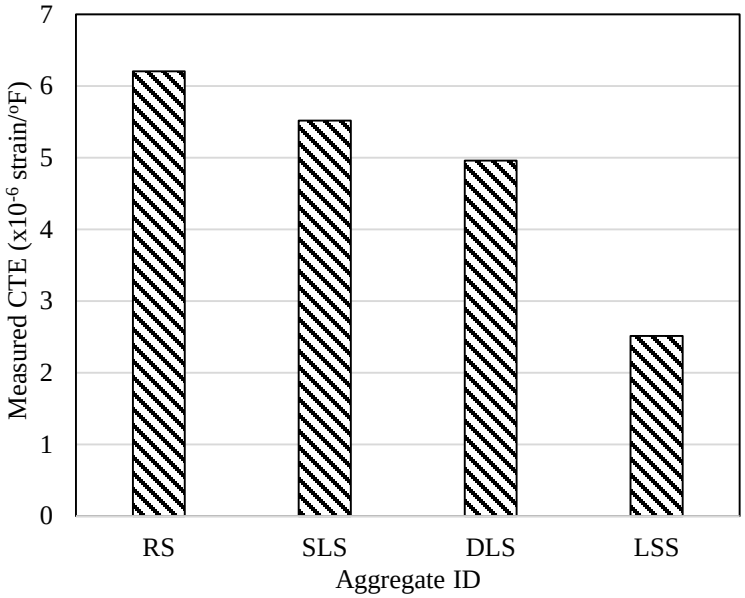

Figure 8.8 Calculated CTE of fine aggregates

To determine the effect of fine aggregate blending on the mortar CTE, mortar cylinders were prepared by replacing RS, SLS, and DLS with LSS. Figure 8.9 illustrates the effect of blending low-CTE fine aggregate with high-CTE fine aggregates on the CTE of mortar. Note that RS-LSS, SLS-LSS, and DLS-LSS represent the mortar made from fine aggregate blends of river sand-limestone, slate-limestone, and dolomite-limestone, respectively. The CTE of mortar decreased with the increased volume of LSS. The relationship between the CTE reduction of mortar and the LSS volume is linear with a coefficient of determination of 0.99 for all three fine aggregate blends. Figure 8.10 presents the relationship between the slope of the best-fit straight lines and the differences between the CTE of the two fine aggregates that were used for blending in mortar mixtures. A best-fit straight line passing through the origin was chosen as a trend line for Figure 8.10. There is a good linear correlation between the rate of CTE reduction and the difference between

the CTE of the two blended fine aggregates. Therefore, the difference in CTE between high- and low-CTE fine aggregates controls the required high-CTE fine aggregate volume replacement by low-CTE fine aggregate to achieve a target CTE reduction. Thus, to achieve a target CTE reduction for a given mortar, the required volume replacement of high-CTE fine aggregate with low-CTE fine aggregate decreases with decreasing CTE of low-CTE fine aggregate.

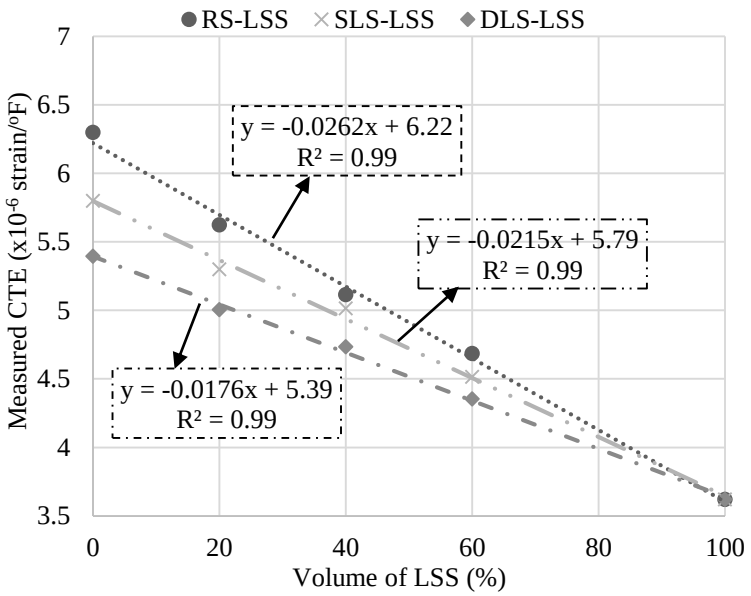

Figure 8.9 Benefit of blending low-CTE fine aggregate with high-CTE fine aggregate to reduce the CTE of mortar

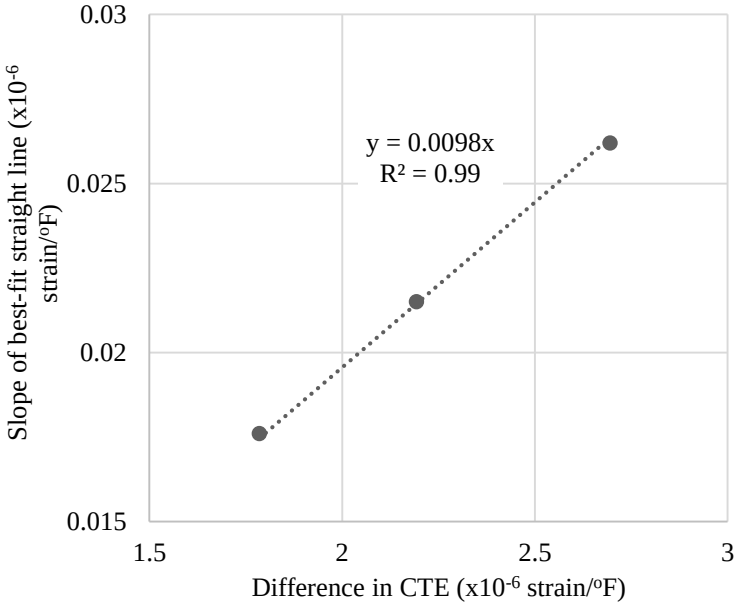

Figure 8.10 Effect of difference in CTE between two fine aggregates on the rate of mortar CTE reduction

Concrete cylinders were made using the same mortar composition as mentioned in the previous section. Two coarse aggregates, RG and SL, were used for concrete mixing. Figure 8.11 and Figure 8.12 show the effect of fine aggregate blending on the CTE of concrete made from RG and SL. The relationship between the CTE of the concrete and the volume of LSS is linear with the coefficient of determination, ranging from 0.96 to 0.99. Figure 8.13 presents the rate of CTE change for mortar and concrete samples. The rate of CTE change is virtually independent of the effect of coarse aggregate type for a given fine aggregate combination. For example, the rate of CTE change for RS-LSS sand is 0.0105 and 0.0117 $x10^{-6}$ strain/^{o}F (0.0189 and 0.0211 $x10^{-6}$ strain/^{o}C) for RG and SL, respectively, which are quite similar results for these two concrete mixtures. The small deviation might be due to the variation of the CTE test procedure. Moreover, the ratio of the rates of CTE change for the concrete and mortar is about 0.45, and that is equal to the volume fraction

of the mortar in the concrete. Hence, the rate of CTE change for concrete can be predicted from the rate of CTE change of the mortar by multiplying the CTE change of the mortar by the volume fraction of mortar in concrete.

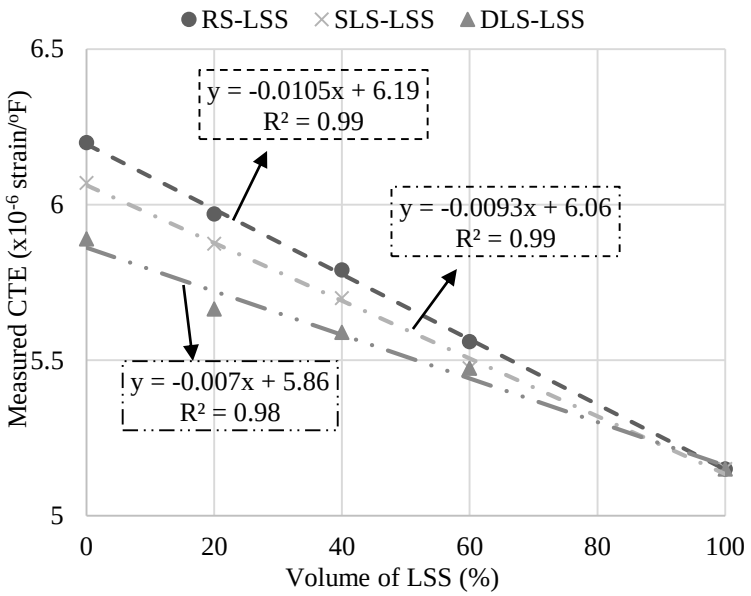

Figure 8.11 Benefit of blending low-CTE fine aggregate with high-CTE fine aggregate to reduce the CTE of concrete made from RG

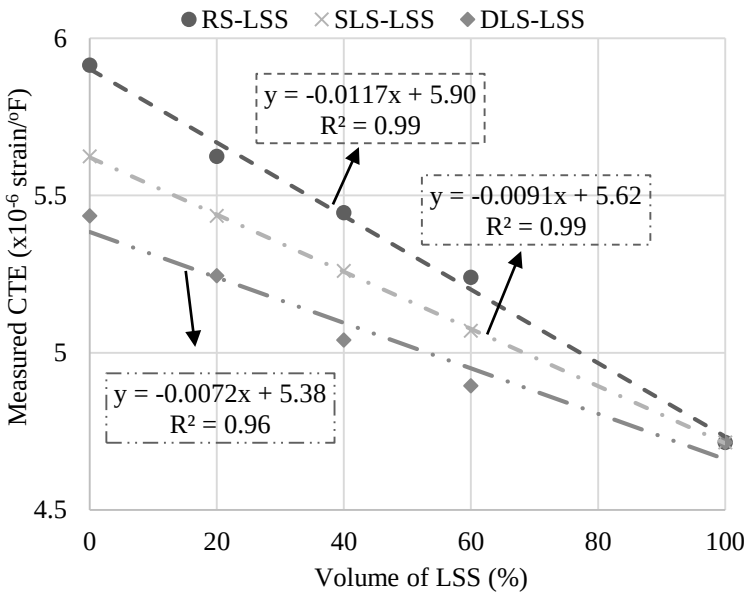

Figure 8.12 Benefit of blending low-CTE fine aggregate with high-CTE fine aggregate to reduce the CTE of concrete made from SL

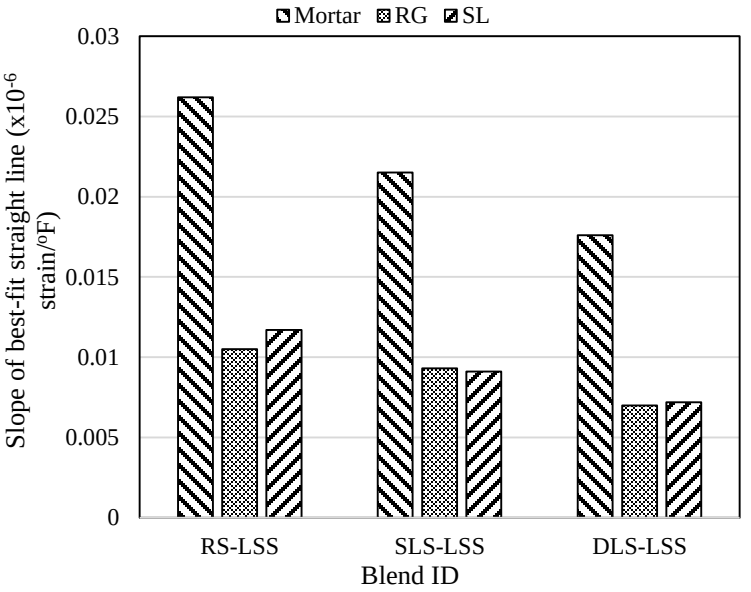

Figure 8.13 Rate of CTE reduction for mortar and concrete

8.4.3.3 Reducing cement paste volume

Seven concrete mixtures with varying cement paste volumes were prepared according to the proportioning technique presented in Chapter 7. Figure 8.14 shows the effect of cement paste volume on the CTE of concrete. Concrete was first proportioned for the cement content required to achieve theoretical paste volume. Then the paste volume was deviated (increased and decreased) from the theoretical paste volume to determine the effect of paste volume on the concrete CTE. The concrete CTE decreased as the cement paste volume decreased up to the theoretical paste volume, but the CTE increased when the paste volume decreased below the theoretical paste volume. The increase in CTE below the theoretical paste volume can likely be explained by the effect of internal water pressure. When the paste content is below the theoretical paste volume, the concrete did not have enough paste to fill all the voids between aggregates. Therefore, additional voids were introduced into the concrete and thus increased the porosity of the concrete. Higher porosity means higher amounts of liquid in the saturated concrete. The liquid phase had a higher CTE than did the solid phase, which increased the overall CTE of the saturated concrete and was the reason for a higher concrete CTE occurring when the paste volume fell below the theoretical minimum paste volume. Additional discussion on the effect of porosity on the measured CTE can be found in Chapter 5.

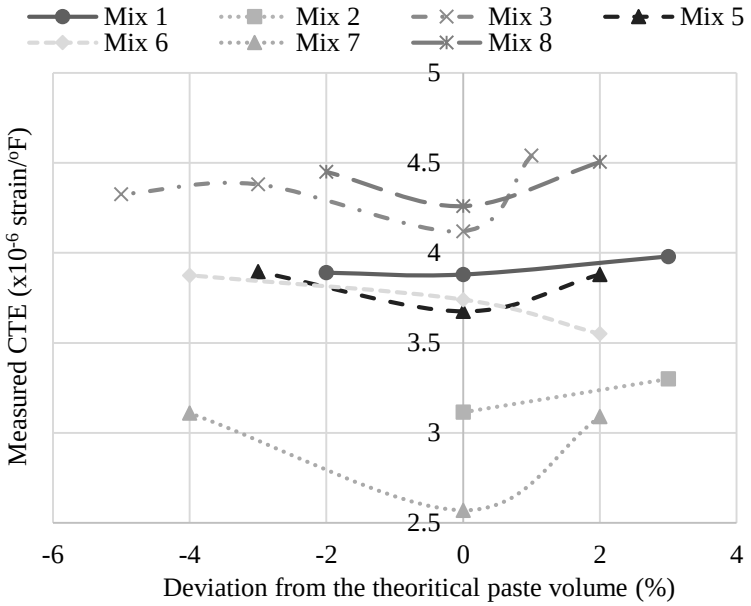

Figure 8.14 Effect of cement paste volume on the CTE of concrete

8.5 DEVELOPING A METHOD FOR CTE OPTIMIZATION

This section will present the comparison between the measured and predicted CTEs of both the mortar and the concrete. Predicted CTEs were determined from the calculated CTE of the constituents using the rule of mixtures proposed by Emanuel and Hulsey (1977). As described in the previous sections, the CTEs of cement paste, fine aggregate, and coarse aggregates were predicted using Eq. (8.4). The CTEs of fine aggregate were determined from the known CTEs of the mortar and the cement paste; similarly, the CTEs of coarse aggregates were determined from the known CTEs of the mortar and the concrete. Clement (2013) showed that Eq. (8.4) can predict the CTE of concrete constituents with a high level of accuracy. Table 8.2 presents the predicted CTE of concrete constituents. SL and SLS are from same source and their predicted CTE was 5.60 and 5.52 x10^{-6} strain/ºF (10.08 and 9.94 x10^{-6} strain/ºC), respectively. The predicted CTEs for SL and SLS were

very similar because the SL and SLS are form same source, thus reinforcing the accuracy of the prediction technique to determine the CTE of concrete constituents.

Table 8.2 Predicted CTE of concrete constituents

Material ID	Predicted CTE in $x10^{-6}$ strain/^{o}F ($x10^{-6}$ strain/^{o}C)
Cement paste	6.55 (11.79)
RG	6.24 (11.23)
SL	5.60 (10.08)
GR	2.46 (4.43)
LS	1.13 (2.0)
RSS	6.21 (11.18)
DLS	5.52 (9.94)
SLS	4.96 (8.93)
LSS	2.51 (4.52)

The CTEs for the mortar and the concrete were calculated using Eq. (8.4) based on the CTEs of the constituents presented in Table 8.2. Figure 8.15 and Figure 8.16 present the comparison of measured and predicted CTEs for the mortar and the concrete, respectively. The points are evenly distributed with respect to the line of equality in both the figures. Therefore, Eq. (8.4) can predict the mortar and concrete CTE with good accuracy from the CTE of the constituents. A t-test also confirmed that statistically there was no difference between predicted and measured CTEs with 99% confidence, where the null hypothesis (H_o) was assumed as the measured and the predicted CTE values were equal. Table 8.3 presents the detailed t-test results.

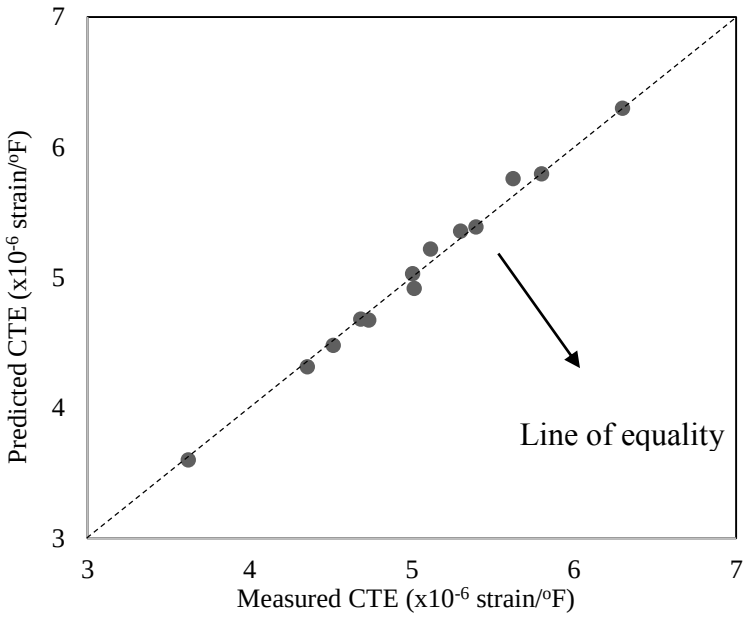

Figure 8.15 Comparison of predicted and measured CTEs of mortar

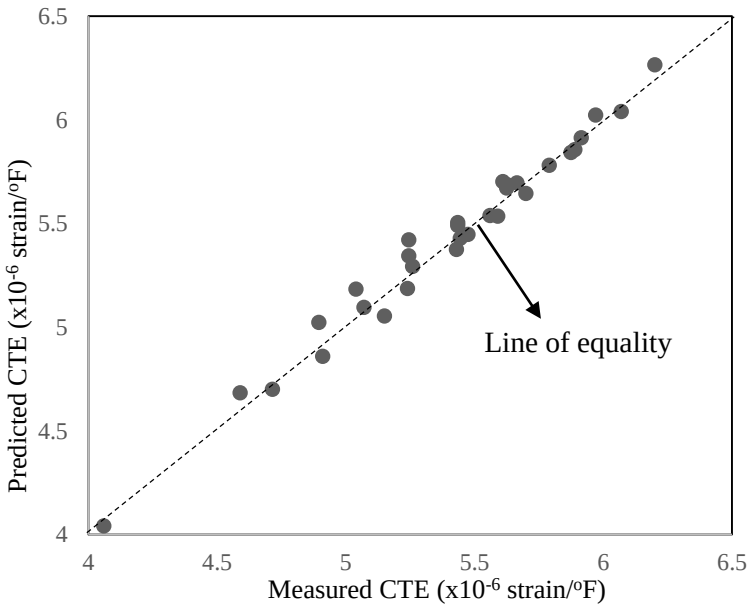

Figure 8.16 Comparison of predicted and measured CTEs of concrete

Table 8.3 Summary of t-test results for mortar and concrete

	Mortar (Figure 8.15)	Concrete (Figure 8.16)
Number of samples	13	26
Average of ΔCTE**	0.005	-0.01
Standard deviation	0.064	0.063
t	0.261	0.84
P (two tail)	0.797	0.41
$P<\alpha$ (α=0.01)	No	No
Null hypothesis (Ho) ($CTE_P=CTE_M$)*	Accepted	Accepted

** CTE_P and CTE_M represent predicted and measured CTE, respectively.*
*** ΔCTE represents the difference in predicted and measured CTE ($\Delta CTE = CTE_P - CTE_M$).*

8.6 PROPOSED METHOD FOR CTE OPTIMIZATION

Based on the previous discussions, a six-step CTE optimization method can be proposed.

- Select the cement, coarse and fine aggregates, and appropriate proportions of concrete constituents.
- Prepare the cement paste, mortar, and concrete specimens that have the same w/c, cement-to-sand, and mortar-to-coarse aggregate ratios of the target concrete mixture. Only one source of fine and coarse aggregates can be used while mixing mortar and concrete. Thus, the concrete mixtures have to be made with one cement, one sand, and one coarse aggregate. Similarly, mortar mixtures are made from similar cement that has been used for the concrete mixtures and one sand. Separate concrete and mortar mixtures have to be made for each coarse and fine aggregate source.

- Measure the CTE of the cement paste, mortar, and concrete prepared in the previous step.
- Determine the CTE of the fine and coarse aggregates using Eq. (8.4) and the known CTE of cement paste, mortar, and concrete. The CTE of fine aggregate can be determined from the known CTE of the cement paste and the mortar. Similarly, the CTE of coarse aggregate can be determined from the known CTE of the cement paste, the sand, and the concrete.
- Determine the required volume fraction of fine and coarse aggregates by using Eq. (8.4) to achieve the target CTE.
- Prepare concrete using the selected volume of fine and coarse aggregates. Measure the CTE of the trial concrete and adjust accordingly to obtain the target CTE; continue to repeat this step until the target concrete CTE is achievable. It is recommended to set the target CTE slightly below the required CTE because of the inconsistent nature of the CTE test procedures.

8.7 CONCLUSIONS

The CTE of concrete plays an important role in the durability and longevity of concrete structures. Concrete, when exposed to temperature change, experiences thermal movements that, under restraint, produce thermal stresses. Optimizing the CTE can alleviate the thermal stress and eventually reduce structural distresses. Following are the major findings of this study:

- A significant reduction of concrete CTE can be achieved by replacing high-CTE coarse aggregate with low-CTE coarse aggregate.

- Replacing high-CTE fine aggregate with low-CTE fine aggregate can also reduce the CTE of mortar, which eventually reduces the CTE of concrete.
- Reducing the cement content up to the theoretical paste volume can also reduce the concrete CTE. Reducing the cement paste volume below the theoretical paste volume introduces voids in the concrete system, which leads to a higher CTE for saturated concrete samples.
- The rule of mixtures can predict the CTE of the concrete from the CTE of its constituents with good accuracy and can be used to determine the volume fraction of each constituent to achieve a target concrete CTE.
- The CTE optimization technique presented in this chapter is simple and does not require complex calculations.
- It is not clear how reduction of the overall CTE of concrete using the proposed method will affect the distresses, such as spalling, that may occur due to the localized incompatibility of CTEs of concrete constituents, particularly for high-CTE coarse aggregate. Therefore, further investigation is needed to address this issue.

Chapter 9: Conclusions and Future Research

9.1 SUMMARY

The goals of this research project were to evaluate the probable causes of the inconsistency of measured CTE and to propose a method to optimize the CTE of concrete according to the need of the structures. This research sought to reveal the inconsistency of the CTE values from a material point of view. Proper understanding of the reasons for the inconsistency in the measured CTEs might help to improve the consistency of the CTE test methods. High-CTE concrete generates higher stress for a given temperature change. Therefore, the cracking potential of concrete can be reduced by reducing the CTE. Optimizing the concrete CTE according to the application can reduce the thermal distresses, thus reducing repair and rehabilitation costs as well as improving the durability and longevity of concrete structures.

During this research program it was noticed that the Texas Department of Transportation (TxDOT) method yielded higher CTE values than did the American Association of State Highway and Transportation Officials (AASHTO) method. This deviation was caused in part by internal water pressure that developed due to the difference in the CTE of the liquid and solid phases of saturated concrete. Internal water pressure is a time-dependent phenomenon that is responsible for instantaneous deformation and time-dependent deformation. A 4-in. x 8-in. (100-mm x 200-mm) concrete cylinder took about 20 to 30 minutes to reach thermal equilibrium. However, even after 10 hours in an isothermal state, length-change equilibrium was not reached.

An analytical model based on the poroelastic behavior of concrete was developed to determine the magnitude of the internal water pressure created in saturated concrete cylinders during heating and cooling cycles. This model can predict the axial strain of saturated concrete cylinders due to temperature change with satisfactory accuracy. According to the model, when concrete cylinders are subjected to a heating cycle, the developed internal water pressure goes as high as 700 psi (4.8 MPa). Internal water pressure increases with increasing porosity, decreasing permeability, and increasing rate of temperature change. Also, internal water pressure increased with increasing sample size (diameter). Internal water pressure could be partially responsible for the inconsistency of the CTE test results. Internal water pressure can be reduced by reducing the porosity, increasing permeability, using a smaller sample size, and reducing the rate of temperature change. Preconditioning saturated concrete samples by applying multiple cycles of heating and cooling prior to CTE testing improved the permeability, thus reducing the internal water pressure development. Moreover, maintaining a lower rate of temperature change reduced the internal water pressure and improved the consistency of measured CTE.

A concrete mixture design was proposed based on the combined gradation of coarse and fine aggregates. The proposed mixture design can use aggregates from any source, regardless of gradation, shape, and texture. Therefore, this might be a suitable method for proportioning concrete when manufactured sand is used as fine aggregate. Typically, manufactured sand has poor gradation, shape, and texture as compared to natural sand. Furthermore, this concrete mixture design method proposed guidelines to reduce cement requirement without sacrificing the performance of the concrete, which has the potential to reduce the cost and the carbon footprint of concrete. Moreover, this concrete mixture

design method is suitable for multiple coarse and fine aggregate blending. Aggregate blending is important, because concrete CTE can be reduced by blending low-CTE aggregate with high-CTE aggregate. Cement paste volume reduction also reduced the CTE of concrete but the effect is not as significant as that of aggregate blending. A CTE optimization technique was proposed based on the rule of mixture that presented systematic guidelines to achieve a target CTE by changing the constituents.

9.2 CONCLUSIONS

This study presented an understanding of the mechanism of internal water pressure development that occurs in a saturated concrete sample when subjected to temperature change. Based on this understanding, methods were presented to improve the consistency of the CTE test results. A CTE optimization technique that provided guidelines to achieve a target concrete CTE by changing concrete constituents was also presented. In addition, a concrete mixture design was presented, which meets the need for CTE optimization and also has the potential to produce economical and sustainable pavement concrete. Major findings of this research project were the following:

- The TxDOT method yielded higher CTE values than did the AASHTO method. Internal water pressure was the reason for this phenomenon.
- Higher porosity, lower permeability, larger sample size, and higher rate of temperature change increased the internal water pressure development in a concrete specimen when subjected to temperature change. Internal water pressure due to temperature change is one of the probable causes of inconsistent CTE test results.

- Preconditioning concrete samples by using heating and cooling cycles and lowering the rate of temperature change improved the consistency of the CTE testing methods.
- Replacing high-CTE aggregates with low-CTE aggregates and reducing cement content can reduce the concrete's overall CTE. Optimizing the CTE of concrete according to the application has the potential to improve the durability and longevity of the concrete structures, as well as achieve significant savings from reduced repair and rehabilitation cost.
- The proposed concrete mixture design method, based on the densest combined gradation of coarse and fine aggregates, can reduce cement content and can use aggregate from any sources. Therefore, this mixture design method can produce more economical and sustainable concrete without sacrificing the performance. This method also meets the need for CTE optimization.

9.3 MAJOR CONTRIBUTIONS

This research program extensively investigated the CTE test methods, evaluated techniques that can improve the consistency of the test results, and finally presented a method based on the rule of mixture to optimize the CTE of concrete. This study makes several contributions that improve the current understanding of concrete CTE. The major contributions of this research program were the following:

- This study compared the TxDOT and AASHTO CTE methods for the first time and identified that the TxDOT method yields higher CTE values than the AASHTO method.

- An analytical model was developed to predict the internal water pressure development in a saturated concrete cylinder. According to the proposed analytical model, porosity, permeability, sample size, and the rate of temperature change were the major factors that significantly influenced the internal water pressure development. Internal water pressure in saturated concrete, created by temperature change, can be reduced by reducing porosity, increasing permeability, reducing the rate of temperature change, and using a smaller sample size.
- Preconditioning concrete sample by applying heating and cooling cycles prior to CTE testing and maintaining a lower rate of temperature change improved the consistency of the CTE test methods by reducing the internal water pressure development in saturated concrete (created when the samples were subjected to temperature change).
- The presented concrete mixture design method was the first reported concrete mixture design based on the densest combined gradation of coarse and fine aggregates to achieve more economical and sustainable pavement concrete. This mixture design method provides a rational way to determine the cement requirement for a concrete mixture and is also suitable for non-standard aggregates that meet the need of CTE optimization requirements.
- Replacing high-CTE aggregates with low-CTE aggregates and reducing the cement paste volume can reduce the CTE of overall concrete. Based on these findings, a CTE optimization technique was proposed that provides a step-by-step guideline for CTE reduction.

9.4 RECOMMENDATIONS FOR FUTURE RESEARCH

Several research extensions would complement the work performed in this study, such as the following:

- Concrete at early age is typically in a saturated condition and might experience internal water pressure when subjected to daily temperature change. Therefore, further investigation is needed to understand the effect of internal water pressure on the early-age cracking potential of concrete.
- The proposed mixture design, based on the combined densest gradation of fine and coarse aggregate, was investigated only for pavement concrete application. Further investigation is needed to determine the suitability of the proposed mixture design for other types of concrete application.
- Additional investigation is needed to better understand the effect of low- and high-CTE aggregate blending on the distress mechanism that occurs due to the local incompatibility of CTE between concrete constituents, such as concrete pavement spalling.

Appendix A

The Laplace Transformation of time derivatives of a function G with respect to θ is defined by

$$\bar{\dot{G}}(\theta) = s\overline{G}(s) - G(\theta = 0) \tag{A1}$$

Therefore, according to Eq. (A1), one may write

$$\bar{\dot{\varepsilon}}_l(u) = s\bar{\varepsilon}_l(u) - \varepsilon_l(u, t = 0) \tag{A2}$$

For this study, there is no temperature change at *t=0*. Hence, no strain development is evident in the liquid phase, which can be expressed as

$$\varepsilon_l(u, t = 0) = 0. \tag{A3}$$

So, Eq. (A1) can be written as

$$\bar{\dot{\varepsilon}}_l(u) = s\bar{\varepsilon}_l(u) = \frac{-\bar{p}}{K_l} + \alpha_l \Delta T. \tag{A4}$$

Similarly, we can write

$$\bar{\dot{\varepsilon}}_s(u) = s\bar{\varepsilon}_s(u) = \frac{-\bar{p}}{K_s} + \alpha_s \Delta T, \tag{A5}$$

$$\bar{\dot{\varepsilon}}_f(u) = s\bar{\varepsilon}_f(u) = \frac{-\bar{p}}{3K_p} + \alpha_p \Delta T, \text{ and} \tag{A6}$$

$$\bar{\dot{\varepsilon}}(u) = s\varepsilon(u) = \frac{4(2s\bar{\nu}_p - 1)\int_0^R rs\bar{\varepsilon}_f \, \mathrm{d}r}{R^2(s\bar{\nu}_p - 1)} - \frac{(1+s\bar{\nu}_p)s\bar{\varepsilon}_f}{(s\bar{\nu}_p - 1)}. \tag{A7}$$

Eqs. (A5) to (A7) were used to obtain Eq. (5.19) from Eq. (5.18).

References

AASHTO T 336-11. (2011). *Coefficient of Thermal Expansion of Hydraulic Cement Concrete*. American Association of State Highway and Transportation Officials, 444 North Capitol Street N.W., Suite 249, Washington, D.C., 20001, 8.

AASHTO TP 60-00. (2000). *Standard Method of Test for Coefficient of Thermal Expansion of Hydraulic Cement Concrete*. American Association of State Highway and Transportation Officials, 444 North Capitol Street N.W., Suite 249, Washington, D.C. 20001, 7.

ACI. (2013). *ACI Manual of Concrete Practice 2013*. American Concrete Institute, Farmington Hills, MI, 1991.

ACI Committee 211. (1991). *Standard Practice for Selecting Proportions for Normal, Heavyweight, and Mass Concrete*. American Concrete Institute, Farmington Hills, MI, 1991, 38.

ACI Committee 318. (2011). *Building Code Requirements for Structural Concrete (ACI 318-11)*. American Concrete Institute, Farmington Hills, MI, 1991, 503.

Ai, H., Young, J. F., and Scherer, G. W. (2001). "Thermal Expansion Kinetics: Method to Measure Permeability of Cementitious Materials: Ii, Application to Hardened Cement Pastes." *Journal of the American Ceramic Society*, 84(2), 385–91.

Alungbe, G. D., Tia, M., and Bloomquist, D. G. (1992). "Effect of Aggregate, Water/Cement Ratio, and Curing on The Coefficient of Linear Thermal Expansion of Concrete." *Transportation Research Record: Journal of the Transportation Research Board*, 1335(1), 44–51.

Andersen, P. J., and Johansen, V. (1993). *Particle Packing and Concrete Properties. Volume 43 of RH & H bulletin*.

ASTM C143 / C143M - 12. (2012). *Standard Test Method for Slump of Hydraulic-Cement Concrete*. ASTM International, 100 Barr Harbor Drive, PO Box C700, West Conshohocken, PA 19428-2959, United States, 8.

ASTM C150 / C150M - 12. (2012). *Standard Specification for Portland Cement*. ASTM International, 100 Barr Harbor Drive, PO Box C700, West Conshohocken, PA 19428-2959, United States, 9.

ASTM C1754 / C1754M - 12. (2012). *Test Method for Density and Void Content of Hardened Pervious Concrete*. ASTM International, 100 Barr Harbor Drive, PO Box C700, West Conshohocken, PA 19428-2959, United States, 3.

ASTM C192 / C192M - 12a. (2012). *Standard Practice for Making and Curing Concrete Test Specimens in the Laboratory*. ASTM International, 100 Barr Harbor Drive, PO Box C700, West Conshohocken, PA 19428-2959, United States, 8.

ASTM C29 / C29M - 09. (2009). *Standard Test Method for Bulk Density ("Unit Weight") and Voids in Aggregate*. ASTM International, 100 Barr Harbor Drive, PO Box C700, West Conshohocken, PA 19428-2959, United States, 5.

ASTM C305-13. (2013). *Standard Practice for Mechanical Mixing of Hydraulic Cement Pastes and Mortars of Plastic Consistency*. ASTM International, 100 Barr Harbor Drive, PO Box C700, West Conshohocken, PA 19428-2959, United States, 3.

ASTM C33 / C33M - 13. (2013). *Standard Specification for Concrete Aggregates*. ASTM International, 100 Barr Harbor Drive, PO Box C700, West Conshohocken, PA 19428-2959, United States, 11.

ASTM C39 / C39M - 12a. (2012). *Standard Test Method for Compressive Strength of Cylindrical Concrete Specimens*. ASTM International, 100 Barr Harbor Drive, PO Box C700, West Conshohocken, PA 19428-2959, United States, 7.

ASTM C469 / C469M - 10. (2010). *Standard Test Method for Static Modulus of Elasticity and Poisson's Ratio of Concrete in Compression*. ASTM International, 100 Barr Harbor Drive, PO Box C700, West Conshohocken, PA 19428-2959, United States, 5.

ASTM C494/C494M. (2013). *Standard Specification for Chemical Admixtures for Concrete*. ASTM International, 100 Barr Harbor Drive, PO Box C700, West Conshohocken, PA 19428-2959, United States, 10.

Bažant, Z. P. (1970). "Delayed Thermal Dilatations of Cement Paste and Concrete Due to Mass Transport." *Nuclear Engineering and Design*, 14(2), 308–318.

Bentz, D. P., Bognacki, C. J., Riding, K. A., and Villarreal, V. H. (2011). "Hotter Cements, Cooler Concretes." *Concrete International*, 33(1), 41–48.

Berwanger, C., and Sarkar, A. F. (1976). "Thermal Expansion of Concrete and Reinforced Concrete." *ACI Journal Proceedings*, ACI.

Bjøntegaard, Ø., and Sellevold, E. J. (2001). "Interaction Between Thermal Dilation and Autogenous Deformation in High Performance Concrete." *Materials and Structures*, 34(5), 266–272.

Bonnell, D. G. R., and Harper, F. C. (1950). "The Thermal Expanson of Concrete. Engineering Research (Summary of a Report to be Published by The Building Research Station)." *Journal of the ICE*, 33(4), 320–330.

Branco, F., and Mendes, P. (1993). "Thermal Actions for Concrete Bridge Design." *Journal of Structural Engineering*, 119(8), 2313–2331.

Brown, T. D., and Javaid, M. Y. (1970). "The Thermal Conductivity of Fresh Concrete." *Matériaux et Construction*, 3(6), 411–416.

Burnham, T., and Koubaa, A. (2001). "A New Approach to Estimate the In-Situ Thermal Coefficient and Drying Shrinkage for Jointed Concrete Pavement." *7th International Conference on Concrete Pavements: The Use of Concrete in Developing Long-Lasting Pavement Solutions for the 21st Century*, International Society for Concrete Pavements, Purdue University, West Lafayette, IN, 9–13.

Campbell-Allen, D., and Thorne, C. P. (1963). "The Thermal Conductivity of Concrete." *Magazine of Concrete Research*, 15(43), 39–48.

Ceylan, H., Coree, B. J., and Gopalakrishnan, K. (2008). "Design of Rigid Pavements in Iowa Using the Mechanistic-Empirical Pavement Design Guide." *Baltic Journal of Road and Bridge Engineering*, 3(4), 219–225.

Choi, S., Ha, S., and Won, M. C. (2011). "Horizontal Cracking of Continuously Reinforced Concrete Pavement Under Environmental Loadings." *Construction and Building Materials*, 25, 4250–4262.

Choinska, M., Khelidj, A., Chatzigeorgiou, G., and Pijaudier-Cabot, G. (2007). "Effects and Interactions of Temperature and Stress-Level Related Damage on Permeability of Concrete." *Cement and Concrete Research*, 37(1), 79–88.

Chung, Y., and Shin, H.-C. (2011). "Characterization of the Coefficient of Thermal Expansion and Its Effect on the Performance of Portland Cement Concrete Pavements." *Canadian Journal of Civil Engineering*, 38(2), 175–183.

Clement, J. C. (2013). "Recommendations for Coarse Aggregate Testing Requirements for use in Portland Cement Concrete." Ph.D. Dissertation, The University of Texas at Austin, Austin, TX.

CSA A23.2-24A. (2004). "Test Method for the Resistance of Unconfined Coarse Aggregate to Freezing and Thawing." Canadian Standards Association, Toronto, Canada.

Darwin, D., Browning, J., Lindquist, W., McLeod, H., Yuan, J., Toledo, M., and Reynolds, D. (2010). "Low-Cracking, High-Performance Concrete Bridge Decks." *Transportation Research Record: Journal of the Transportation Research Board*, 2202(-1), 61–69.

Dettling, H. (1964). *The Thermal Expansion of Hardened Cement Paste, Aggregates, and Concrete*. Deutscher Ausschuss filr Stahlbeton, Berlin, 64.

Dewar, J. D. (1999). *Computer Modeling of Concrete Mixtures*. Routledge, New York, NY.

Dobrowolski, J. A. (1998). *Concrete Construction Handbook*. McGraw-Hill, New York, USA.

El-Dieb, A. S., and Hooton, R. D. (1995). "Water-Permeability Measurement of High Performance Concrete Using a High-Pressure Triaxial Cell." *Cement and Concrete Research*, 25(6), 1199–1208.

Emanuel, J. H., and Hulsey, J. L. (1977). "Prediction of the Thermal Coefficient of Expansion of Concrete." *ACI Materials Journal*, 74(4), 149 – 155.

Emerson, M. (1981). "Thermal Movements of Concrete Bridges: Field Measurements and Methods of Prediction." *ACI Special Publication*, 70.

G.M.Idorn Consult A/S. (1995). *User manual Europack version 1.1*. G.M.Idorn Consult A/S.

Garboczi, E. J. (1997). "Stress, Displacement, and Expansive Cracking Around a Single Spherical Aggregate Under Different Expansive Conditions." *Cement and concrete research*, 27(4), 495–500.

Glavind, M., Olsen, G. S., and Munch-Petersen, C. (1993). "Packing Calculations and Concrete Mix Design." *Nordic Concrete Research*, 13(2), 21–34.
Goltermann, P., and Johansen, V. (1997). "Packing of Aggregates: an Alternative Tool to Determine the Optimal Aggregate Mix." *ACI Materials Journal*, 94(5), 435–442.
Grasley, Z. C. (2006). "Measuring and Modeling the Time-Dependent Response of Cementitious Materials to Internal Stresses." Ph.D., University of Illinois at Urbana-Champaign, United States -- Illinois.
Grasley, Z. C., and Lange, D. A. (2007). "Thermal Dilation and Internal Relative Humidity of Hardened Cement Paste." *Materials and Structures*, 40(3), 311–317.
Grasley, Z. C., Scherer, G. W., Lange, D. A., and Valenza, J. J. (2007). "Dynamic Pressurization Method for Measuring Permeability and Modulus: Ii. Cementitious Materials." *Materials and Structures*, 40(7), 711–721.
Grasley, Z., and Leung, C. (2011). "Quasi-Static Axial Damping of Poroviscoelastic Cylinders." *Journal of Engineering Mechanics*, 137(8), 561–570.
Hale, W. M., John, E. E., Peyton, S. W., and Sanders, C. L. (2012). "Bridge Deck Cracking: A Field Study on Concrete Placement, Curing, and Performance." *Construction and Building Materials*, 34(1), 70+.
Hobbs, D. W. (1971). "The Dependence of the Bulk Modulus, Young's Modulus, Creep, Shrinkage and Thermal Expansion of Concrete Upon Aggregate Volume Concentration." *Matériaux et Construction*, 4(2), 107–114.
Hoseini, M., Bindiganavile, V., and Banthia, N. (2009). "The Effect of Mechanical Stress on Permeability of Concrete: A Review." *Cement and Concrete Composites*, 31(4), 213–220.
Hossain, M., Khanum, T., Tanesi, J., Schieber, G., and Montney, R. A. (2006). "The PCC Coefficient of Thermal Expansion Input for the Mechanistic-Empirical Pavement Design Guide." *85th Annual Meeting of the Transportation Research Board, National Research Council,* Washington, DC.
Huang, Y. H. (2003). *Pavement Analysis and Design*. Prentice Hall.
Hudson, B. (2003). "Blending Sands for Concrete." *Field Evaluation*, Austin, TX.
Im, C. K., and Chang, S. P. (2000). "Thermal Behaviour of Composite Box-Girder Bridges." *Proceedings of the ICE - Structures and Buildings*, 140(2), 117–126.
Imbsen, R. A., Vandershaf, D. E., Schamber, R. A., and Nutt, R. V. (1985). *Thermal Effects in Concrete Bridge Superstructures*. National Cooperative Highway Research Program report, Transportation Research Board, National Research Council, Washington, DC.
Iskander, M., Parikh, S., and Aboumoussa, W. (2012). "Apparent Thermal Coefficient of Expansion of Concrete Building with Restraint." *ACI Materials Journal*, 109(1).
Jahangirnejad, S., Buch, N., and Kravchenko, A. (2009). "Evaluation of Coefficient of Thermal Expansion Test Protocol and Its Impact on Jointed Concrete Pavement Performance." *ACI Materials Journal*, 106(1), 64–71.

Johansson, L. (1979). "The Effect of Aggregate Grading and Mix Proportions on the Workability for Concrete Made with Entirely Crushed Aggregate." *Studies on Concrete Technology, Swedish Cement and Concrete Research Institute*, 147–160.

Kada, H., Lachemi, M., Petrov, N., Bonneau, O., and Aïtcin, P.-C. (2002). "Determination of the Coefficient of Thermal Expansion of High Performance Concrete from Initial Setting." *Materials and Structures*, 35(1), 35–41.

Kannekanti, V. N., and Harvey, J. T. (2006). "Sensitivity Analysis of 2002 Design Guide Distress Prediction Models for Jointed Plain Concrete Pavement." *Transportation Research Record: Journal of the Transportation Research Board*, 1947(1), 91–100.

Khan, A. A., Cook, W. D., and Mitchell, D. (1998). "Thermal Properties and Transient Thermal Analysis of Structural Members During Hydration." *ACI Materials Journal*, 95(3), 293–303.

Kim, S., and Won, M. C. (2004). "Horizontal Cracking in Continuously Reinforced Concrete Pavements." *ACI Structural Journal*, 101(6), 784–791.

Kim, W., and Laman, J. A. (2010). "Integral Abutment Bridge Response Under Thermal Loading." *Engineering Structures*, 32(6), 1495–1508.

Koehler, E. P., and Fowler, D. W. (2007). *Aggregates in Self-Consolidating Concrete*. Research Report, International Center for Aggregates Research, The University of Texas at Austin, Austin, TX, 353.

Kohler, E., Alvarado, R. F., and Jones, D. J. (2007). "Measurement and Variability of Coefficient of Thermal Expansion for Concrete Pavements." *Transportation Research Board 86th Annual Meeting*, Washington, D.C., 13.

Krauss, P. D., and Rogalla, E. A. (1996). *Transverse Cracking in Newly Constructed Bridge Decks*. National Highway Cooperative Research Program (NCHRP) Report, National Highway Cooperative Research Program (NCHRP) Report, Transportation Research Board, Washington D.C., 132.

De Larrard, F. (1999). *Concrete Mixture Proportioning: A Scientific Approach*. Taylor & Francis.

Leung, C., and Grasley, Z. (2012). "Poromechanical Damping of Cementitious Materials." *Journal of Materials in Civil Engineering*, 24(2), 232–238.

Leung, C. K., and Grasley, Z. C. (2012). "Effect of Micrometric and Nanometric Viscoelastic Inclusions on Mechanical Damping Behavior of Cementitious Composites." *Construction and Building Materials*, 35, 444–451.

Mallela, J., Abbas, A., Harman, T., Rao, C., Liu, R., and Darter, M. (2005). "Measurement and Significance of the Coefficient of Thermal Expansion of Concrete in Rigid Pavement Design." *Transportation Research Record: Journal of the Transportation Research Board*, 1919(1), 38–46.

Mallet, A. (2000). *NumericalInversion*. University of Mauritius.

McCullough, B. F., Zollinger, D., and Dossey, T. (2000). *Evaluation of the Performance of Texas Pavements Made with Different Coarse Aggregates*.

Mehta, P. K., and Monteiro, P. J. (2006). *Concrete: Microstructure, Properties, and Materials*. McGraw-Hill New York.
Meyers, S. L. (1951). "Thermal Expansion Characteristics of Hardened Cement Paste and of Concrete." *Highway Research Board Proceedings*.
Mindess, S., Young, J. F., and Darwin, D. (2002). *Concrete*. Prentice Hall, New Jersey, U.S.
Moorty, S. (1990). "Thermal Movements in Bridges." Ph.D., University of Washington, United States -- Washington.
Moorty, S., and Roeder, C. W. (1990). "Thermal Responses of Skewed Bridges." *Third International Conference on Short and Medium Span Bridges*, Canadian Society for Civil Engineering, Toronto, Canada, 343–353.
Mukhopadhyay, A. K., Neekhra, S., and Zollinger, D. G. (2007). *Preliminary Characterization of Aggregate Coefficient of Thermal Expansion and Gradation for Paving Concrete.* Technical Report, Texas Transportation Institute and Texas Department of Transportation., FHWA, U.S. Department of Transportation, Washington, DC.
Mukhopadhyay, A. K., Zollinger, D. G., and Sarkar, S. L. (2003). "New Mineralogical Approach to Predict Aggregate Coefficient of Thermal Expansion (cote) Based on Dilatometer and Bulk Chemical Analysis." *ICAR 11th Annual Symposium*, National Sand and Gravel Association, Alexandria, VA.
Naik, T., Kraus, R., and Kumar, R. (2011). "Influence of Types of Coarse Aggregates on the Coefficient of Thermal Expansion of Concrete." *Journal of Materials in Civil Engineering*, 23(4), 467–472.
Naranjo, A. (2013). "Two Lift Concrete Paving -TxDOT Perspective." Two-Lift Paving Workshop, The University of Texas, Austin, TX.
National Cooperative Highway Research Program (NCHRP), and Applied Research Associated, Inc. (ARA). (2004). *Guide for Mechanistic-Empirical Design of New and Rehabilitated Pavement Structure*. Washington, D.C.
Ndon, U. J., and Bergeson, K. L. (1995). "Thermal Expansion of Concretes: Case Study in Iowa." *Journal of Materials in Civil Engineering*, 7(4), 246–251.
Neville, A. M., and Brooks, J. J. (1987). *Concrete Technology*.
Paul, V. (1981). "Composite Construction and Bearings." *Design of Steel Bridges*, Granada Publishing, London, England, 10.68–10.70.
Pritchard, B. (2003). *Continuous and Integral Bridges*. CRC Press.
Quiroga, P. N., and Fowler, D. W. (2004). *The Effects of Aggregates Characteristics on the Performance of Portland Cement Concrete*. Research Report, International Center for Aggregates Research, The University of Texas at Austin, Austin, TX, 382.
Rached, M., De Moya, M., and Fowler, D. W. (2009). *Utilizing Aggregates Characteristics to Minimize Cement Content in Portland Cement Concrete*. Research Report,

International Center for Aggregates Research, The University of Texas at Austin, Austin, TX, 117.
Rogers, C. A. (1998). "Canadian Experience with the Micro-Deval Test for Aggregates." *Geological Society, London, Engineering Geology Special Publications*, 13(1), 139–147.
Rogers, C. A., Lane, B. C., and Senior, S. A. (2003). "The Micro-Deval Abrasion Test for Coarse and Fine Aggregate in Asphalt Pavement." *International Center for Aggregates Research 11th Annual Symposium*, National Sand and Gravel Association, Alexandria, VA.
Sakyi-bekoe, K. (2008). "Assessment of the Coefficient of Thermal Expansion of Alabama Concrete." Master of Science, Auburn University, Auburn, Alabama.
Sakyi-Bekoe, K. O. (2008). "Assessment of the Coefficient of Thermal Expabsion of Alabama Concrete." Master of Science, Auburn University, Auburn, Alabama.
Sandepudi, K. S. (1991). "Thermal Response in Florida Bridges." M.S. Thesis, Florida Atlantic University, United States, Florida.
Saunders, C. H. (1995). "Manufactured Sand Usage in North Carolina." Austin, TX.
Scherer, G. W. (1994). "Stress in Aerogel During Depressurization of Autoclave: I. Theory." *Journal of Sol-Gel Science and Technology*, 3(2), 127–139.
Scherer, G. W. (2000a). "Measuring Permeability of Rigid Materials by a Beam-Bending Method: I, Theory." *Journal of the American Ceramic Society*, 83(9), 2231–2239.
Scherer, G. W. (2000b). "Thermal Expansion Kinetics: Method to Measure Permeability of Cementitious Materials: I, Theory." *Journal of the American Ceramic Society*, 83(11), 2753–2761.
Scherer, G. W. (2006a). "Dynamic Pressurization Method for Measuring Permeability and Modulus: I. Theory." *Materials and structures*, 39(10), 1041–1057.
Scherer, G. W. (2006b). "Dynamic Pressurization Method for Measuring Permeability and Modulus: I. Theory." *Materials and Structures*, 39(10), 1041–1057.
Schindler, A., and McCullough, B. F. (2002). "Importance of Concrete Temperature Control During Concrete Pavement Construction in Hot Weather Conditions." *Transportation Research Record: Journal of the Transportation Research Board*, 1813(-1), 3–10.
De Schutter, G., and Taerwe, L. (1995). "Specific Heat and Thermal Diffusivity of Hardening Concrete." *Magazine of Concrete Research*, 47(172), 203–208.
Sellevold, E. J., and Bjøntegaard, Ø. (2006). "Coefficient of Thermal Expansion of Cement Paste and Concrete: Mechanisms of Moisture Interaction." *Materials and Structures*, 39(9), 809–815.
Al-Shemmeri, T. (2012). *Engineering Fluid Mechanics*. Ventus Publishing, Telluride, CO.
Shilstone, J. M. (1999). "The Aggregate: The Most Important Value-Adding Component in Concrete." Austin, TX.
Shilstone Sr, J. M. (1990). "Concrete Mixture Optimization." *Concrete International*, 12(6), 33–39.

Siddiqui, M. S., and Fowler, D. W. (2013a). "Coefficient of Thermal Expansion of Concrete: Some Rational Modifications to Improve the Reliability of Current Testing Practices." Conference presentation, Ames, IA.

Siddiqui, M. S., and Fowler, D. W. (2013b). "Optimizing the COTE of Concrete by Blending High and Low COTE Aggregates to Meet TxDOT Limit." *Sustainable pavements and materials, 2nd T&DI Green Street, Highways and Development 2013*, American Society of Civil Engineers, Reston, VA, 125–134.

Siddiqui, M. S., and Fowler, D. W. (2014a). "Evaluation of Current Concrete Coefficient of Thermal Expansion Test Procedures and Their Response to Internal Water Pressure." Conference presentation, Washington, D.C.

Siddiqui, M. S., and Fowler, D. W. (2014b). "Effect of Internal Water Pressure on the Measured Coefficient of Thermal Expansion of Concrete." *Journal of Materials in Civil Engineering*, 04014151.

Tanesi, J., Crawford, G., Gudimettla, J., and Ardani, A. (2012). "Coefficient of Thermal Expansion of Concrete changes to Test Method will enhance Pavement Design." *Concrete International*, 55–60.

Tanesi, J., Gudimettla, J. M., Crawford, G. L., and Ardani, A. A. (2013). "Ruggedness Study on the Coefficient of Thermal Expansion of Concrete Test Method (AASHTO T336)." *Transportation Research Board 92nd Annual Meeting*, Washington, D.C., 15.

Tanesi, J., Hossain, M., Khanum, T., Schieber, G., and Montney, R. A. (2006). "Portland Cement Concrete Coefficient of Thermal Expansion Input for Mechanistic-Empirical Pavement Design Guide." *Transportation Research Board 85th Annual Meeting*, Washington, D.C., 21.

Tanesi, J., Kutay, M., Abbas, A., and Meininger, R. (2007). "Effect of Coefficient of Thermal Expansion Test Variability on Concrete Pavement Performance as Predicted by Mechanistic-Empirical Pavement Design Guide." *Transportation Research Record: Journal of the Transportation Research Board*, 2020(1), 40–44.

Tex-1xx-E. (Unpublished). *Aggregate Crushing Value*. Texas Department of Transportation, Austin, TX.

Tex-403-A. (1999). *Saturated Surface-Dry Specific Gravity and Absorption of Aggregates*. Texas Department of Transportation, Austin, TX, 8.

Tex-410-A. (1999). *Abrasion of Coarse Aggregate Using the Los Angeles Machine*. Texas Department of Transportation, Austin, TX, 1.

Tex-411-A. (2004). *Soundness of Aggregate Using Sodium Sulfate or Magnesium Sulfate*. Texas Department of Transportation, Austin, TX, 11.

Tex-418-A. (2008). *Compressive Strength of Cylindrical Concrete Specimens*. Texas Department of Transportation, Austin, TX, 1.

Tex-428-A. (2011). *Determining the Coefficient of Thermal Expansion of Concrete*. Texas Department of Transportation, Austin, Tx, 8.

Tex-461-A. (2005). *Degradation of Coarse Aggregate by Micro-Deval Abrasion*. Texas Department of Transportation, Austin, TX, 3.

Timoshenko, S., and Goodier, J. N. (1951). *Theory of Elasticity*. Mcgraw Hill, New York, USA.

Tindal, T., and Yoo, C. (2003). "Thermal Effects on Skewed Steel Highway Bridges and Bearing Orientation." *Journal of Bridge Engineering*, 8(2), 57–65.

TxDOT. (2004). *Standard Specifications for Construction and Maintenance of Highways, Streets, and Bridges*. Texas Department of Transportation, Austin, TX.

Vichit-Vadakan, W., and Scherer, G. W. (2002). "Measuring Permeability of Rigid Materials by a Beam-Bending Method: III, Cement Paste." *Journal of the American Ceramic Society*, 85(6), 1537–1544.

Wittmann, F., and Lukas, J. (1974). "Experimental Study of Thermal Expansion of Hardened Cement Paste." *Matériaux et Construction*, 7(4), 247–252.

Wolfram Research, Inc,. (2012). *Wolfram Mathematica*. 100Trade Center DriveDrive, Champaign, IL, 61820–7237, USA.

Won, M. (2005). "Improvements of Testing Procedures for Concrete Coefficient of Thermal Expansion." *Transportation Research Record: Journal of the Transportation Research Board*, 1919(1), 23–28.

Yeon, J., Choi, S., and Won, M. (2009). "Effect of Relative Humidity on Coefficient of Thermal Expansion of Hardened Cement Paste and Concrete." *Transportation Research Record: Journal of the Transportation Research Board*, 2113(1), 83–91.

Ziegeldorf, S. W., Kleiser, K., and Hilsdorf, H. K. (1978). "Effect of Thermal Expansion of Aggregate on Thermal Expansion of Concrete." *Colloque international sur les materiaux granulaires. International symposium on aggregates and fillers. Budapest, 9-12 oct. 1978*, Omkdk-technoinform, 452–464.

Zoldners, N. G. (1971). "Thermal Properties of Concrete Under Sustained Elevated Temperatures." *ACI Special Publication*, 25.